Title

Design and Synthesis of Conjugated Polymers and Small Molecules Based on Thiophene-Substituted Isoindigo, 5-acetyl-4H- cyclopenta[c]thiophene-4,6(5H)-dione, and Diketopyrrolopyrrole Electron-Deficient Units

Author

Richard, Eric Thomas

Publication Date

2014

Peer reviewed|Thesis/dissertation

UNIVERSITY OF CALIFORNIA
Los Angeles

Design and Synthesis of Conjugated Polymers and Small Molecules Based on Thiophene-Substituted Isoindigo, 5-acetyl-4*H*-cyclopenta[*c*]thiophene-4,6(5*H*)-dione, and Diketopyrrolopyrrole Electron-Deficient Units

A dissertation submitted in partial satisfaction of the
requirements for the degree Doctor of Philosophy
in Materials Science and Engineering

by

Eric Thomas Richard

2014

ABSTRACT OF THE DISSERTATION

Design and Synthesis of Conjugated Polymers and
Small Molecules Based on Novel Electron Deficient Units

by

Eric Thomas Richard
Doctor of Philosophy in Materials Science and Engineering
University of California, Los Angeles, 2014
Professor Yang Yang, Chair

Pi-Conjugated polymers and small molecules are useful for their semiconductor properties in organic electronic devices such as organic photovoltaics, light emitting diodes, and thin film transistors. They also find application in chemical detection for their high sensitivity to fluorescence quenching species. Described herein are the syntheses of two new electron deficient monomer units for polymers and small molecules. 5-acetyl-1,3-dibromo-4H-cyclopenta[c]thiophene-4,6(5H)-dione was synthesized for the first time. It can be conveniently polymerized by Stille coupling to form polymers initially insoluble in common solvents, which can be rendered soluble by deprotonation with various organic amines. Solutions in methanol are highly fluorescent and show strong quenching when exposed to Ni^{2+} and Cu^{2+}. Additionally, films can be cast from chloroform or dichlorobenzene solutions with triethylamine. New polymers and small molecules based on the recently reported thiophene substituted isoindigo were also synthesized and employed in photovoltaic devices reaching a maximum of 3.75 % power conversion efficiency, the highest yet reported for this unit. Also discussed is a series of

low band gap small molecule semiconductors incorporating two diketopyrrolopyrrole units and their photovoltaic applications. The best power conversion efficiency for a molecule in this series was 2.22 %.

This dissertation of Eric Thomas Richard is approved.

_____

Dwight C. Streit

_____

Kang L. Wang

_____

Benjamin J. Schwartz

_____

Yang Yang, Committee Chair

University of California, Los Angeles

2014

This thesis is dedicated to my parents for their unwavering support and their cultivation from an early age of my love of science.

Table of Contents

List of Abbreviations

LED light-emitting diode

EL electroluminescence or electroluminescent

PL photoluminescence

ITO indium tin oxide

CuPc Copper Phthalocyanine

PLED polymer LED

PT poly(thiophene-2,5-diyl)

SCLC space charge limited current

AM1.5G Air Mass 1.5 Global

$PC_{61}BM$ [6,6]-phenyl C_{61}-butyric acid methyl ester

$PC_{71}BM$ [6,6]-phenyl C_{71}-butyric acid methyl ester

P3HT poly(3-hexylthiophene-2,5-diyl)

DI de-ionized

PEDOT:PSS poly(3,4-ethylenedioxythiophene):poly(styrenesulfonate)

PV photovoltaic

PVK Poly(N-vinylcarbazole)

TCNQ tetracyano-p-quinodimethane

TTF tetrathiafulvene

HOMO highest occupied molecular orbital

LUMO lowest unoccupied molecular orbital

PCE power conversion efficiency

OPV organic photovoltaic

DMSO dimethylsulfoxide

ACT 5-acetyl-4*H*-cyclopenta[*c*]thiophene-4,6(5*H*)-dione

DPP 1,4-diketo-pyrrolo[3,4-c]pyrrole

II Isoindigo

TII thiophene-substituted isoindigo

TFT thin film transistor

DFT density functional theory

EH 2-ethylhexyl

BDT Benzodithiophene

QRE quasi-reference electrode

TLC thin layer chromatorgraphy

DTT dithienothiophene

NBS N-bromosuccinimide

n-BuLi n-Butyl Lithium

DMF N,N-Dimethylformamide

THF Tetrahydrofuran

CF Chloroform

DCB 1,2-dichlorobenzene

DIO 1,8-Diiodooctane

CN 1-Chloronaphthalene

List of Figures and Tables

Chapter 2

Chapter 3

Figures

Tables

Chapter 4

Chapter 5

Figures

Tables

Acknowledgements

I would like to sincerely thank everyone who made my PhD studies and research possible. I need to first of all thank my advisor Professor Yang Yang for inviting me to join his dynamic and creative research group and for his support and guidance over the years it took to complete this work. His wisdom and insight into the world of academia were indispensible to me and to all of the students who have passed through the group.

I would also like to thank my committee members Professors Dwight Streit, Kang Wang, and Benjamin Schwartz for their valuable input.

My labmates in the YY group played a huge part in my research. I would like to first thank the device experts who contributed directly to much of the data presented in this work. To Johnny Chen, Jing Gao, Zhenyi Wang, Steve Hawks, Yang Yang (the student), Enping Yao, and Brett Beekly I owe a debt of gratitude for their patience, hard work, and critical insight. I would also like to thank all of the fantastic organic chemists I worked with during my time at UCLA, Letian Dou, Lijun Huo, Youjun He, Jase Chang, Yongsheng Liu and Shirong Lu for many fruitful discussions and for their spirit of camaraderie during the long hours spent in the lab.

This work was supported in part by the NSF IGERT: Materials Creation Training Program at UCLA

I would like to thank the chair of the MCTP program Prof. Robin Garrell as well as the other MCTP faculty for enthusiastically leading this excellent program.

Vita of Eric Thomas Richard

2004	**Graduated Palos Verdes Peninsula High School**
	Boy Scouts of America Eagle Scout Award
	Varsity Letter in Track and Field
	Awarded Regents' Scholarship to UC Irvine
2008	**Astronomy Club at UCI President**
	Tau Beta Pi Engineering Honor Society
	Graduated from UC Irvine with a BS In Chemical Engineering with a minor in Materials Science
2009	**Chemist I at Solarmer Energy Inc. in El Monte, California**
2010	**Awarded UCLA Materials Creation Training Program (MCTP) Fellowship**
2011	**MCTP Seminar Oral Presentation "Low Bandgap Polymer Synthesis for Organic Photovoltaics"**
2012	**Internship at National Chiao Tung University, Hsinchu, Taiwan**
	Advisor: Prof. Kung-Hwa Wei, Research topic: Crosslinkable Organic Semiconductors

2013 **Advanced to candidacy for Doctor of Philosophy degree in Materials Science and Engineering**

Chapter 1

General Introduction

The field of organic electronics has grown rapidly over the past few decades. Organic light emitting diodes (OLEDs) are already part of consumer electronics products and other devices including organic photovoltaics (OPV), photodetectors, chemical sensors, and transistors show considerable promise.[5] Organic materials can be employed as conductors and semiconductors in electronic devices. Organic semiconductors can be processed by vacuum evaporation,[6] electropolymerization,[7] and from solution by a range of printing processes.[8] The solution approach is very attractive for making large area printed electronics such as solar cells and emissive displays. Such devices could be manufactured on continuous roll-to-roll printing equipment, enabling a revolution in inexpensive large area electronics.

Applications like these require soluble organic semiconductors with a range of properties. Organic materials with specific light absorption or emission spectra and electronic properties such as energy level position and charge carrier mobility are required for each application. These properties are controlled by chemical structure and can be adjusted by judicious modification.

The focus of this thesis is the design and application of novel organic semiconductor materials. It will begin with an introduction to the history of the field and a discussion of the operating principles of organic photovoltaic devices and the thought process involved in designing materials for this application. Chapters are dedicated to individual research projects centered on a particular structural unit.

Chapter 2

Introduction to organic electronics

2.1 History of organic electronics

The electrical conduction properties of organic materials have been investigated since the early 20th century[9] with early reports of photoconductivity in anthracene and it's solutions coming from Pochettino in 1906,[10] Byk and Bork in 1910[11] and Volmer in 1913[12] who measured an increase in conductivity of hexane and benzene solutions of anthracene upon illumination with an arc lamp, which may have been due to the photogeneration of mobile ions.

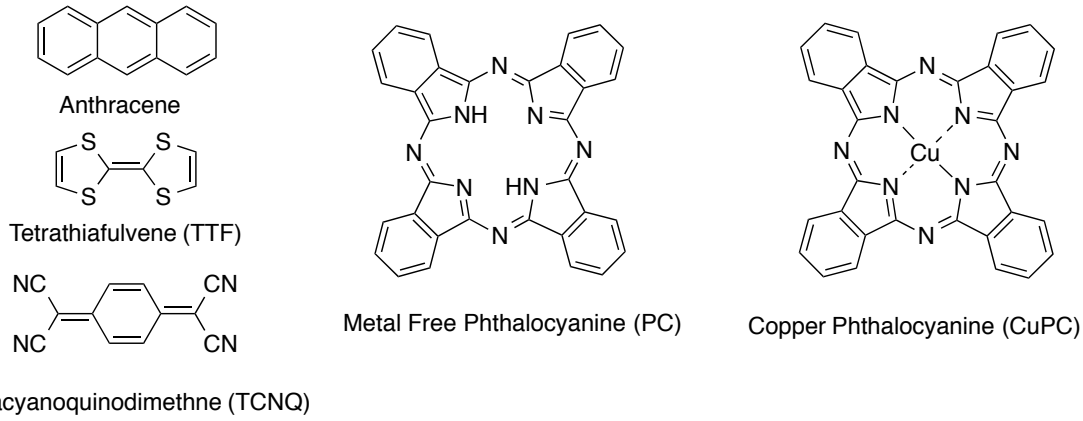

Figure 2.1: Structures of early organic semiconductors

By the late forties, these phenomena were being revisited and studied in the context of semiconductor research. In 1946 D. D. Eley reported perhaps the first conclusive evidence for intrinsic semiconducting properties in an organic material.[13] Crystals of phthalocyanine and its copper complexes were shown to exhibit an Arrhenius

relationship between conductivity and temperature analogous to inorganic semiconductors. Organic charge transfer complexes of tetrathiafulvene(TTF) and halogens and later tetracyanoquinenmethide (TCNQ) were found to have metal like conductivities up to 1.47 x 10^4 S/cm.[14] The π-conjugated polymer polypyrrole, prepared by pyrolosis was reported in the literature in 1963 and showed conductivity up to 1 S/cm upon doping with iodine.[15] It was also reported that both p and n-type chemical doping could be achieved with electron-poor and electron-rich dopants. Research in conductive polymers accelerated tremendously after Shirakawa, MacDiarmid, and Heegar reported on the synthesis and conductivity of films of polyacetylene doped with halogen vapors.[16] Iodine doped films were initially reported to have a conductivity of 38 S/cm, which was later improved to over 10^5 S/cm in stretch-oriented films.

A variety of electronic devices based on organic materials have been developed over the years. The first organic electroluminescent (EL) device based on the organic dye acridine orange was reported in 1955,[17] but required high voltages and operated via an impact ionization mechanism analogous to inorganic EL devices. The first organic light emitting devices to operate via a charge injection and recombination mechanism were patented by R.H. Partridge,[18] and consisted of poly(vinylcarbazole) (PVK) with emitting dye molecules added sandwiched between a cesium electrode and a transparent conductor coated with $SbCl_5$ doped polyvinylcarbazole as a hole injecting layer. The first OLED to operate at a voltage < 10V was reported by Tang et. al. at Kodak in 1987[19] which lead to an explosion of interest in the field of organic electronics.

Organic photovoltaic (OPV) cells, the devices which are the main focus of this thesis, were first reported by Kearns and Kalvin in 1958.[20] They measured a photovoltage of 200 mV when using air-oxidized N,N,N',N'-tetramethyl-p-phenylenediamine as the

electron accepting material in a bilayer configuration. The power output of these first devices was only several picowatts. It was not until the work of C.W. Tang which was patented in 1979[21] and published in 1986[22] that an OPV device with a power conversion efficiency over 1% was reported. These devices contained a heterojunction of copper phthalocyanine and an o-phenylenediamine adduct of perylene tertracaboxylate. The two materials formed a heterojunction with CuPc as the electron donor and the perylene derivative as the acceptor. Tang attributed the high performance to exciton (bound electron hole pair) separation at the interface under the influence of an electric field present at the donor-acceptor interface.[22]

The field of OPV was advanced further with the development of the bulk heterojunction, a phase-separated mixture of donor and acceptor that allows more photogenerated excitons to make it to the interface and be separated. This approach was first reported by Hiramoto et. al. for evaporation-processed small molecules in 1991 and in solution-processed MEH-PPV:C_{60} photodetectors by Yu and Heeger in 1994.[23] The approach was later successful in producing 2.9% power conversion efficiency (PCE) devices.[24] Improvements in bulk heterojunction morphology by more controlled processing methods such as controlling solvent evaporation rate for “solvent annealing” lead to further improvements.[25]

Around the same time, there was an increasing emphasis on lower band gap polymers, which absorb more of the solar spectrum.[1] Synthesis of new organic semiconductor materials became a major driver for improvements in power conversion efficiency. At the time of writing this thesis, the efficiency of organic photovoltaics has increased to 12%[26] overall and 10.6%[27] for a solution processed cell, both from stacked tandem devices.

2.2 Organic Semiconductors and Conductors

Semiconductors are materials, which have the ability to conduct charge carriers, mobile electrons and/or holes (empty electron states), but have a lower concentration of these carriers than a conductor.{Blakemore:ud} This concentration and hence the conductivity can be altered by introduction of impurities (doping), exposure to light or other radiation, or electric fields. Conductivity is related to carrier concentration by the equation:

$$\sigma = ne\mu \qquad 2.1$$

Where σ is conductivity n is the charge carrier density e is the elementary charge and μ is a material parameter known as charge carrier mobility and is the ratio of the drift velocity of carriers to the electric field.[28] The ability of charge carriers to move depends on a large system of overlapping orbitals, which is usually a conjugated π system (except for the case of polysilanes).[29] π-conjugation results when the p-orbitals in a chain of atoms overlap, resulting in new molecular orbitals of varying energy depending on the way in which the p-orbitals interact, as can be seen from the 1,3-butadiene example in figure 2.2. Depending on the phases of the interacting p-orbitals, the resulting molecular orbitals have nodes where destructive interference occurs; the more nodes, the higher the energy. The highest occupied molecular orbital is referred to as the HOMO level and the lowest energy unoccupied one is referred to as the LUMO. Organic semiconductors consist of much larger conjugated π electron systems which result in HOMO and LUMO energies close enough that charge carriers are reasonably stable and excited states can be generated by ultraviolet and visible light.

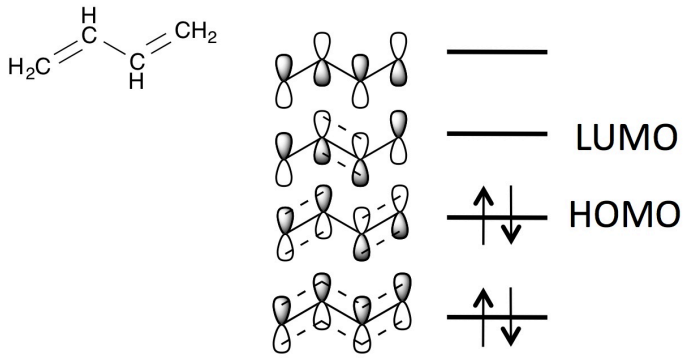

Figure 2.2 Molecular orbitals in 1,3-butadiene

Carrier transport

The extended π-conjugation leads to a delocalization of the molecular orbitals, which allows extra electrons and holes to travel within a molecule. In order for a carrier to move through an organic material, it must hop from one molecule to another. This process depends on the spatial overlap of orbitals between adjacent molecules and requires sufficient energy to overcome any differences in energy between the two orbitals, except in highly ordered materials, which may exhibit band-like transport (as evidenced by the high mobility and its increase with decreasing temperature).[30] Orbital energy differences may arise from relaxation of molecular structure on the molecule(s) bearing a charge carrier, and structural or conformational variation due to disorder (known as energetic disorder). The energy to hop between molecules is provided by quanta of vibrational energy known as phonons. The process is known as phonon-assisted hopping and shows a characteristic $\mu \propto T^{1/4}$ dependence of mobility on temperature, which is observed in many, but not all,[30] organic semiconductors.

Doping

Conjugated polymers can be rendered conductive by chemical doping, which results in holes or electrons on the backbone balanced by counter ions of opposite charge. The

simple conjugated polymer polyacetylene, for example, can be doped with iodine vapor, which leads to the oxidation of the polymer chain giving rise to a cation known as a polaron.[31] In other conducting polymers, which are more complex and consist of aromatic units, charge carriers may pair up to form bipolarons if the carrier concentration is high enough.[31] This configuration is lower in energy than two separate polarons since the introduction of a polaron causes a switch in the bond order represented in *fig. 2.10* from the aromatic structure to the less stable quinoid structure. There is a driving force in these polymers to bring the polarons together to reduce the number of repeat units in the quinoid structure.

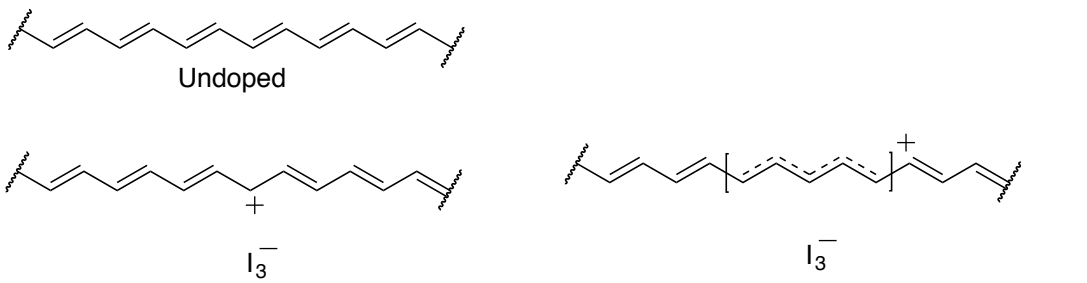

Figure 2.3 Iodine doping in polyacetylene

2.3 Operating Principles of Organic Electronic Devices

Organic Photovoltaics (OPV)

Photovoltaic cells, organic or otherwise, are devices which produce a voltage upon illumination with light. If current is allowed to flow, power will be generated based on the equation $P = IV$, where P is power, I is current, and V is voltage. A graph of current or current density vs. applied potential is known as a *J-V* or *I-V* curve of a device.{Wurfel:tu} This graph is often used to evaluate the performance of photovoltaic

devices and determine the ideal load to extract the maximum power from a device. The basic features of this graph are shown in fig 2.4. The current at zero voltage applied is known as the short circuit current or current density if it is expressed on a per-area basis (I_{SC} or J_{SC}, respectively). This is the maximum current the device can generate without external power. The voltage at zero current is known as the open circuit voltage or V_{OC}. The power output of the device reaches a maximum at one point on the graph. The ratio of this power to the product J_{SC} x V_{OC} is a parameter known as the fill factor, and can be thought of graphically as the ratio of area 1 to area 2 shown on the graph in *figure 2.4.*

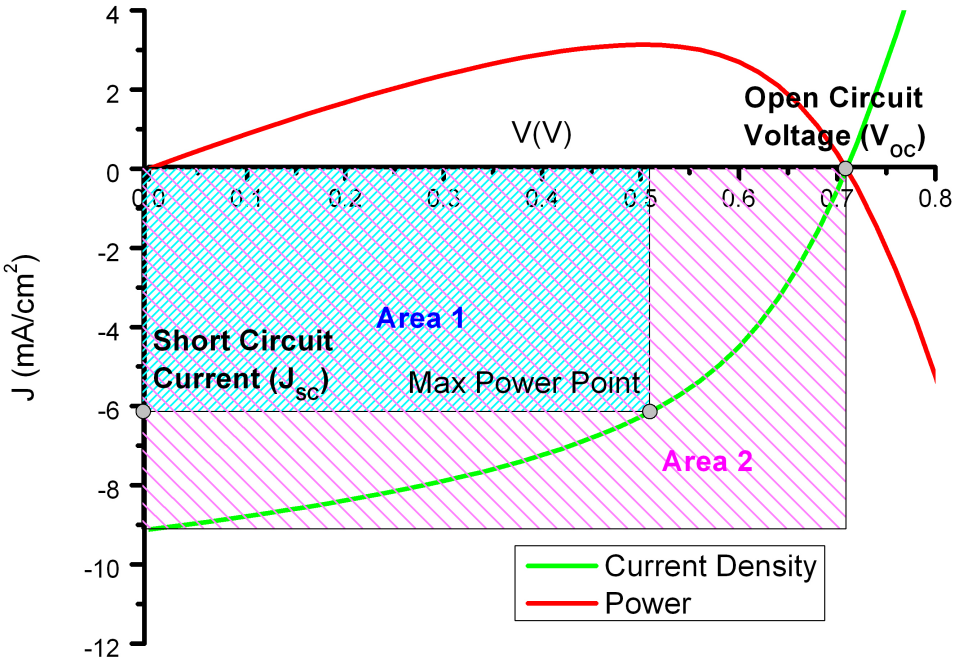

Figure 2.4 Critical parameters of a photovoltaic cell J-V curve

Organic photovoltaics typically are made from at least two different organic semiconductors, an electron donor material and an electron acceptor. These materials form a heterojunction, which is necessary for efficient device operation. Unlike many

inorganic semiconductors, such as silicon, germanium, and gallium arsenide, most organic semiconductors do not form free electrons and holes upon absorption of a photon; instead a bound electron-hole pair, or exciton, is formed.[32]{Wurfel:tu} Because of their low dielectric constants and molecular reorganization, the binding energies of excitons in organic semiconductors are larger than in most inorganic ones. Estimates for this value range from 0.05 – 1.6 eV depending on the material.[32] The consequence of this is that a heterojunction is required to separate excitons into free electrons and holes that can be collected to generate photocurrent. The excitons generated must also reach an interface before they recombine or they will not contribute to device current.

The basic steps of photocurrent generation are illustrated in *fig 2.5*. First, an exciton is generated in the donor (or acceptor) by an incident photon. Second, it diffuses to an interface in what is thought to be a random walk process. Third, the exciton separates, with an electron dropping into the LUMO level of the acceptor (or a hole going from the acceptor to the HOMO level of the donor). The exact way in which this happens is controversial and may depend on the specific materials used for the device.[33,34] One possibility is that when an exciton reaches an interface, a bound pair of charge carriers, an electron in the acceptor and a hole in the donor, results. This charge-transfer state then dissociates to form free carriers. There is considerable evidence from transient absorption studies that this occurs in some cases and that recombination of these states is a limiting factor in the photocurrent generation in some material combinations.[35] The role of non-thermally-relaxed “hot” excitons in charge separation has also been investigated and also seems to be significant in some materials.[36] The extra energy and delocalization of hot excitons may be responsible for the ultrafast (<1 - 10ps) charge

separation observed by transient absorption and PL.

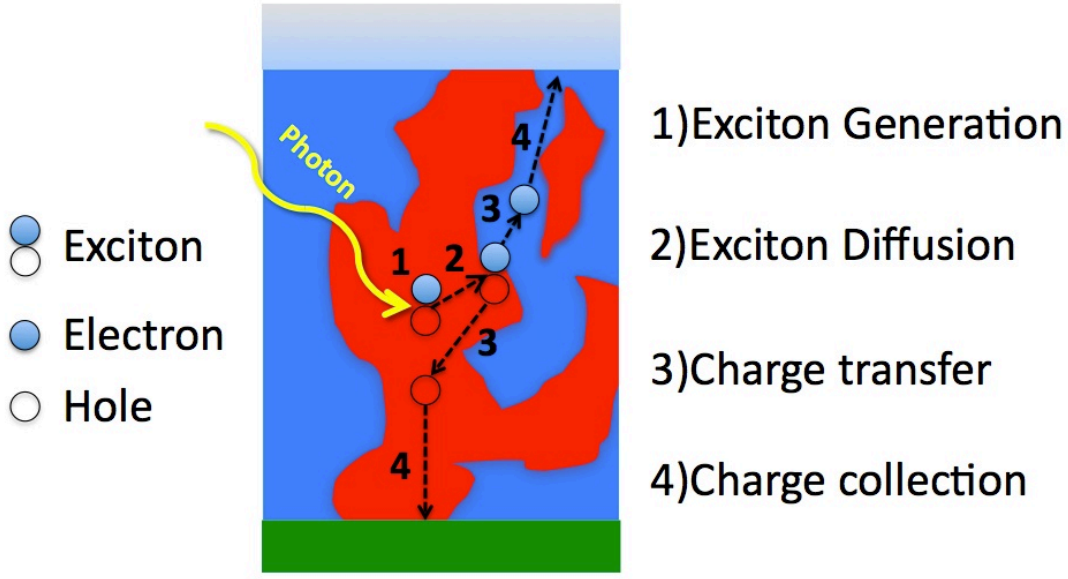

Figure 2.5 Process of photocurrent Generation in organic solar cells

The final step in photocurrent generation is collection of the free electrons and holes. This is accomplished with carrier-selective contacts, which are typically conductive materials with Fermi energy levels that are close to the LUMO level of the acceptor for the negative electrode (cathode) and close to the HOMO level of the donor for the positive electrode (anode). The carrier motion is driven by the built-in potential in the devices.

With the typically short exciton diffusion lengths in organic semiconductors (around 20 nm) in a devices with a planar heterojunction, as in the first heterojunction OPV by Tang et al.,[22] excitons generated far from the interface are not collected. To overcome this problem, an interpenetrating network of donor and acceptor materials can be used so the generated excitons are close enough to a donor/acceptor interface to diffuse to it

before recombining. For this to be the case, the size of the domains must be less than the exciton diffusion length. This concept is shown schematically in *fig 2.4.*

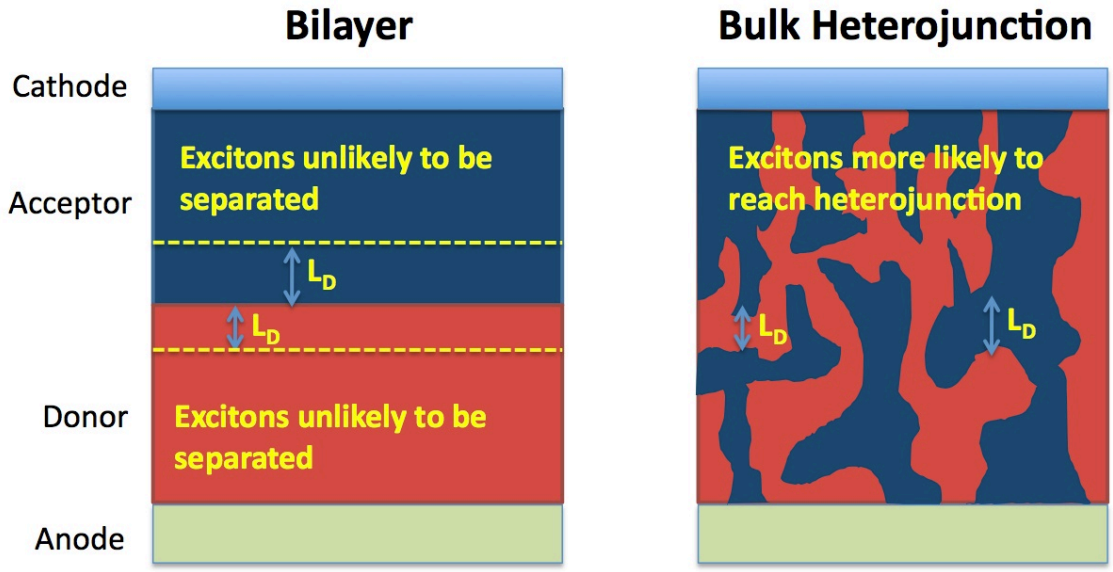

Figure 2.6 Bulk heterojunction and bilayer structures in OPV

To make bulk heterojunction devices like this, the materials may be deposited by thermally evaporating donor and acceptor materials simultaneously onto the substrate or by solution processing from a mixed solution of donor and acceptor in one solution, or sequentially from separate solutions of donor and acceptor. With solution processing, the two materials phase separate upon evaporation of the solvent.{Nardes:2012kp}{Ayzner:2012kp} Controlling the scale of this phase segregation is important to achieving good performance. With many small molecule materials, for example, their rapid crystallization leads to overly large domains if they are coated from high boiling point solvents, so for these materials, highly volatile solvents such as chloroform are used.[37-39]

2.4 Design of materials for OPV

The focus of this thesis is the design and synthesis of novel materials for OPV and other applications. The material properties that are important for performance in OPV devices are determined by chemical structure as well as supramolecular ordering on nanometer to micron length scales. Materials with appropriate properties can be designed by modifying chemical structure. The structure-property relationships in organic semiconductors are very complicated and most structural modifications can be expected to affect all of the relevant material properties to some degree, often in unexpected ways.

Perhaps the most straightforward aspect of material design is control over the HOMO and LUMO energy levels. The energy levels can be adjusted via a variety of design approaches and structural motifs, and there are an abundance of materials reported in literature with a wide range of both HOMO and LUMO positions.{Bundgaard:2007ci}{Chen:2009hy} The energy level requirements for donor materials in OPV are as follows: 1) a HOMO-LUMO gap that achieves a balance of absorbance of the solar spectrum and open circuit voltage for maximum efficiency 2)a HOMO level as deep as possible for the highest open circuit voltage and 3) a LUMO level that is high enough to allow for charge transfer to the acceptor.{Bundgaard:2007ci}

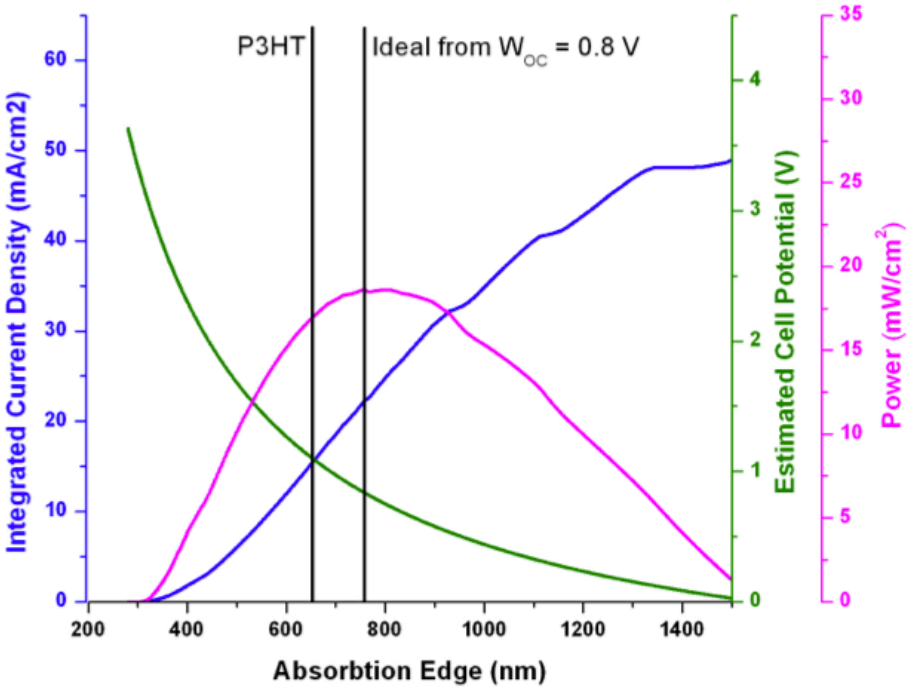

Figure 2.7 *Energy level optimization based on a simple performance model*

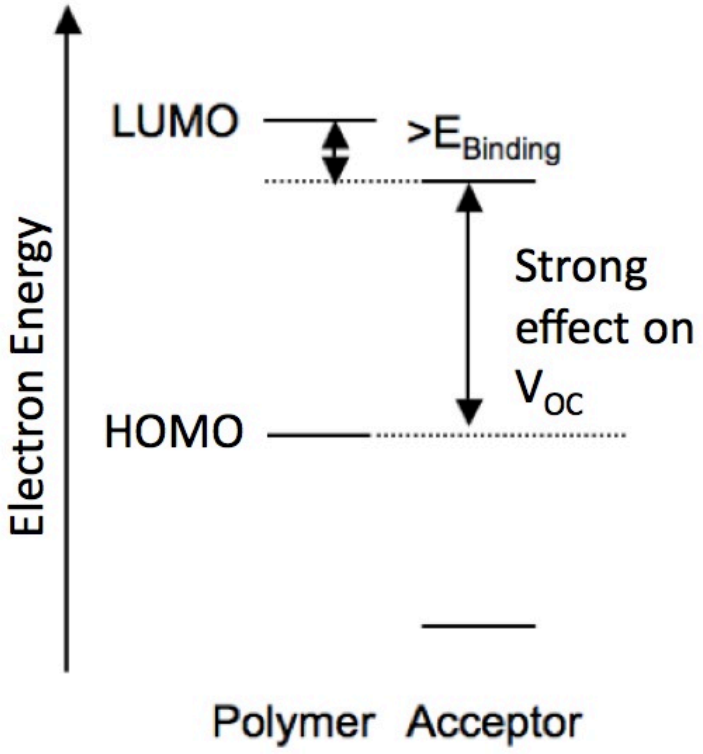

Figure 2.8 Energy level diagram for a polymer solar cell

To satisfy requirement 1, the HOMO-LUMO gap needs to be adjusted to a value of 1.4 – 1.7eV. Using a simple model of OPV performance assuming that the open circuit voltage will be 0.8 V lower than the bandgap, a typical empirical value, it can be estimated that the ideal band gap when using sunlight at the earth's surface is 1.65 eV. This optimization is shown in *fig. 2.7*. In practice, the highest performance materials for single junction cells have had band gaps around 1.6 – 1.7 eV[40]. This is higher than the optimum value of 1.4 derived by Shockley and Queisser[41] using thermodynamics and the detailed balance of carrier concentrations. The various additional losses in organic solar cells beyond radiative recombination are the reason for this observed discrepancy.

The structural effects on the band gap of an organic semiconductor include:

Conjugation Length. An increase in the length of the conjugated π-system will reduce the bandgap. This effect tapers off at high molecular weight and is generally only a factor in oligomers with molecular weights below 5000 g/mol.

Aromatic Stabilization. Since the LUMOs of aromatic conjugated polymers typically have a quinoid electronic structure and the HOMOs have an aromatic structure,[42] increased aromaticity stabilizes the HOMO level and destabilizes the LUMO level. This effect is particularly apparent in the difference in band gaps of polyphenylenes, polythiophenes, and polyselenophenes,[1,43] with a trend of decreasing band gaps and aromatic character of the rings in the polymer chains. Another approach is using fused ring systems that favor the quinoid electronic structure over the aromatic one. This can be demonstrated with a resonance structure argument shown in *fig 2.10* where in poly(thieneothiophene), only one of the rings can be drawn with three electron pairs, and in the quinoid structure, the upper thiophene gains an electron pair.

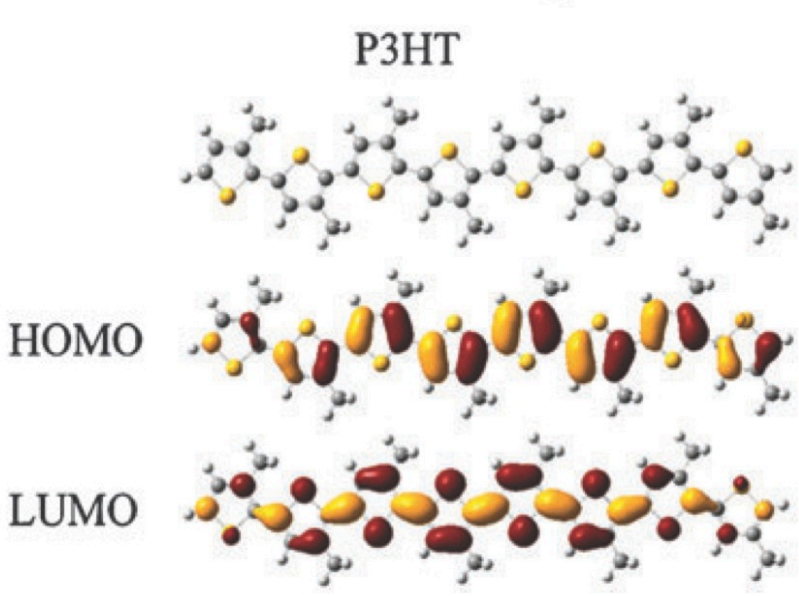

Figure 2.9 DFT Frontier Orbitals of Poly-3-hexylthiophene adapted from literature.{Mike:2011jo}

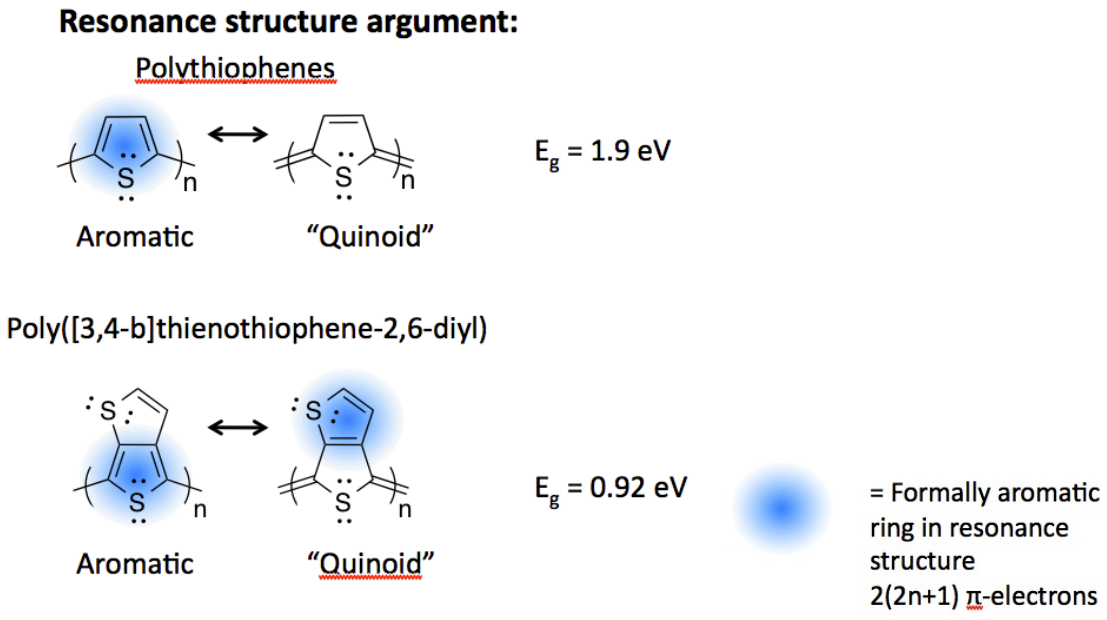

Figure 2.10 The effect of a fused thiophene ring on the quinoid structure stability and band gap in conjugated polymers. Band gap values are from literature.[1]

Intramolecular Charge Transfer. Combining electron-rich and electron-deficient parts into one conjugated system is a well-established strategy from dye chemistry. When electron rich an electron deficient units are combined, the orbitals of both units will combine to form new molecular orbitals, as shown schematically in fig 2.11.{Bundgaard:2007ci} The HOMO level will be above the HOMO of the electron-rich unit and the LUMO level will be below that of the electron deficient unit. This approach is used in most of the reported OPV materials to achieve appropriate band gap.[1]

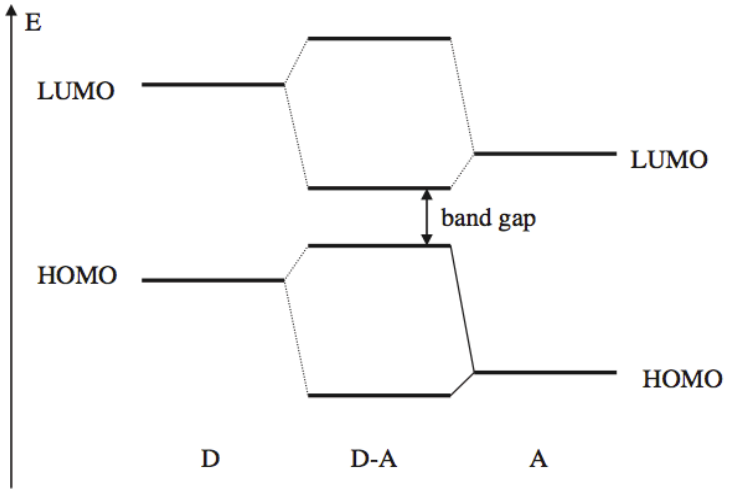

Figure 2.11 Conceptual illustration of the combination of electron rich "donor" units (D) and electron poor "acceptor" units (A). Adapted from literature.[1]

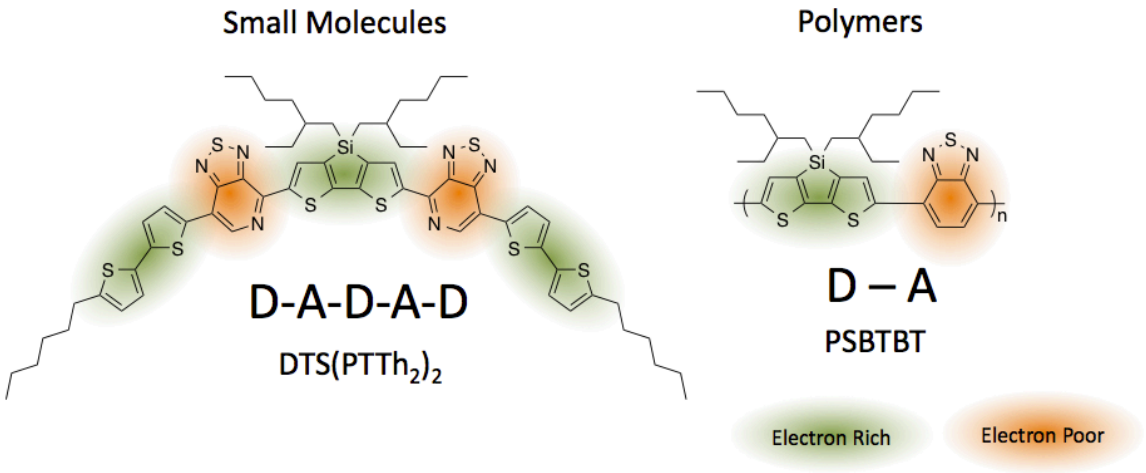

Figure 2.12 Examples of donor-acceptor design in OPV donor materials. DTS($PTTh_2$)$_2$[2] and PSBTBT[3]

Metal-ligand charge transfer

Organometallic complexes like copper phthalocyanine owe their low bandgap to charge transfer from a metal center to an organic ligand bound to them.{Carniato:2002cg}

Effect of electron-withdrawing groups

In order to adjust the positions of the energy levels to get better open circuit voltage, electron-withdrawing groups can be introduced. Fluorine atoms are a commonly employed electron withdrawing unit that can be substituted for hydrogen to lower the HOMO level of materials because of their small atomic radius and limited disruption of molecular packing compared to polyatomic electron withdrawing groups such as carbonyl, cyano, sulfonyl, and trifluoromethyl groups,[44,45] which are also used. Fluorine atoms do, however, still significantly affect solubility, usually making molecules less soluble in organic solvents. There are many examples of fluorine substitution in literature.[46-48]

2.5 Solubility of Organic Semiconductors

In addition to control over band gap and energy, another important consideration for solution-processed materials is solubility. Conjugated polymers have very strong π-π stacking interactions, and ones lacking substitution (or dopant counter ions[49]) are, without exception, highly insoluble materials. In order for them to be soluble, they must be substituted with alkyl groups or ionic groups. Alkyl groups provide steric repulsion to prevent strong π-π interactions and have a high entropy in the liquid phase due to their

flexibility. Alkyl chains with branching enhance solubility more than linear ones, and groups like 2-ethylhexyl, 2-butyloctyl, 2-hexyldecyl etc. are commonly used since precursors are commercially available.[50,51] However, alkyl chains are a non-conjugated part of the material and can reduce charge carrier mobility by inhibiting chain to chain charge transport and lead to reduced J_{SC} in polymer solar cells if they are excessive.[52] The positioning of the alkyl chains on a molecule or polymer also has a major influence on the supramolecular packing. The effect of even small modifications on alkyl groups has been shown many times to have a major effect on performance due to changes in film packing.[38,53] If there is steric repulsion between adjacent units in a polymer chain, the bonds may rotate out of planarity and lead to a breaking of conjugation and often a drop in mobility and increase in band gap.[54,55] Alkyl side chains also act as significant electron donating groups due to hyperconjugation.[56] Because of the many effects of alkyl chains on different properties, the process of molecular design in organic electronics still requires a great deal of trial and error when it comes to alkyl side chain selection.

Chapter 3 Thiophene-Substituted Isoindigo Materials

3.1 Introduction

In this chapter, I will discuss the design and synthesis of thiophene-substituted isoindigo (TII) unit based polymer and small molecule semiconductors. The TII unit gives materials with lower band gap than DPP and isoindigo based small molecules with similar structure.[57] In donor-acceptor-donor small molecules, the energy gaps range from 1.30eV for bithiophene as the donor to 1.59eV for naphthalene. The highest efficiency of 3.77% was obtained using benzofuran as the donor unit.

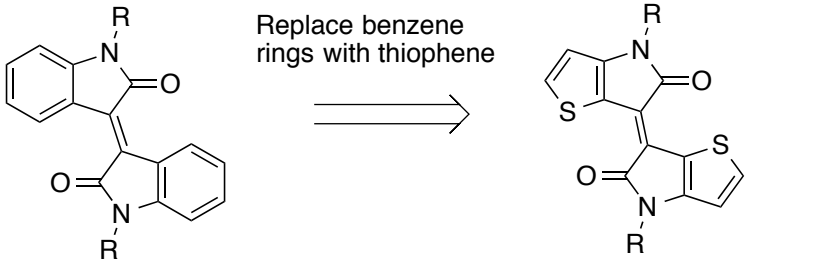

Isoindigo Thiophene Isoindigo (TII)

Figure 3.1 Thiophene substituted isoindigo

Isoindigo is a chromophore due to its low lying LUMO level, which results from the structure which can be thought of as two donor acceptor chromophores that share a common ethylene bridge[58] which gives rise to many possible charge transfer resonance structures, as shown in fig. 3.2. This makes it a promising candidate for low band gap materials, and it indeed has been employed in polymeric and small molecule

semiconductors that have been used in organic field effect transistors (OFET)[59-62] and OPV cells[62-67]. Isoindigo, when copolymerized with common donor units, gave band gap energies ranging from 1.50 – 1.61 eV. This is sufficiently small for efficient collection of the solar spectrum, but when isoindigo is employed in donor-acceptor-donor type small molecules, the band gap energy is about 1.67 eV.[67]

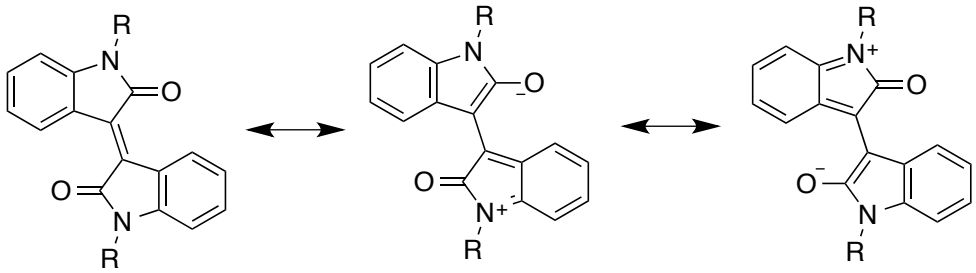

Figure 3.2 Some charge transfer resonance structures in isoindigo

Reducing the band gap further could lead to improvements in current by improving light absorption. This would be helpful for making small molecules suited to tandem solar cell applications. This led us to explore small molecules incorporating the more recently-developed thiophene-substituted isoindigo unit as a way to explore the properties of molecules with lower band gaps. Replacing one or both of the benzene rings in the isoindigo unit with thiophene has been shown to reduce the band gap and reduce the twisting of the central double bond as well as the twisting between units in the backbone.[62,63] Previously-reported polymers containing thiophene-substituted isoindigo (TII) show band gaps of 1.0 – 1.6 eV[62,68,69] The widest band gap of 1.6 eV reported was a copolymer with fluorene,[68] and the narrowest was with dithienothiophene.[69]

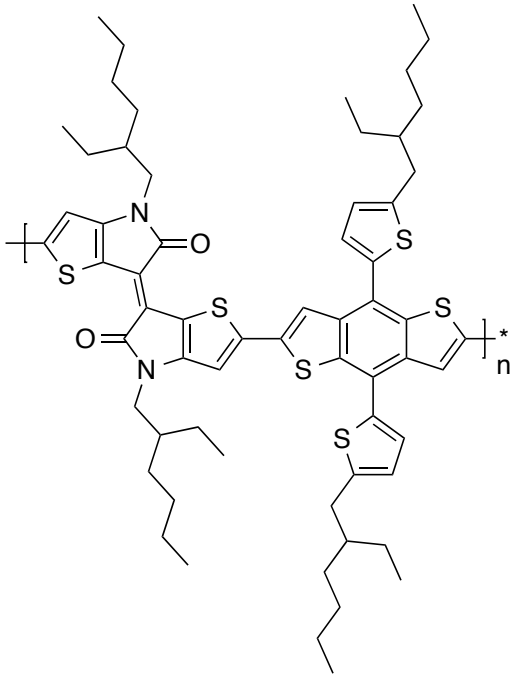

Figure 3.3 Structure of TII-BDTT (P-1) Polymer

In this work, the TII unit was copolymerized with a bis-(2-thienyl)benzodithiophene donor comonomer to yield a polymer with an optical band gap of 1.24 eV. Device performance reached a maximum of 2.53% PCE. In order to make materials with somewhat larger band gaps more appropriate for OPV applications, small molecules also were prepared as the reduced conjugation length in small molecules should result in an increased band gap. The thiophene isoindigo unit was coupled to five different electron donor units of varying electron-donating ability: Alkylbithiophene, 2-phenylthiophene, benzothiophene, benzofuran, and naphthalene. This gave materials with varying band gaps and energy levels as shown in table 3.1.

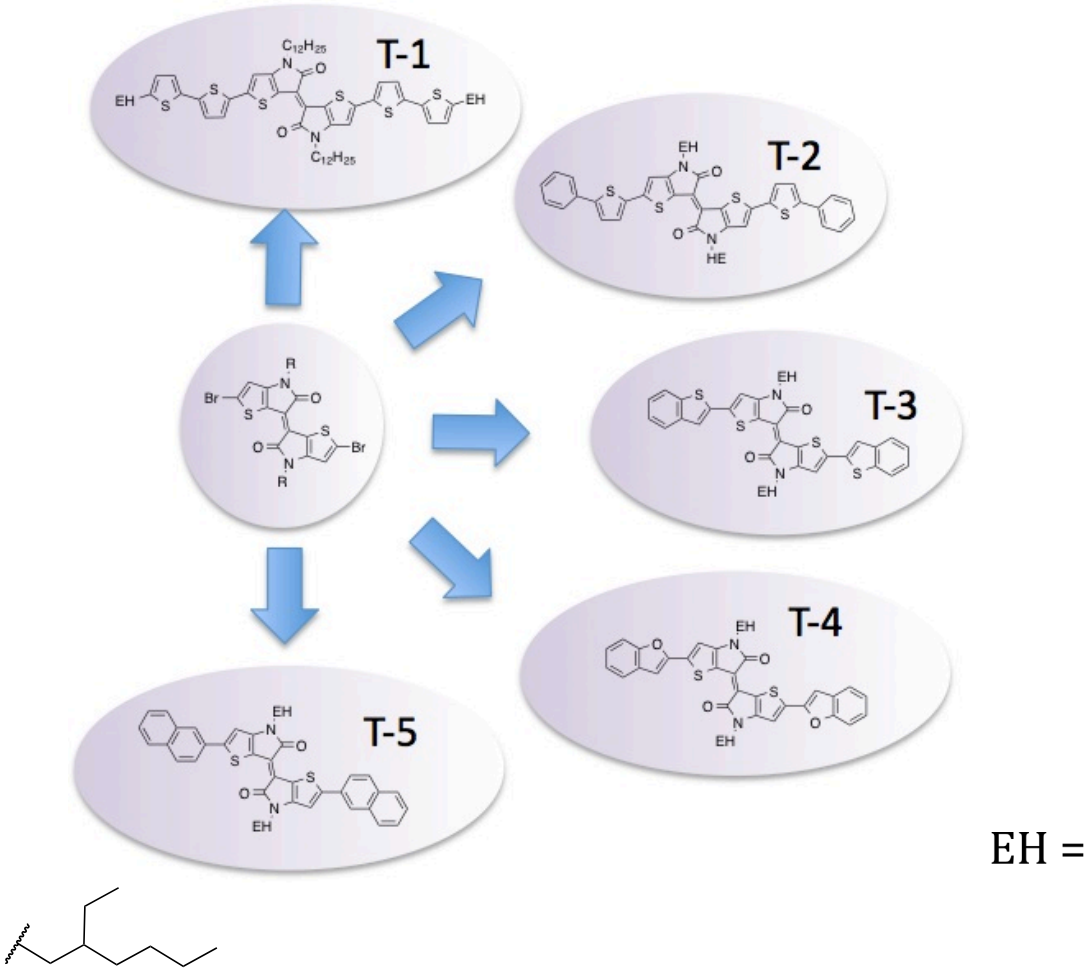

Figure 3.4 Small molecules made from TII unit

Donor-acceptor-donor type small molecules were synthesized by Stille coupling of the dibromoisoindigo with several different trimethylstannylarenes (see experimental section for details). The thiophene isoindigo unit was coupled to 5 different electron donor units of varying electron donating ability: 5'-octyl-2,2'-bithiophene, 2-phenylthiophene, benzothiophene, benzofuran, and naphthalene giving materials T-1 through T5 respectively. The molecular structure of the products were verified by NMR, and in some cases, matrix-assisted laser desorption ionization time-of-flight (MALDI-TOF) mass spectrometry. All products were soluble in chloroform, but poorly soluble in most other organic solvents, except for T-5 which dissolves well in toluene.

3.2 Results and Discussion:

Optical and electrochemical properties

All compounds possess strong visible light absorption in solution and thin films (fig. 3.5). T-2, T-3, and T-4 showed blue shifts of the absorption maximum in films relative to solution, while T-5 showed a 4-nm red shift and T-1 showed a large red shift from 730 to 854 nm. The blue shift in the absorption maxima is probably due to H-type aggregation in the solid state.[70] This behavior has been previously observed in certain diketopyrrolopyrrole (DPP) based donor-acceptor-donor small molecules.[71]

a)

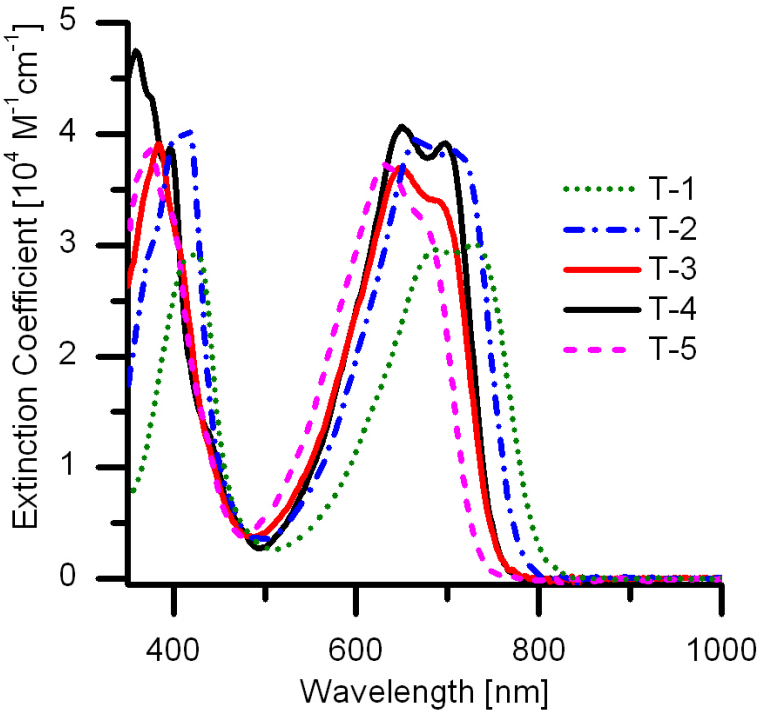

b)

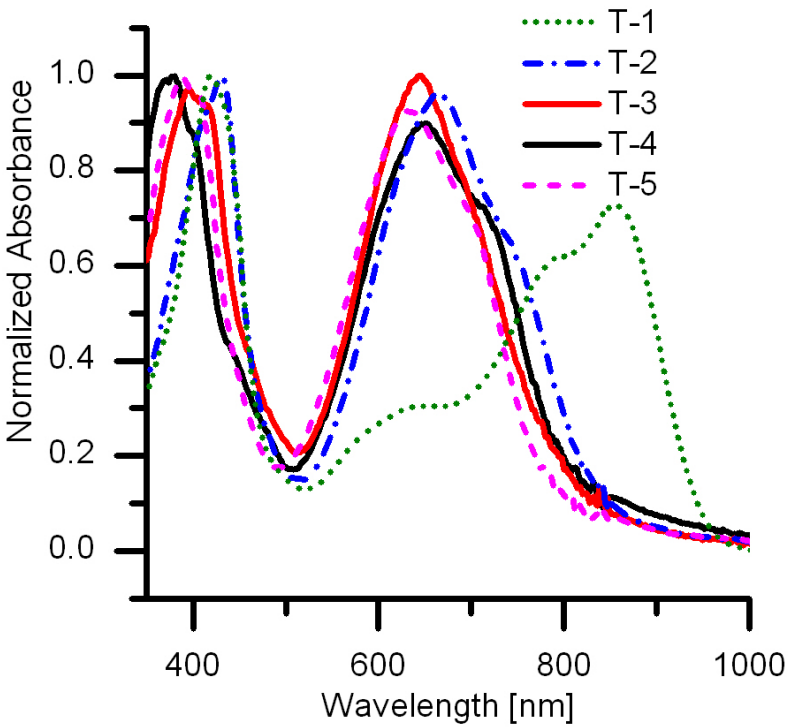

Figure 3.5 Absorption spectra of T-1 through T-5 small molecules a) solution extinction coefficients and b) Normalized thin film absorbance

H-aggregation may also explain the annealing behavior of bulk heterojunction films of TII(BFu)$_2$ and PC$_{71}$BM. The absorbtion peak shifts from 650 to 625 nm and the shoulder at 715 nm disappears upon annealing for 10 min at 110ºC (fig.). This also suggests that the H-aggregated structure is thermodynamically favored. Similar behavior also has been reported with alkylphenyl DPP based D-A-D molecules upon annealing.[72]

Table 3.1 Photophysical and electrochemical properties of TII small molecules

Material	Solution λ_{max} (nm)	Film λ_{max} (nm)	λ_{edge} (nm)	$E_{g.opt}$ (eV)	E_{HOMO} (eV)	E_{LUMO} (eV)	$E_{g,E.C.}$ (eV)
T-1	424, 686, 730	418, 854	960	1.29	-5.08	-3.63	1.45
T-2	416, 666, 710	432, 666	840	1.48	-5.11	-3.58	1.53
T-3	384, 648	396, 644	834	1.49	-5.21	-3.66	1.55
T-4	358, 650, 698	379, 651	840	1.48	-5.19	-3.74	1.45
T-5	374, 630	388, 634	806	1.54	-5.13	-3.57	1.56

TII(BiTh)$_2$ (T-1) shows clear J-type aggregation in films and likely has a different structure in the solid state due to its terminal alkyl chains and unbranched dodecyl side chains on the isoindigo unit. Straight dodecyl side chains might be responsible for the effect and could be tested with other donors, but solubility is expected to be poor without terminal side chains.

All of the molecules tested showed photoluminescence in solution, but none was detected in films in the regions studied (700 – 850 nm and 950 – 1200 nm) at an excitation wavelength of 650 nm. Photoluminescence spectra in solution are shown in figure 3.6

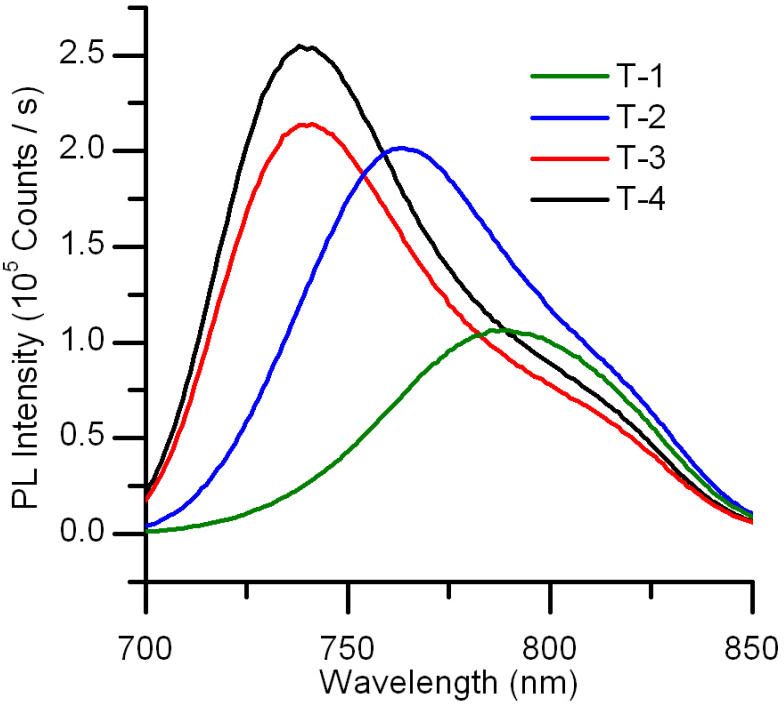

Figure 3.6 Photoluminescence spectra of T-1 through T-4

Frontier orbital energies were estimated by cyclic voltammetry (CV) of thin films on a platinum disk electrode with a 0.1 M tetrabutylammonium hexafluorophosphate electrolyte in acetonitrile. Benzofuran and benzothiophene as donors gave the deepest highest occupied molecular orbital (HOMO) energy levels at -5.19 and -5.21 eV, respectively based on the onset of the oxidation and reduction waves. The orbital energy level diagram showing energy levels for one TII polymer and the five small molecules discussed are shown in fig 3.7. The CV curves used to create the diagram are shown in fig. 3.8.

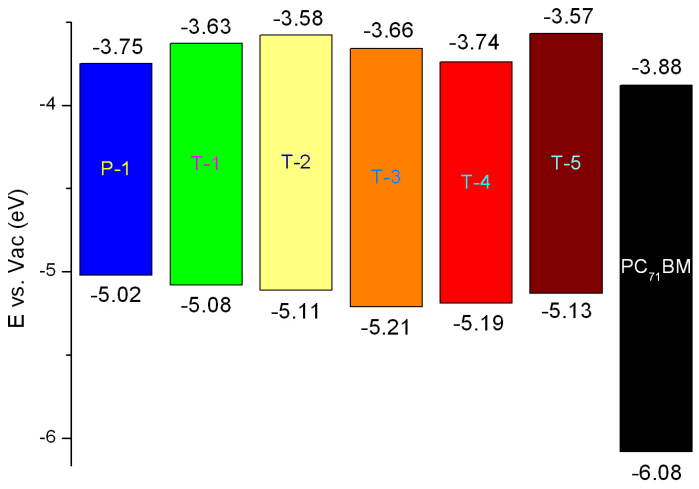

Figure 3.7 Energy levels of TII polymer and small molecule materials and $PC_{71}BM$ acceptor derived from cyclic voltammetry of thin films.

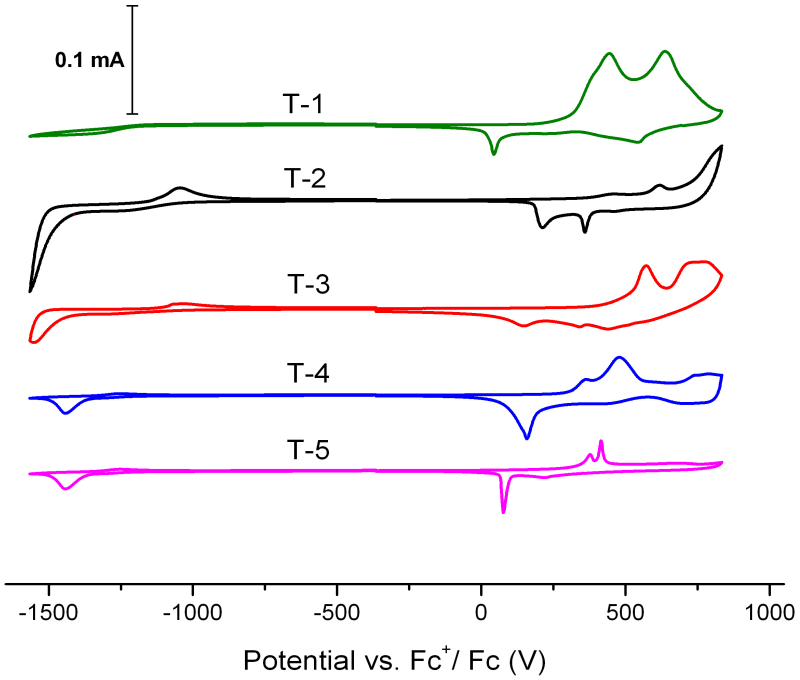

Fig 3.8 Cyclic voltammetry curves of small molecule films on a Pt disc in 0.1 M Bu_4NPF_6 solution in acetonitrile at 21ºC. Ag wire quasi-reference electrode was used and Fc^+ / Fc redox couple was used as an external standard.

3.3 Solar cell device performance

The polymer P-1 was tested using a regular device structure (ITO/PEDOT:PSS/Polymer:PCBM/Ca/Al) and 1,2-dichlorobenzene (DCB) as the solvent and 3% (v/v) 1,8-diiodooctane (DIO) as an additive to modify morphology. The results of device testing with and without adding DIO are shown in table 3.2. and figure 3.9. The addition of DIO caused a moderate increase in power conversion efficiency (PCE). Based on P-1's absorption spectrum, a much higher short circuit current (J_{SC}) would be expected. High-performance polymers often achieve currents higher than 75% of the theoretical maximum from solar irradiance (see fig 2.5) and based on this, a material with an absorbtion edge of 1000 nm should have a maximum current of 33 mA/cm^2, and 25 mA/cm^2 should be practically achievable. The best J_{SC} of 13 mA/cm^2 falls far short of this.

Table 3.2 Device performance of P-1:PCBM solar cell devices made with and without DIO additive.

Spin Speed	DIO (wt. %)	J_{SC} (mA/cm^2)	V_{OC} (V)	FF (%)	Max PCE (%)	Average PCE (%)
3000	0	13.0	0.40	42.3	2.21	2.13
3000	3	12.3	0.42	48.8	2.53	2.36

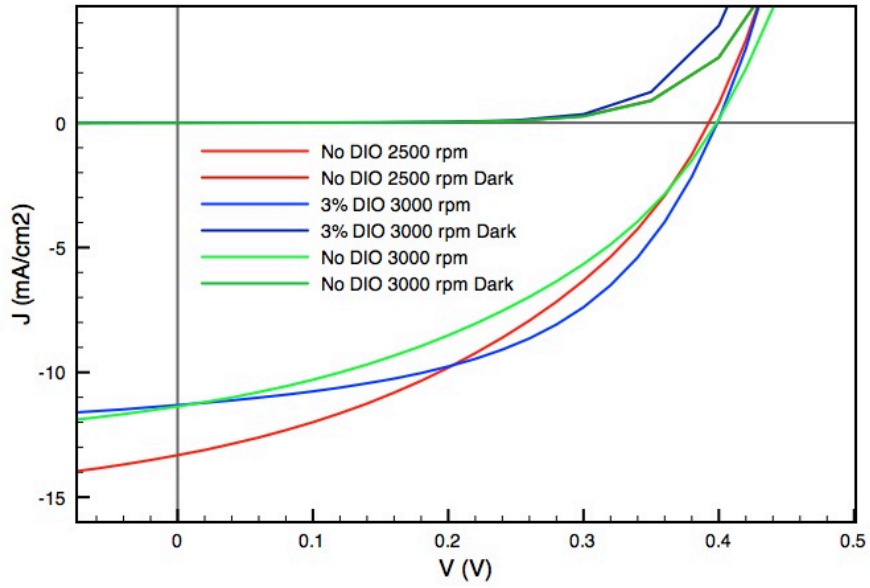

Figure 3.9: J-V curves for P-1 devices

The small molecules were also tested, each with a range of donor:acceptor blend ratios, but with the small molecule concentration kept constant at 20 mg/ml, except for T-3, for which the poor solubility necessitated a lower concentration of 10 mg/ml. The device structure used for these tests was: ITO/PEDOT/Small molecule:PC71BM/Ca/Al. The best performance for each of these materials is listed in table 3.3. The expected increasing open circuit voltage (V_{OC}) trend due to the lowering of HOMO level energy with decreasing donor strength was observed.

The gas-phase first ionization energies of the parent molecules from which the donor units were derived are shown in figure 3.10. These values correctly predict the progression of HOMO energy levels measured by CV except for T-3, and also predict the V_{OC} in solar cells, except forT-3, which had a lower V_{OC} than T-5. This may, however, be a result of device conditions being less than optimum for T-3 because of difficulties in preparing films due to poor solubility. The use of gas-phase ionization energies, which are available in databases[73] for a large number of molecules, to predict the effect of a

structural motif on photophysical properties and device performance could be a powerful tool for material design.

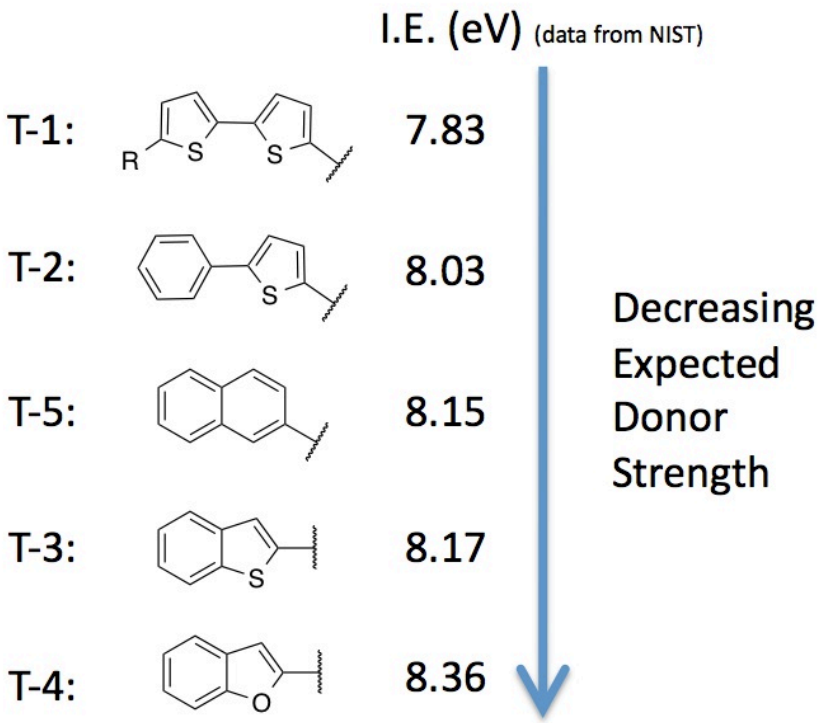

Figure 3.10 Gas phase ionization energy of heterocycle systems used as electron donors.

Table 3.3 Device performance of small molecule materials

Material	Voc (V)	Jsc (mA/cm^2)	FF (%)	Max PCE (%)	D:A Ratio	Annealing	Spin Speed (RPM)
T-1	0.55	4.29	40.2	0.94	1:0.8	120ºC 1 min	1200
T-2	0.55	4.98	44.8	1.22	2:1	100ºC 10 min	3500
T-3	0.61	2.67	45.2	0.73	2:1	100ºC 10 min	3500
T-4	0.72	8.67	51	3.18	3:2	100ºC 10 min	3500
T-5	0.65	6.79	42.7	1.88	3:2	100ºC 10 min	3500

V_2O_5 as an alternate anode buffer layer

In the initial device structure, PEDOT:PSS is used to improve the interface between the device active layer and ITO. PEDOT is a p-doped conductive polymer with

a work function of 5.1 eV.[74] It is heavily doped enough to make ohmic contact with ITO and its energy level position close to the HOMO level of many donor materials allows it to efficiently collect holes. Transition metal oxides are also often employed as buffer layers, and have the advantage of greater stability, better chemical compatibility with some materials due to lack of acidic poly(styrenesulfonic acid) (PSS),[2] and better energy level alignment. Vanadium pentoxide (V_2O_5) is an oxide material commonly used in organic electronics and has a work function of -5.3 to -5.6 eV depending on processing conditions.[75] This interlayer was tried in place of PEDOT with the highest performing material, T-4, to see if performance could be improved. Switching from PEDOT to V_2O_5 lead to an improvement in power conversion efficiency from 3.18% to 3.73% under the same processing conditions, mainly due to an increase in J_{SC}. The work function of V_2O_5 used in these devices should be around -5.3 eV for our processing conditions. The alignment of the Fermi level with the HOMO of T-4 is still good, but PEDOT should be acceptable as well.

Table 3.4 Performance of devices with V_2O_5 vs. PEDOT as an Interlayer

Interlayer	V_{OC} (V)	J_{SC} (mA/cm^2)	Fill Factor (%)	Max PCE (%)	Average
PEDOT	0.719	8.67	51.03	3.18	3.16
V_2O_5	0.717	9.96	52.2	3.73	3.64

Annealing effect

All materials tested showed increases in performance upon annealing. In T-4 devices, performance increased from 10 min of annealing at 100º C and less so at a higher temperature of 125º C. In order to investigate the origin of this effect, BHJ films of T-4 with PCBM were investigated with UV-Vis spectroscopy and transmission electron microscopy (TEM).

Table 3.5 Annealing effect on T-4 Devices with PEDOT interlayer

Annealing	V_{OC} (V)	J_{SC} (mA/cm^2)	Fill Factor (%)	Max PCE (%)	Average
None	0.783	2.93	28.18	0.65	0.60
100ºC	0.715	9.04	46.66	3.01	2.68
125ºC	0.708	7.38	48.52	2.54	2.34

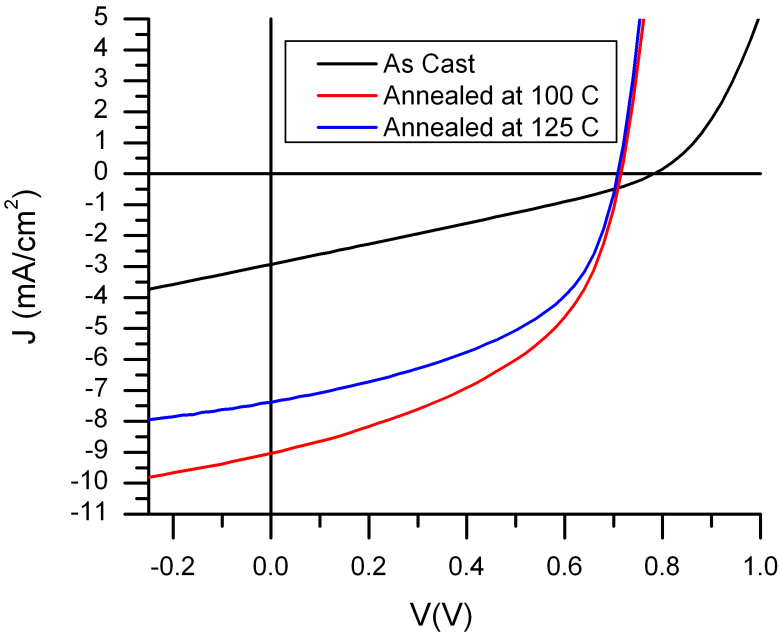

Figure 3.11 J-V curves for T-4 devices with annealing

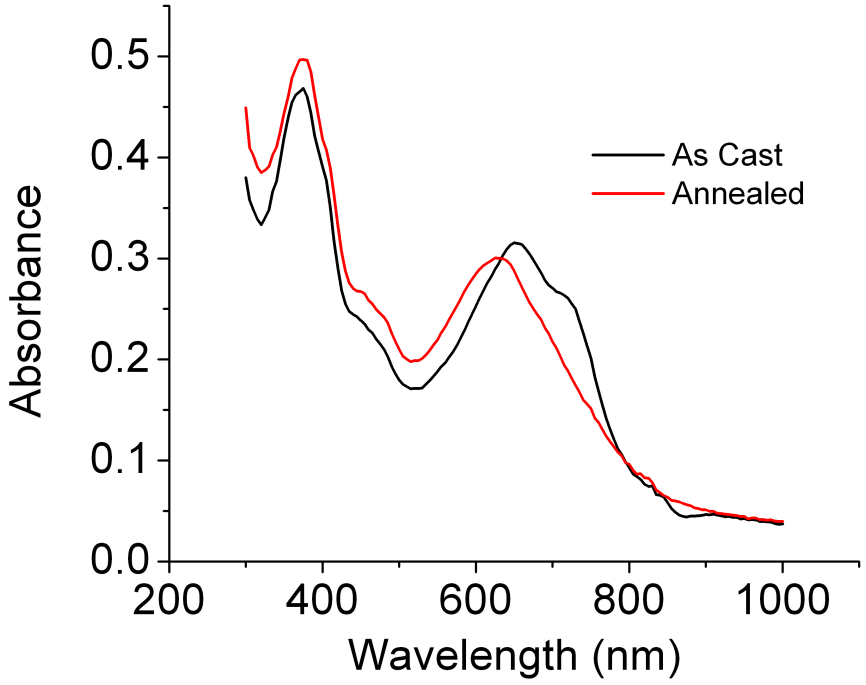

Figure 3.12 Annealing effect on T-4:$PC_{71}BM$ UV-Vis absorption

A pronounced blue shift of the absorption spectrum and a loss of the long wavelength absorption shoulder around 750 nm were found upon annealing. This is unusual, but not unheard of[72] in OPV materials, which more often show a red shift upon annealing as the process improves molecular packing and increases aggregation. Chromophores can have either a red-shift upon aggregation or a blue-shift depending on how they interact with each other. If there is a more favorable interaction energy in the excited state, then there will be a red-shift and if the interaction energy is unfavorable, there will be a blue shift. These kinds of aggregates are known as j-aggregates and h-aggregates respectively. The absorption energies in the excited state of an aggregated chromophore system often show both red-shifted and blue shifted bands ("j-band" and "h-band") relative to the chromophore in dilute solution. Both bands have been seen together in thin films of diketopyrrolopyrrole (DPP) based small molecules.[72] It seems

that a change in the relative intensity of the h and j-bands is responsible for the change in absorption spectrum of T-4. Its longest wavelength absorption peak in solution lies at 698 nm and its thin film spectrum has a peak at 651 nm (h-band) and shows a shoulder around 750 nm (possibly the j-band). In h-aggregate forming materials, the j-band absorption has very low oscillator strength, but this can be increased by disorder. It has been found computationally that imperfect molecular overlap in h-aggregates of terphenylene restores some oscillator strength to the j-band.[70] This may be the reason for the loss of the 750 nm absorption shoulder upon annealing, the increased order in the film reduces the residual j-band oscillator strength. H-aggregation is also consistent with the loss of fluorescence upon casting the molecules into films. H-aggregates typically lack strong fluorescence because excitons are formed in the h-band where light absorption is strong and then drop in energy to the j-band where the low oscillator strength means light emission is slow, and the excitons decay non-radiatively.

3.3 TEM Characterization

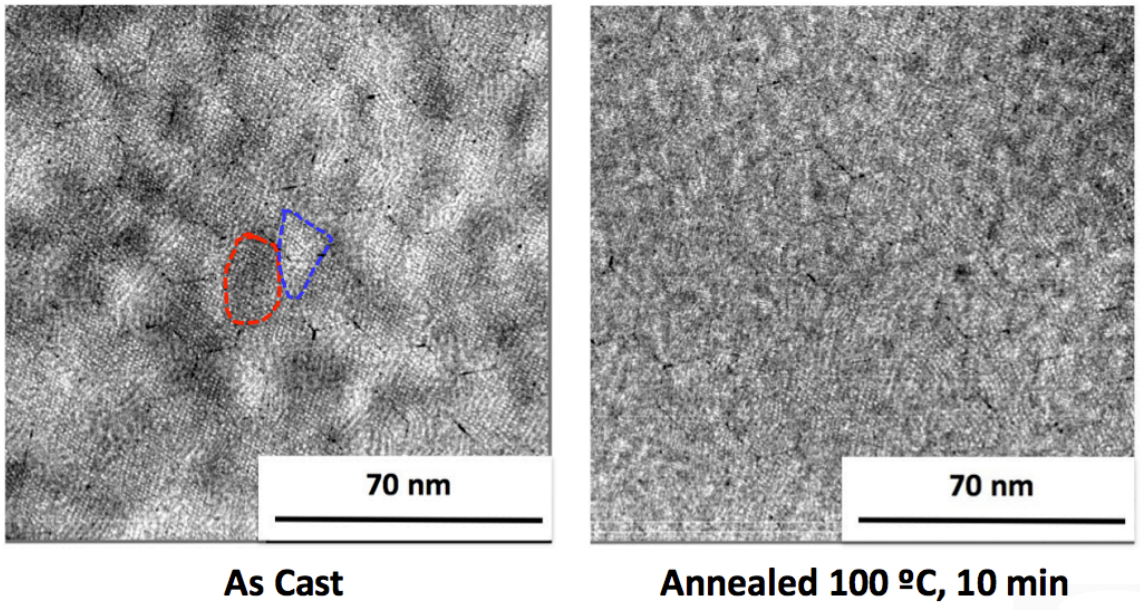

Figure 3.13 Annealing effect on T-4:PCBM films studied by TEM

In order to gain insight into the effects of annealing on the device bulk heterojunction morphology, T-2:PCBM and T-4:PCBM blends were examined with TEM. The results were somewhat surprising as the length scale of the light and dark features in the films were actually diminished in size upon annealing (*fig. 3.13*). The reason for this effect is unclear. The possibility of the film melting and resolidifying upon was investigated by measuring the melting point of T-4. It was found to be thermally stable enough to melt into a dark blue liquid and resolidify at 270ºC. As a side note, this suggests the possibility of melt-processing an organic semiconductor. Other possible explanations for the annealing behavior include increased solid-phase miscibility of the small molecule and PCBM at high temperatures followed by rapid phase separation upon cooling, and a phase change at high temperature and a return to the original phase by rapid nucleation and growth upon cooling.

T-2 films showed more typical behavior upon annealing, as the domain size was increased after annealing

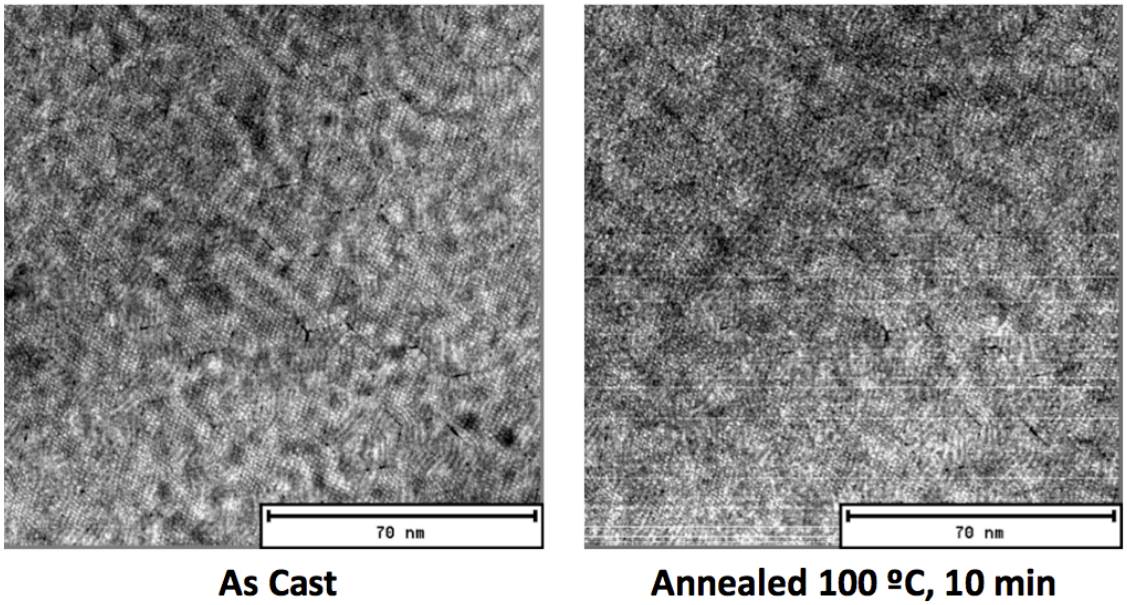

Figure 3.14 T-2 annealing effect on T-2:PCBM films studied by TEM

3.4 Device Characterization: Ideality Factor under Dark and Illuminated Conditions

In order to gain insight into the diode properties and recombination mechanisms in the devices, ideality factors were studied using dark current analysis and light intensity – open circuit voltage measurements. The diode ideality factor of a solar cell can be used to gain insight into the types of recombination mechanisms at work in the device. A value close to 1 can be derived for the case where bimolecular recombination is dominant. When trap-induced recombination becomes prevalent values closer to two are expected.[76]

The values obtained by the dark current and light intensity methods were not in agreement, as is often the case for organic solar cells.[76] The ideality factor *n* was obtained from the dark current-voltage data using the equation:

$$n = \left(\frac{kt}{q} \frac{\partial \ln J}{\partial V} \right)^{-1} \qquad 3.1$$

The calculated ideality factor varied greatly with voltage, indicating a poor fit to the one diode model, and the minimum ideality factor at 0.7 V was 3.0 (*fig. 3.15)* unexpectedly high values for dark ideality are often encountered in OPV devices and are not necessarily indicative of the recombination in the device. Using variable light intensity measurements is generally more reliable.

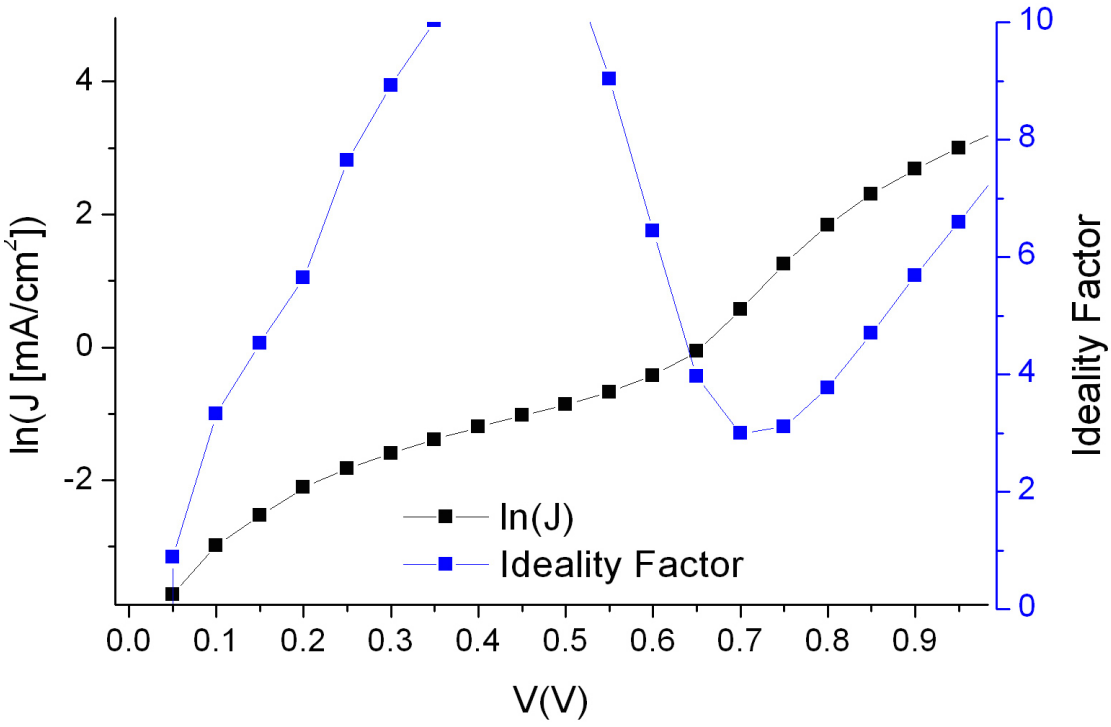

Figure 3.15: Ideality factor determined from the dark current voltage characteristics of a T – 4 device with PEDOT interlayer.

The ideality factor determined from the dark current was not taken to be a reliable indication of the recombination mechanisms since the series and shunt resistance can have a major impact on the measurements. In this case series and shunt resistance were 2.51 Ωcm^2 and 2.53 x 10^3 Ωcm^2, respectively. For a more reliable determination, the ideality factor under illumination was studied by measuring V_{OC} vs. light intensity. A PEDOT interlayer T-4 device was tested under a range of light intensities from 0.015 sun to 1 sun. The ideality factor was determined from the dependence of open circuit voltage on light intensity using the following equation from reference 61:

$$n = \frac{q}{kt}\frac{dV_{OC}}{d\ln(I)} \qquad 3.2$$

In equation 3.2 *I* is light intensity, and using a set of neutral density filters the light intensity of AM 1.5G from a solar simulator was adjusted. The intensities were measured using a silicon reference photodiode with each combination of filters in order to

The resulting ideality factor was 0.91. Since the value is close to 1, the recombination seems to be bimolecular in origin, with no indication of a trap-assisted mechanism. The plot used for the calculation is shown in figure 3.16. The data showed the expected linear relation of open circuit voltage on the logarithm of light intensity and are a good fit to equation 3.2

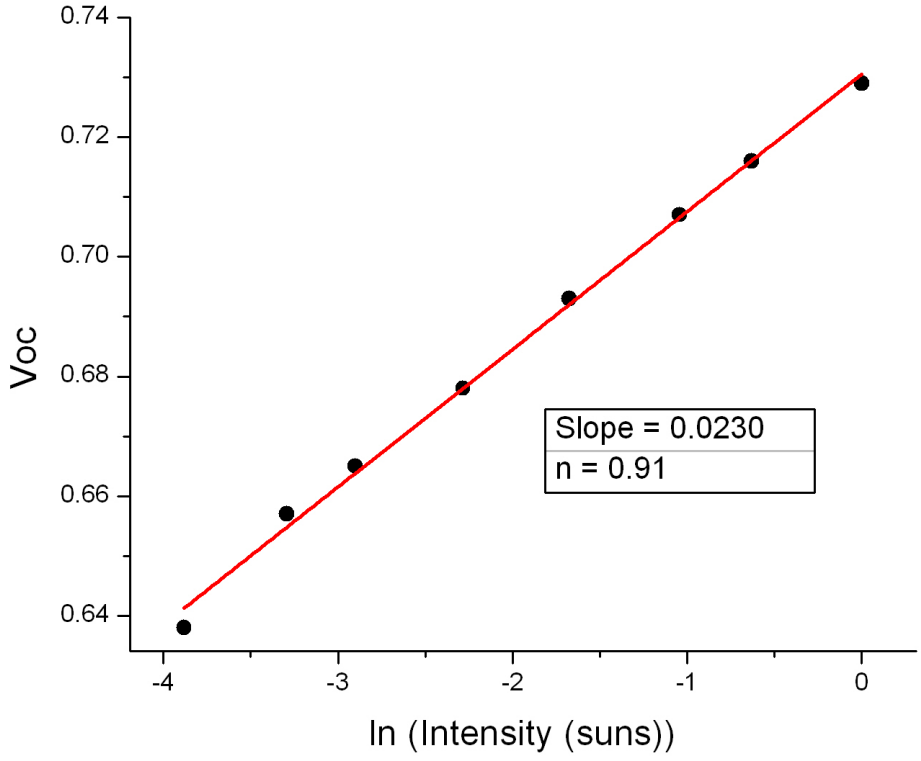

Figure 3.16 Ideality factor determination by the variable light intensity method

3.5 Experimental Details

Small Molecule Device Fabrication:

Solar cells with the structure ITO/PEDOT/Small molecule:PC71BM/Ca/Al were fabricated. Cells were fabricated on ITO-coated glass substrates, with sheet resistance of 15Ω/□. The pre-cleaned ITO substrates were treated with UV/ozone prior to the spin-coating of PEDOT-PSS solution (Baytron AI 4083) at 4000 rpm. Then, in a nitrogen atmosphere, a solution containing the donor material at a concentration of 15 mg/ml in chloroform and PCBM in the ratios shown in table 3.3 was dropped onto the already spinning substrates ("spin-drop casting" technique). Top electrodes were evaporated through a shadow mask, calcium followed by aluminum. Device areas were determined by the top electrode overlap with the ITO coated part of the glass, and were approximately 0.1 cm^2.

Synthesis

Dibrominated thiophene isoindigo, (*E*)-2,2'-dibromo-N,N'-bis(2-ethylhexyl)-[6,6'-bithieno[3,2-*b*]pyrrolylidene]-5,5'(4*H*,4'*H*)-dione), compound 1 was synthesized via a route similar to the reported methods,[63] but with some differences. The procedure used is as follows:

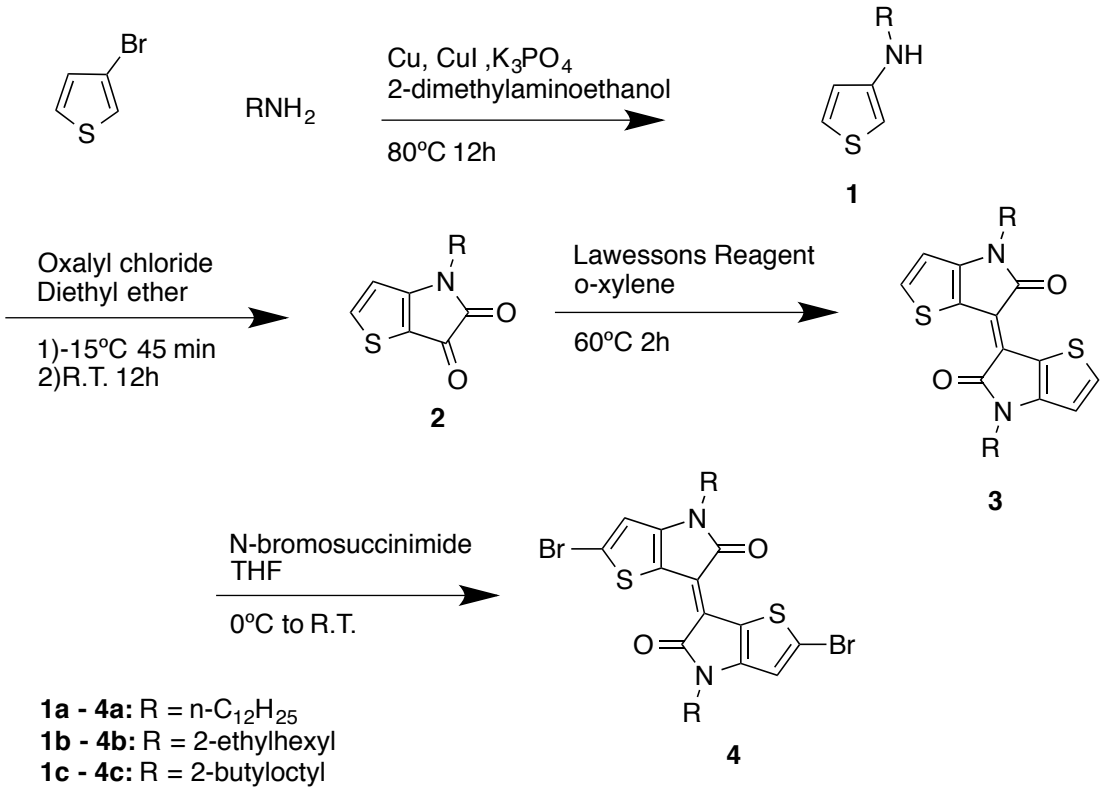

Figure 3.17 Synthesis of dibrominated isoindigo unit

3-(2-ethylhexylamino)thiophene (1b) 3-bromothiophene (3.75 ml, 40 mmol), 2-ethylhexylamine (9.82 ml, 60 mmol), 200 mesh copper metal powder (0.127 g, 2 mmol), copper (I) iodide (0.381 g, 2 mmol), and potassium carbonate (16.96 g, 80 mmol) were mixed with 60 ml of N,N-dimethylethanolamine in a round bottom flask. The atmosphere was replaced with argon by evacuating and refilling three times. The flask was then heated to 80 ºC in an oil bath and stirred for 12 hours. The product was detected by GCMS (M/Z = 211 amu). The reaction mixture was poured into 300 ml of water in a separatory funnel and extracted with two 100 ml portions of ether. The combined organic washings were washed with water (3 x 50 ml) and then brine (2 x 25 ml) and then the solvent evaporated in vacuum leaving a red colored oil. This residue was purified by column chromatography (100 -200 mesh silica, 2” diameter, 8” tall, eluent:

hexane, then 25% dichloromethane (DCM)) to yield the product as clear oil which rapidly turns red upon exposure to air. The product was used in the next step immediately (same day) without further purification. Yield (2.33 g, 27.5%)

4-(2-ethylhexyl)-4*H*-thieno[3,2-*b*]pyrrole-5,6-dione (2b). Compound 2a (2.33 g, 11 mmol) was dissolved in 70 ml of diethyl ether and added dropwise to a solution of oxalyl chloride (4.72 ml, 55 mmol) in 70 ml diethyl ether at -15 ºC over 45 min under argon and then stirred at room temperature for 3 h. The solvent and excess oxalyl chloride were then evaporated in vacuum and recovered. The residue was purified immediately by column chromatography (25% DCM in hexane to 60%) The product was recovered as a red-orange oil that can crystallize upon standing at room temperature. Yield 1.73 g, 59%.

(*E*)-4,4'-bis(2-ethylhexyl)-[6,6'-bithieno[3,2-*b*]pyrrolylidene]-5,5'(4*H*,4'*H*)-dione (3b). Compound 2b (1.73g, 6.52 mmol) was dissolved in o-xylene and Lawesson's reagent[77] (1.32g, 3.26 mmol) was added. The flask was flushed with argon and heated to 60 ºC for 2 hours. The solvent was then evaporated in vacuum and the residue was purified by silica gel column (33% DCM:hexane). The product was a dark purple solid. The yield was 0.803 g, (49 %).

(E)-2,2'-dibromo-4,4'-bis(2-ethylhexyl)-[6,6'-bithieno[3,2-b]pyrrolylidene]-5,5'(4H,4'H)-dione 4b. Compound 3b (0.564 g, 1.31 mmol) was dissolved in tetrahydrofuran (THF) (44 ml) and cooled to 0 ºC and protected from light. N-bromosuccinimide (NBS) (0.490 g, 2.75 mmol) was added in small portions with stirring. The reaction was stirred at room temperature overnight. The reaction mixture was then poured into 5% aqueous $Na_2S_2O_3$ solution (100 ml), and then extracted with

dichloromethane (2 x 50 ml). The DCM was evaporated and the residue was purified by column chromatography (SiO_2 100-200 mesh, 2" diameter x 16" high, 33% dichloromethane in hexane). The chromatography procedure was repeated once more to yield product which was pure by thin layer chromatography (TLC) and NMR and suitable for polymerizations or coupling with donor units for small molecules.

^{1}H NMR (300 MHz, $CDCl_3$) δ ppm 0.76 - 1.02 (m, 12 H) 1.11 - 1.47 (m, 16 H) 1.68 - 1.96 (m, 2 H) 3.62 (d, J=7.32 Hz, 4 H) 6.79 (s, 2H)

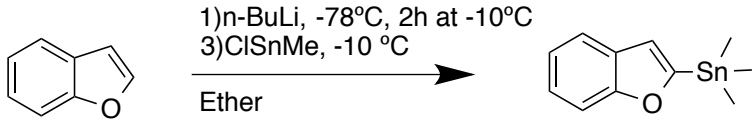

Figure 3.18 Synthesis of 5-trimethylstannyl-benzo[2,3-b]thiophene

Aryltrimethylstannanes (compounds 5-8) of 5'-(2-ethylhexyl)-2,-2'-bithiophene, benzofuran, benzothiophene, and 2-phenyl thiophene were synthesized by addition of butyllithium at -78 ºC in diethyl ether or THF and warming to -10 ºC for 2 h, then cooled back to -78 ºC before addition of trimethyltin chloride solution in THF. The reactions were then stirred at room temperature for 2 h. Purification was accomplished by pouring the reaction mixture into water and extracting with ether followed by vacuum distillation at < 1 torr.

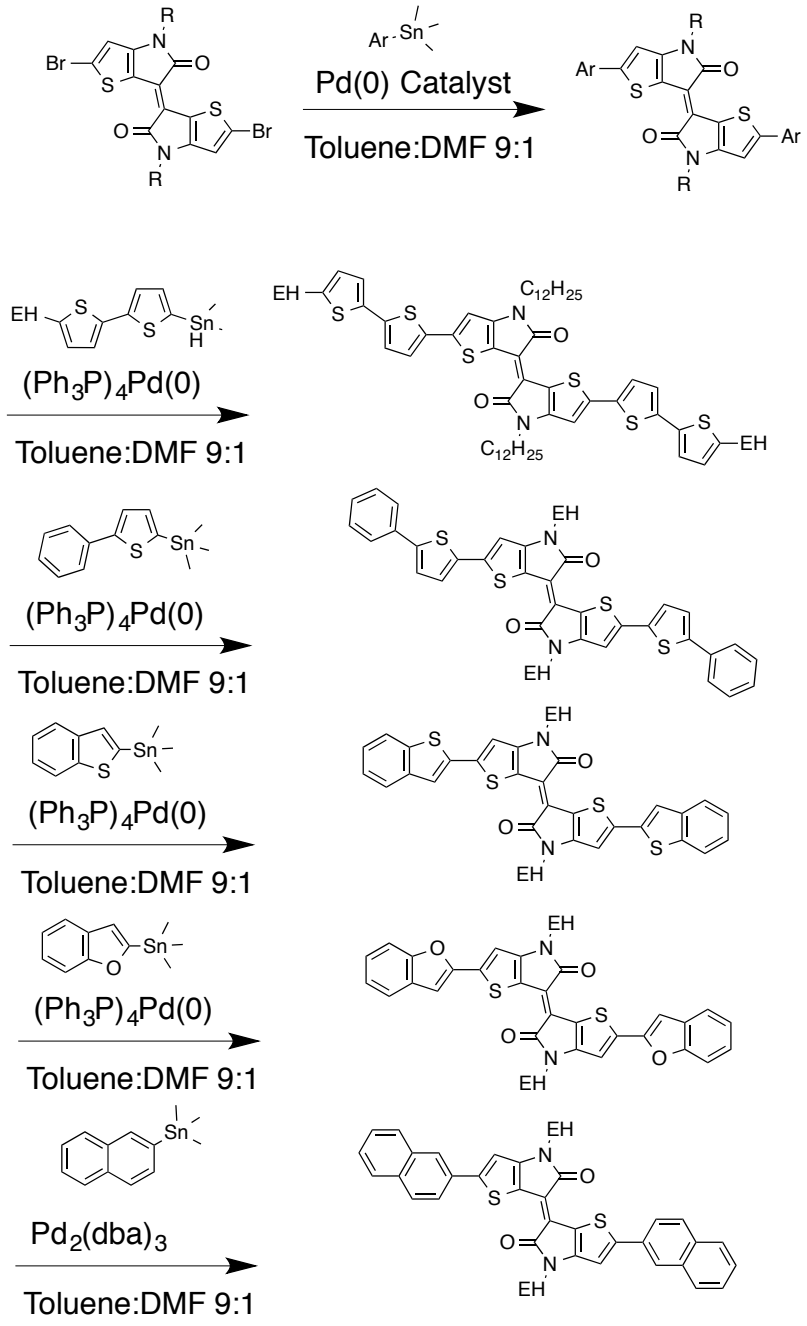

Figure 3.19 Coupling reactions to yield molecules T-1 through T-5

Coupling reactions to yield compounds T-1 through T4 were conducted in 9:1 toluene:DMF using tetrakis-triphenylphosphinepalladium(0) ($Ph_3P_4Pd(0)$) as catalyst (*fig 3.19*). In a typical reaction for T-4, 0.2 mmol of 1, 0.5 mmol of aryltrialkylstannane and 5mg of $Ph_3P_4Pd(0)$ were put into a flask and the atmosphere was replaced with argon.

3.6 ml of toluene and 0.4 ml of DMF (both degassed by bubbling with argon for 20+ min) were injected and the reaction was heated to reflux overnight. After cooling to room temperature, black crystals formed, which were collected by filtration and washed with hexanes and methanol. These were dissolved in dichloromethane and evaporated onto silica gel. This was loaded onto an 18” tall by 2” diameter silica column and eluted with 20% DCM in hexane, which was increased to 30-35% to cause the product to elute. This chromatography procedure was repeated and then the products were crystallized from toluene by dissolving in a minimum of toluene at reflux and allowed to slowly cool to room temperature in a cotton-insulated box. The resulting black crystals with a reddish luster were collected by filtration and dried in vacuum.

The reaction for compound T-5 was conducted in 9:1 toluene:DMF using tris-dibenzylidineacetone dipalladium (Pd_2dba_3) as catalyst(*fig. 3.19*). In a typical reaction for T-5, 0.2 mmol of 1, 0.5 mmol of aryltrialkylstannane and 5 mg of Pd_2dba_3 were put into a flask and the atmosphere was replaced with argon. 3.6 ml of toluene and 0.4 ml of DMF (both degassed by bubbling with argon for 20+ min) were injected and the reaction was heated to reflux overnight. After cooling to room temperature, black crystals formed, which were collected by filtration and washed with hexanes and methanol. These were dissolved in dichloromethane and evaporated onto silica gel. This was loaded onto an 18” tall by 2” diameter silica column and eluted with 30% DCM in hexane, which was increased to 35% to cause the product to elute. The procedure was repeated one more time and then the product was crystallized from ethyl acetate by dissolving in a minimum of ethyl acetate at reflux and allowed to slowly cool to room temperature in a cotton-insulated box. The resulting black crystals with a reddish luster were collected by filtration and dried in vacuum.

NMR Spectroscopy Data:

T-1: ^{1}H NMR (300MHz, CDCl3): δ ppm0.82-0.98(m,21H)1.23-1.39 (m,54H) 1.56 (s,5H) 1.65-1.79 (m,4H) 2.74 (d, J=6.59Hz,4H) 3.78 (s,4H) 6.67 (d, J=3.48Hz,2H) 6.76(s,2H) 6.98 (d, J=3.48Hz,2H) 7.01(d, J=3.84Hz,2H)7.21(s,1H)

T-2: ^{1}H NMR (300MHz,$CDCl_3$)δppm 0.86-0.99 (m,12H), 1.28-1.44 (m,16H), 1.56 (s,2H), 2.36 (s,2H), 3.68 (s,1H), 3.70(d, J=7.50 Hz, 3 H), 6.80 (s, 2 H), 7.13 - 7.20 (m, 2 H), 7.23 - 7.34 (m, 9 H), 7.36 - 7.42 (m, 4 H), 7.57 - 7.63 (m, 4 H).

T-3: ^{1}H NMR (300 MHz, $CDCl_3$) δ ppm 0.75 - 1.04 (m, 12 H) 1.20 - 1.50 (m, 16 H) 1.77 - 1.96 (m, 2 H) 3.54 - 3.79 (m, 4 H) 6.87 (s, 2 H) 7.29 - 7.44 (m, 4 H) 7.58 (s, 2 H) 7.67 - 7.82 (m, 4 H)

T-4: 1H NMR (300 MHz, $CDCl_3$) δ ppm 0.82 - 1.03 (m, 12 H) 1.21 - 1.51 (m, 16 H) 1.78 - 2.00 (m, 2 H) 3.71 (d, J=7.50 Hz, 4 H) 6.95 - 7.08 (m, 4 H) 7.19 - 7.36 (m, 5 H) 7.42 - 7.50 (m, 2 H) 7.51 - 7.60 (m, 2 H)

T-5:^{1}H NMR (300 MHz, $CDCl_3$) δ ppm 0.71 - 1.07 (m, 12 H) 1.19 - 1.54 (m, 16 H) 1.81 - 1.99 (m, 2 H) 3.52 - 3.85 (m, 4 H) 7.04 (s, 2 H) 7.40 - 7.63 (m, 4 H) 7.68 - 7.97 (m, 8 H) 8.19 (s, 2 H)

Chapter 4: Development of the 5-acetyl-4*H*-cyclopenta[*c*]thiophene-4,6(5*H*)-dione (ACT) monomer unit for conjugated polymers

4.1 Introduction

One of the challenges in application of conjugated polymers to any device is processing. Conjugated polymers are often difficult to process because of their limited solubility and inability to melt before decomposition. The lack of solubility results from strong attractive intermolecular interactions between π orbitals. Several approaches have been used to overcome this. Dissolving the polymer can be avoided by electropolymerization onto a substrate,[78] or by preparing suspensions of small particles,[79] or the polymers may be made soluble by adding alkyl side chains that have favorable interactions with solvents,[80] or a large counterion may be used to render a doped polymer soluble as with polyaniline (as partially oxidized emeraldine base), which can form a salt with p-dodecylbenzenesulfonic acid, which is soluble in the organic solvent m-cresol.[49]

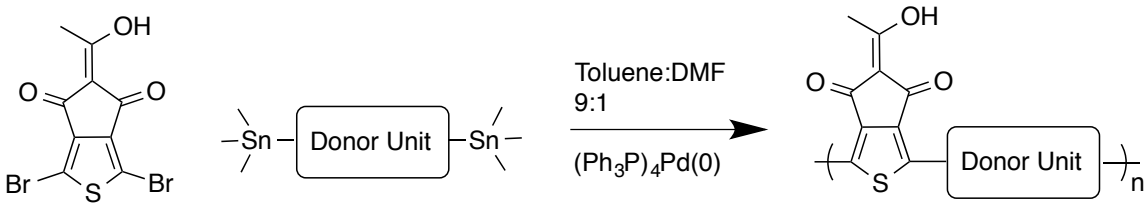

Figure 4.1 Synthesis of conjugated polymers based on the ACT unit

In this chapter I will discuss the synthesis of two copolymers bearing the acidic 5-acetyl-4*H*-cyclopenta[*c*]thiophene-4,6(5*H*)-dione (ACT) unit, which can be rendered soluble in organic solvents by polyelectrolyte salt formation with trialkylamine bases. The resulting solutions are also highly florescent, while the neutral polymer is not. As little as 1.5 molar equivalents of triethylamine added per acid unit is enough for one copolymer to be soluble to more than 10 g/l. The salt formation is reversible by annealing films of the polymer when a volatile amine is used. This gives solvent-resistant films of semiconducting polymer. The monomer unit, compound 7, is insoluble in water, but dissolves in 40 g/l sodium bicarbonate solution as a result of salt formation indicating that the p*Ka* is below 8. Enolized five membered ring triketones investigated in literature have been found to have p*Ka* as low as 3.1 for aliphatic compounds.[81]

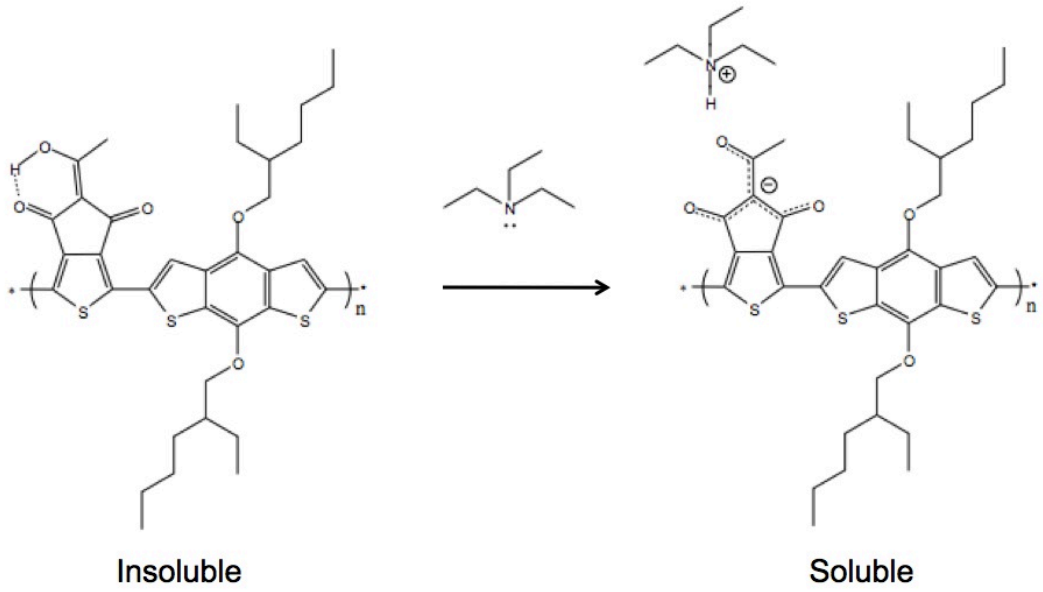

Figure 4.2 Deprotonation of ACT-1 polymer by triethylamine

Polymers with amine-induced solubility could be useful in fabricating multi-layered organic electronic devices like tandem solar cells or organic light emitting diodes because of the resistance of the films to solvents without amines. This will prevent coating of other polymers from dissolving the layer underneath. This represents a new type of orthogonal solvent processing approach, where solubility in moderate polarity solvents like chloroform and dichlorobenzene can be controlled by deprotonation of an acidic unit in the polymer chain. Conjugated polyelectrolytes typically show solubility in polar solvents, but combining alkyl chains with the ACT ionic groups leads to good organic solubility.

4.2 Synthesis

The synthesis for the new monomer was developed based on an alternative way to prepare 2-acetylindanedione that was reported in 1964.[82] . The method was adopted after attempts to prepare related compounds by Claisen condensations of dimethyl 2,4-dibromothiophene-3,4-dicarboxylate with ethyl acetate, dimethyl malonate, and acetylacetone were unsuccessful.

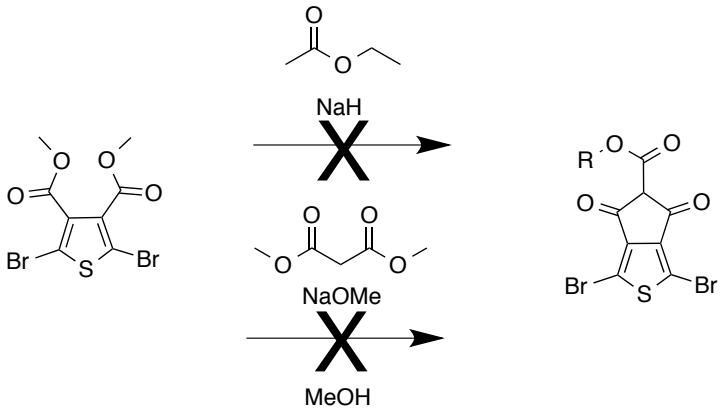

Figure 4.3 Attempts to prepare alkyl 5-carboxy-4*H*-cyclopenta[*c*]thiophene-4,6(5*H*)-dione via Claisen condensation.

The reaction that was successful in producing the target ACT monomer was based on acylation of isopropenyl acetate with 2,5-dibromothiophene-3,4-dicarboxylic anhydride in 1,1,2,2-tetrachloroethane. The reaction likely occurs by initial $AlCl_3$ - catalyzed Friedel-Crafts acylation of the alkene in isopropenyl acetate followed by transfer of the acetate group via intermolecular reaction of an intermediate which can be viewed as a vinylogous acid anhydride. Another Friedel-Crafts acylation closes the ring to yield the final product as shown in *figure 4.4.*

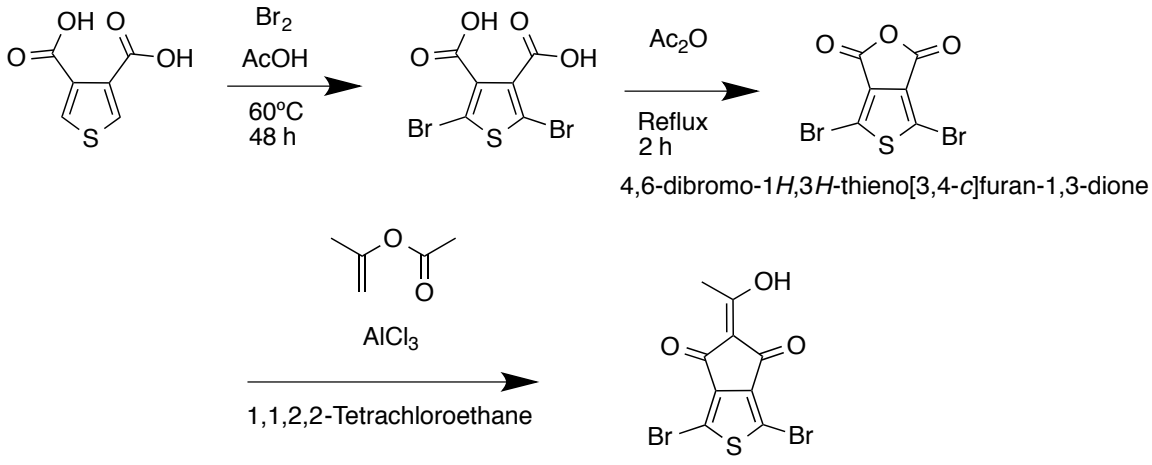

Figure 4.4 Successful route for preparing ACT monomer.

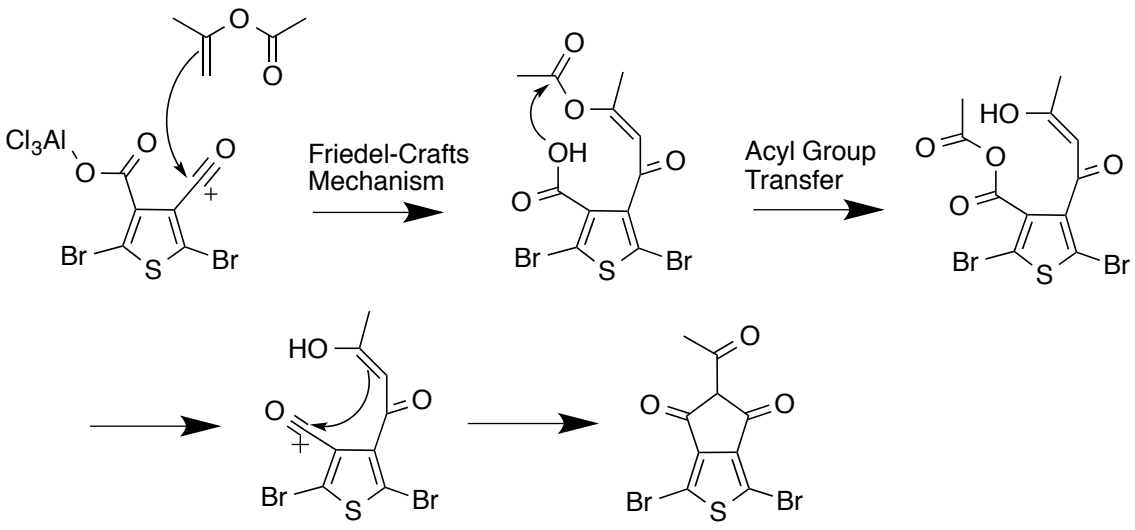

Figure 4.5 Abbreviated proposed mechanism for the final step in formation of the ACT monomer.

4.3 Investigation of Tautomerism in the ACT Monomer

The final product is expected to exist as several tautomer forms with the acidic proton in various positions on the molecule. The nominal tautomer form convention for 2-acetyl-1,3-cyclopentadiones is structure 1 (*figure 4.6*), however, the closest analogue in literature, 2-aceyl indanedione is expected to exist mainly in a structure similar to 2 based on DFT calculations.[4] Structure 2 is likely the most stable tautomer, but this has not been conclusively determined as of this writing. Structure 1 can be ruled out as a dominant tautomer based on ^{13}C NMR and fluorescence data.

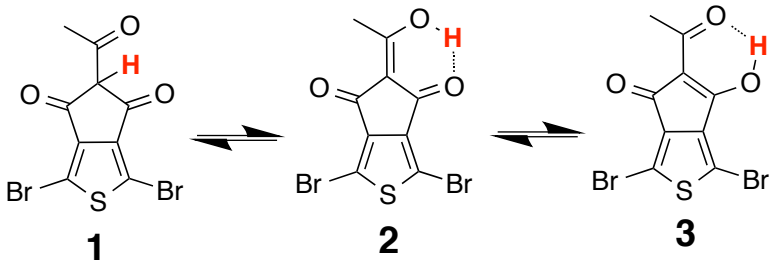

Figure 4.6 Tautomer forms of ACT monomer

The carbon 13 NMR spectrum in deuterated chloroform of the compound shows 9 distinct peaks, one for each carbon atom, which indicates that there are no chemically equivalent carbons in the structure. Structure 1 should show only 6 peaks due to symmetry of the carbonyl carbon atoms and the 3 and 4 carbons and 2 and 5 carbons on the thiophene ring. This is evidence for the predominance of one of the asymmetric structures 2 or 3.

Some 2-acetyl-1,3-cyclopentanediones are known to exhibit excited state electron transfer in solution.[4] This occurs because the energetically-preferred tautomer form is different in the excited state than in the ground state, and the proton is held in an intramolecular hydrogen bond, which places it close to the other oxygen atom, facilitating rapid transfer. A consequence of this is that florescent emission occurs mainly through a different tautomer than absorbtion. The excited state preferred tautomer has a lower energy gap and thus emits at a much longer wavelength, leading to a very large Stokes shift as can be seen in *figure 4.7*. Thus Stokes shift can be used as an indication of this kind of tautomerism.

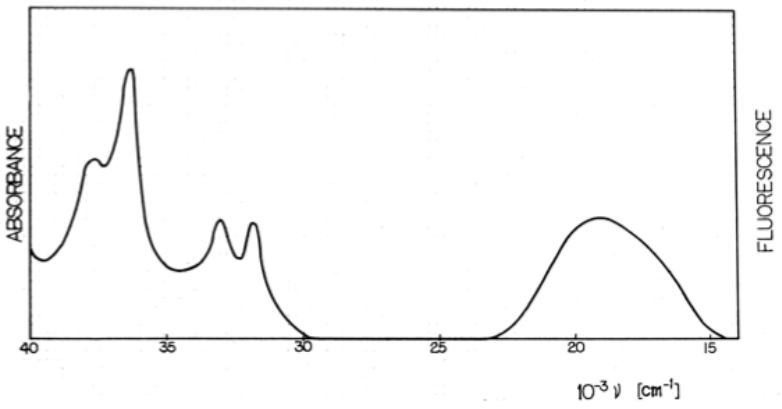

Figure 4.7 2-Acetylindanedione absorbtion and fluorescence in cyclohexane solution. Adapted from Enchev et. al.[4]

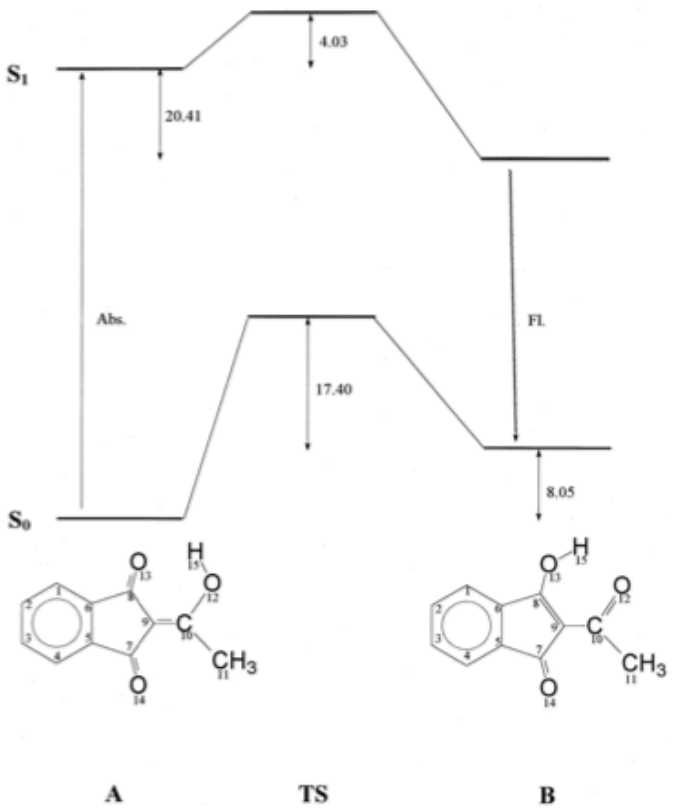

Figure 4.8 2-Acetylindanedione energy levels. Differences shown in kcal/mol. Adapted from Enchev et. al.[4]

The ACT monomer shows strong evidence for excited state intermolecular proton transfer similar to 2-acetylindanedione. The fluorescence and absorption spectra in dilute chloroform solution show a large Stokes shift. This Stokes shift is drastically reduced when the solvent is changed to dimethylsulfoxide (DMSO). The DMSO is a hydrogen bond donor solvent and likely disrupts the intramolecular hydrogen bond and inhibits the proton transfer.[83] The presence of this effect strongly suggests that the predominate form is one of the structures with an intramolecular hydrogen bond (2 or 3) thus providing further evidence for one of these structures as the main tautomer.

Structure number 2 will be used to represent the ACT monomer in this thesis, but it should be noted that structure 3 cannot be ruled out.

The monomer is clearly an acidic molecule. The material can be dissolved in diethyl ether and can be extracted from this organic solution into aqueous, half-saturated sodium bicarbonate solution. Adding HCl to acidify the solution causes the product to precipitate and it can be filtered of extracted with additional ether. This procedure is a very convenient way to purify the product, which leaves behind many of the impurities including a deep green truxenone-like self-condensation product that is non-acidic. The acidity of tautomers 2 and 3 can be rationalized structurally by thinking of them as vinylogous carboxylic acids (acids where the the carbonyl group and OH group are separated by a vinyl group whose conjugation allows for the carbonyl group to still stabilize the deprotonated form of the OH group).

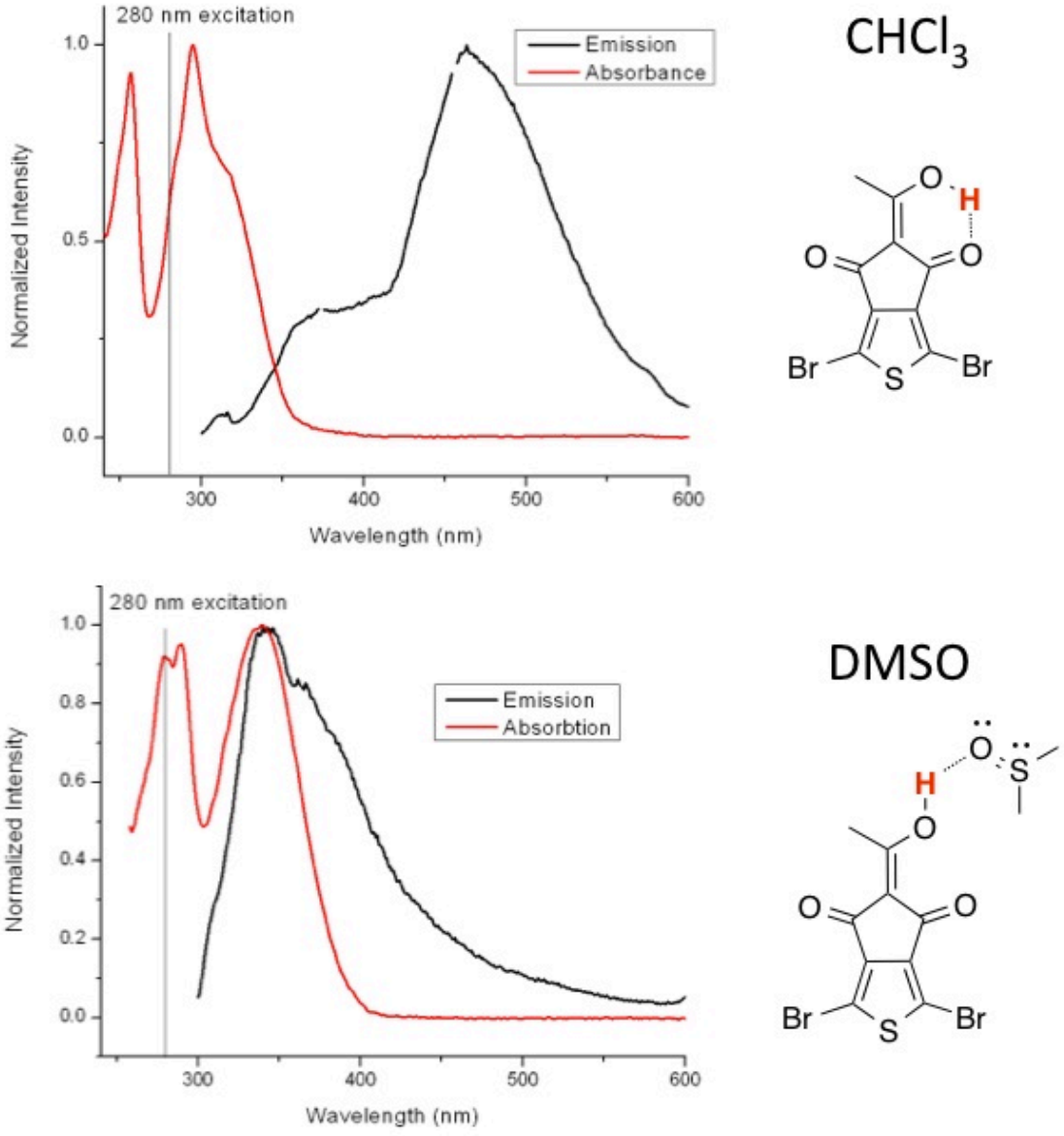

Figure 4.7 Absorption and fluorescence evidence for excited state intramolecular proton transfer in chloroform and disruption of hydrogen bonding by DMSO.

4.4 Polymer synthesis

Two polymer materials were prepared from the dibromide monomer via Stille coupling with two bistrimethylstannyl arenes. The first material, ACT-1, was made by

copolymerizing with the commonly used dialkoxy benzodithiophene unit. The presence of the alkyl chains on this unit was not enough to give this polymer solubility in organic solvents. The polymerization was done at various lengths of time. The first time the procedure was done, precipitation was observed after 6 hours of polymerization and the reaction was immediately stopped. Polymer from this batch showed some solubility in organic solvents such as chloroform without any other additives. In later experiments, the polymerization time was increased from 6 h to 13 h and then to 20 h. 13 h and 20 h batches showed almost no solubility in pure organic solvents, but the 13 h polymerized material could be rendered soluble by addition of organic amines or slightly soluble (~0.1% w/v) by the addition of 10% methanol in chloroform.

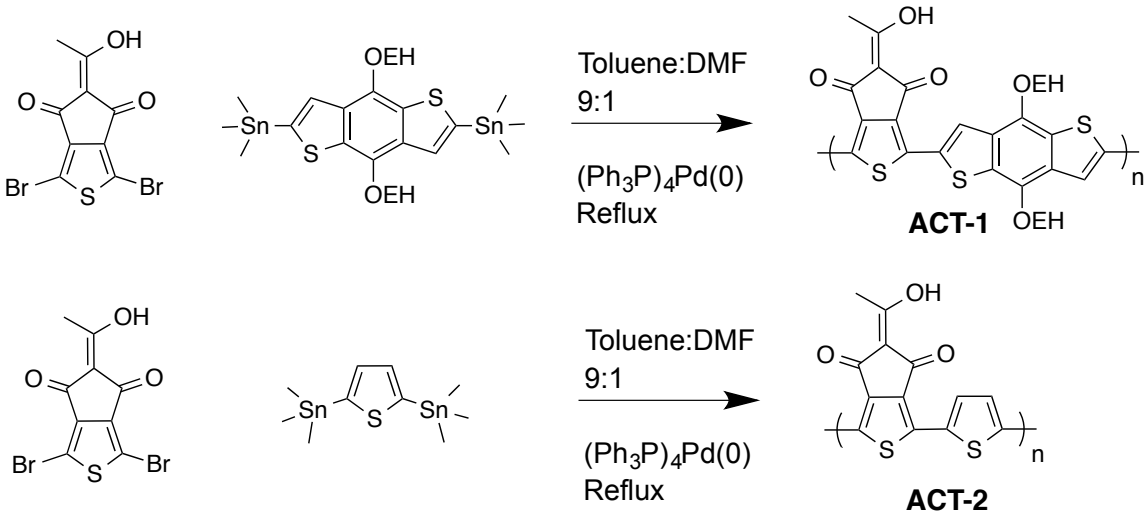

Figure 4.8 Synthesis of ACT polymer materials.

The second polymer was synthesized in order to see weather a polymer without alkyl side chains could be rendered soluble by deprotonation of the acidic ACT unit. Unsubstituted thiophene was chosen as a co-monomer and the reaction was kept at reflux for 13 hours.

The resulting polymer precipitated from the toluene:DMF reaction mixture and was found to be insoluable in DCB, with only a small amount dissolving to form a brownish solution when up to 2.5 molar equivalents of triethylamine or tributylamine were added with respect to the repeat unit. It was found to be quite soluble in dimethylsulfoxide (DMSO) with 1 % v/v triethylamine added and slightly soluble (<1% w/v) in methanol with 1 % triethylamine and has trace solubility in ammonia water (fluorescence observable, but solution appears colorless)

4.5 Solubility

The effect of addition of organic amines to ACT-1 was studied. 10 mg of the polymer was found to be mostly insoluble in 1 ml of 1,2-dichlorobenzene (DCB) leading to only a pale purple solution with black particles suspended. Addition of 10 µl (1% of solvent volume) of triethylamine lead to complete dissolution of the polymer giving a deep orange, highly fluorescent solution. This effect was observed in chloroform solution as well. Other amines, tributylamine and 1-methylpiperidine also showed the same effect. Solutions prepared from chloroform and dichlorobenzene could be spin coated to give blue colored films. The resulting films cannot be washed away by rinsing with chloroform or DCB.

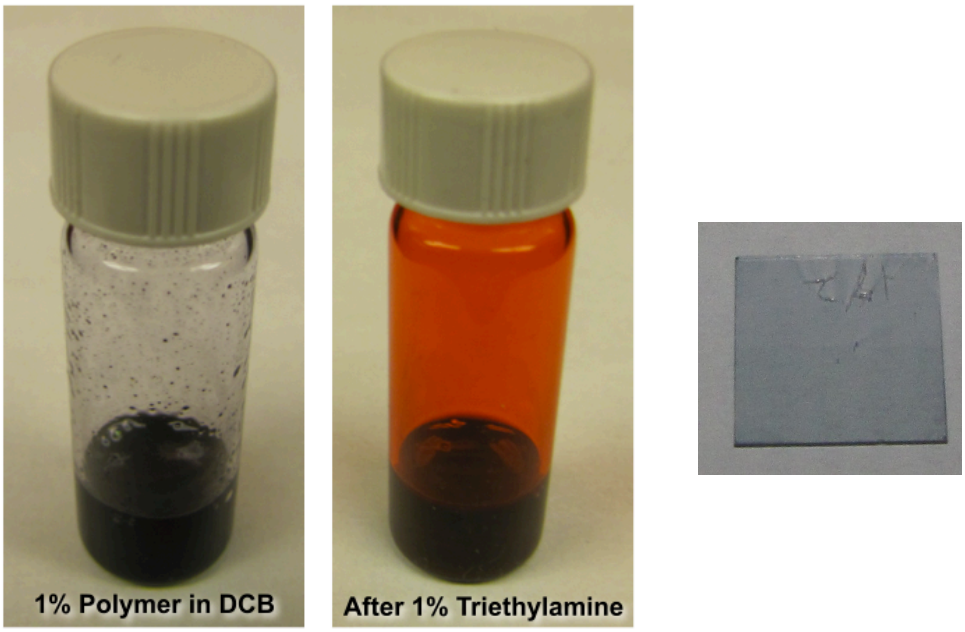

Figure 4.9 ACT – Polymer in DCB with and without triethylamine and a film spin-coated from the solution.

This approach shows promise for coating films for multilayer devices. So far, the solar cell devices, which were made using PCBM as the acceptor, have poor performance, with an open circuit voltage of 0.47 V, short circuit photocurrents of 0.61 mA / cm^2, and fill factors below 25% due to s-curve shaped I-V curves, which are an indication of a poor interface.[84] The performance of these cells might be improved with an inverted structure, that does not use a reactive metal cathode. An acceptor material with similar solubility properties might also be more suitable for fabricating devices with ACT-1. The initial device data at least shows a proof of concept.

ACT-2 also was tested for solubility; it showed limited solubility in chloroform and dichlorobenzene solutions with triethylamine. Methanol with 1 % v/v triethylamine can partially dissolve the polymer when 10 mg/ml polymer is combined with the solvents.

The only solvent system found to fully dissolve ACT-2 was DMSO with 1% v/v of triethylamine or tributylamine, which can form 1 % w/v solutions. This solution was not capable of good making films by spin coating. Only porous brown crusts were formed. The likely reason for this was that the amine evaporated more quickly than the DMSO, causing the polymer to precipitate before the solvent dried. This might be overcome in future work by using an amine with similar vapor pressure to DMSO. The films could be characterized by cyclic voltammetry by coating onto a platinum disc electrode (*fig. 4.10*) the HOMO and LUMO levels were found to be -5.4 eV and -3.8 eV based on the ferrocenium / ferrocene couple as an external standard.

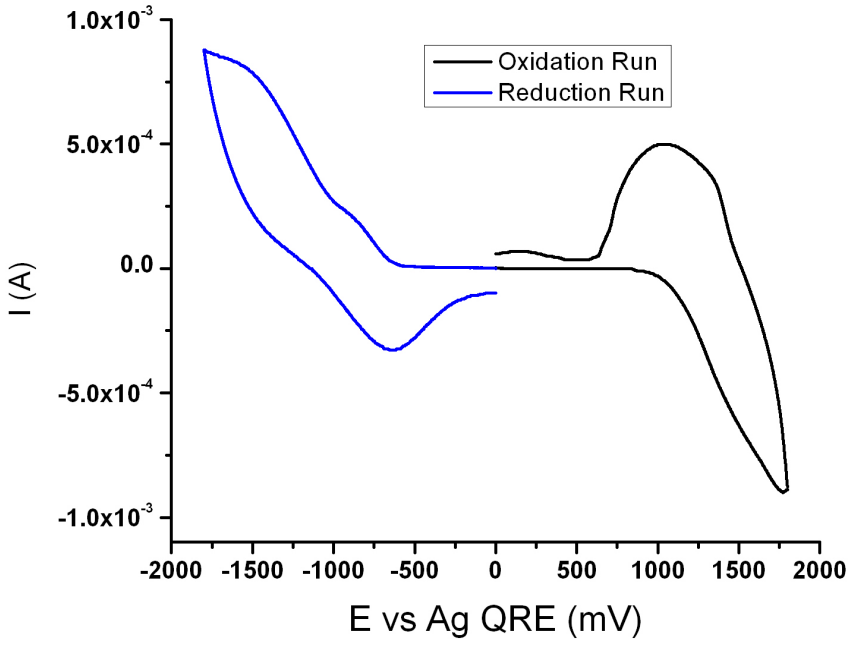

Figure 4.10 ACT-2 thin film cyclic voltammetry (CV) in acetonitrile / 0.1M Bu_4NPF_6 at 21ºC. Pt disk working electrode, silver wire quasi-reference electrode. Ferrocenium / ferrocene couple used as external standard.

4.6: Fluorescence quenching of ACT-2 polymer by metal ions

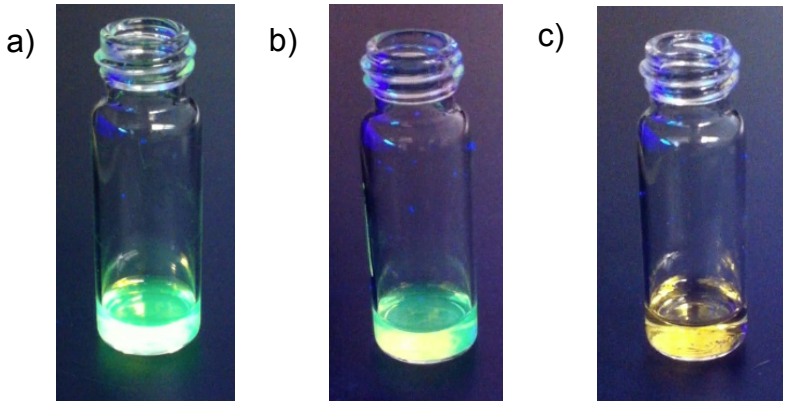

Figure 4.11 Fluorescence of ACT-2 polymer solution in methanol with a) No $Ni(OAc)_2$ b) 17 μM $Ni(OAc)_2$ and c) 29 μM $Ni(OAc)_2$

Solutions of ACT-2 in methanol with 1 % v/v triethylamine were highly fluorescent in longwave UV. Since the related molecule 2-acetylindanedione can form complexes with copper (II) and zinc (II) ions,[83,85] the effect of these ions and others on the polymer were investigated. The fluorescence of the polymers in solution was found to be strongly quenched by the addition of both ions to methanol solutions of ACT-2 (*fig 4.11*)

Solutions were prepared by adding 10 mg of each polymer to 1 ml of 1% v/v triethylamine in methanol, and stirring for 2 h, giving pink and yellow solutions for ACT-1 and ACT-2 respectively. Undissolved polymer was removed by filtering using a 2.7 μm glass fiber syringe filter. This solution was further diluted with methanol. For experiments, 60 μl of the polymer solution was diluted with 3 ml of methanol. Portions of 0.1 mM solutions of various metal salts in methanol were added to increase the concentration. The raw data for nickel (II) acetate is shown in *figure 4.12.* Strong photoluminescence quenching was observed with this salt as well as copper (II) chloride and zinc acetate.

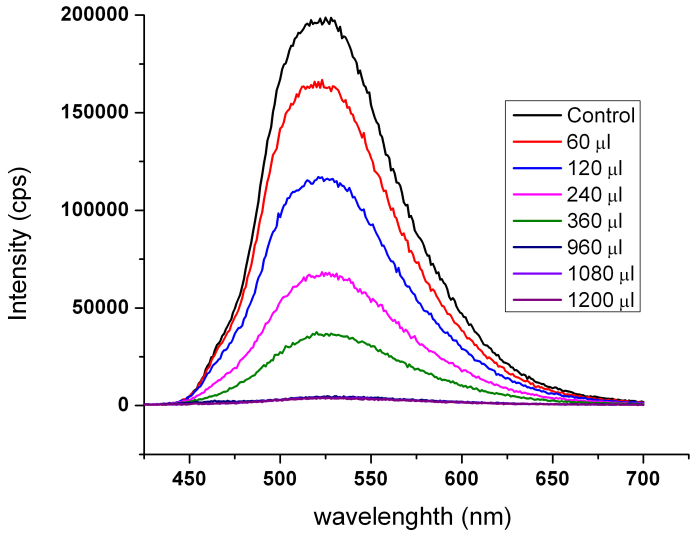

Figure 4.12: Raw fluorescence quenching for nickel (II) acetate

Integrated intensities from 400 to 700 nm were used for Stern-Volmer analysis.

$$\frac{\Phi_e^{\circ}}{\Phi_e} = \frac{I^{\circ}}{I} = 1 + k_q \tau_a [Q] = 1 + k_{SV}[Q] \qquad 4.1$$

Equation 4.1 is the form of the Stern –Volmer equation used for the analysis. Measurements of steady state fluorescence intensity were used to calculate k_{SV}, the fluorescence lifetime τ and quenching constant k_q were not measured. The initial over final intensity (I_o / I) was plotted verses quencher concentration [Q] in units of molarity (M).

Stern-Volmer plots for nickel (II) acetate, zinc (II) acetate, and copper (II) chloride showed fluorescence quenching. The Stern-Volmer constants (K_{SV}) for the low concentration linear region of nickel acetate, copper chloride, and cadmium acetate plots are 3.5 x 10^5 M^{-1} and 7.1 x 10^4 M^{-1}, and 6.9 x 10^4 M^{-1} respectively. The data in the

hyperlinear region was excluded from the fit. The quenching by nickel and copper salts was very strong. No quenching was observed with mercury acetate, and the intensity was observed to increase slightly when corrected for dilution of the polymer. The PL quenching by zinc was found to increase rapidly at 5 μM ion concentration and level off at 15 μM at a value of $I_o / I \approx 2$. Cadmium (II) acetate quenching increased linearly and saturated . The data for nickel (II) acetate and copper chloride showed a linear Stern-Volmer plot until 10.5 and 16.4 μM respectively, after which the quenching increased in a hyperlinear manner.

The likely reason for the hyperlinear behavior may be aggregation-induced fluorescence quenching. 2-Acetylindanedione (2-AID) is known to form $M(2\text{-AID})_2$ complexes with divalent ions of zinc, copper, cadmium, and lead.[85] The attachment of two binding groups to one metal ion would be expected to lead to coiling or aggregation of the polymer chains, which may be responsible for the observed behavior. As the concentration of the metal ion increases, the probability of double binding increases and eventually causes aggregation. It may also explain the saturation behavior in the zinc acetate data. Zinc may be a poor quencher on its own, but leads to aggregation that causes some quenching.

a)

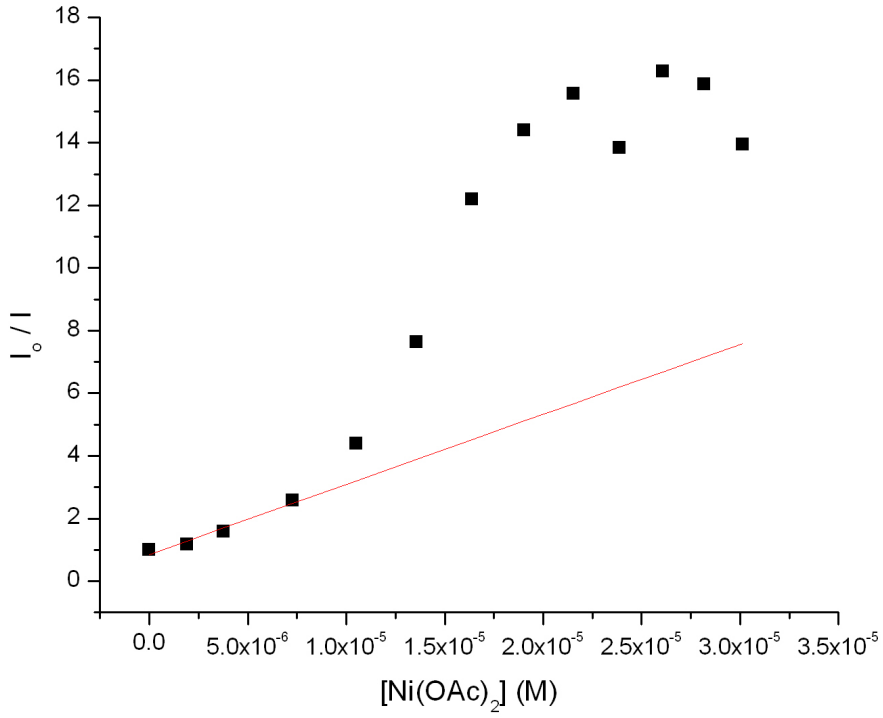
18
16
14
12
10
8
6
4
2
0
I_o / I
0.0
5.0x10^{-6}
1.0x10^{-5}
1.5x10^{-5}
2.0x10^{-5}
2.5x10^{-5}
3.0x10^{-5}
3.5x10^{-5}
[Ni(OAc)$_2$] (M)

b)

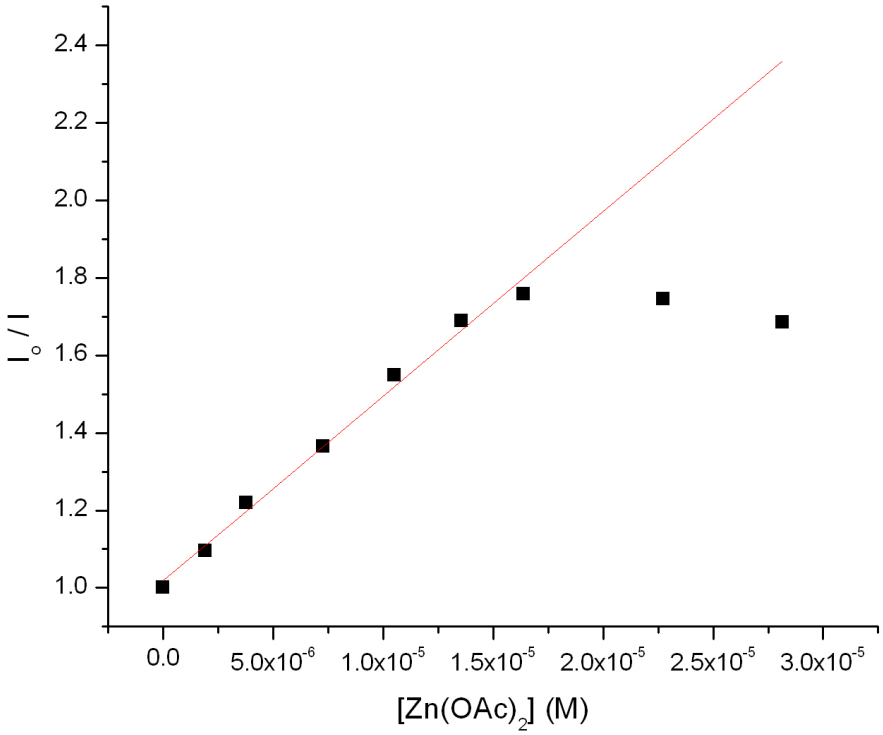
2.4
2.2
2.0
1.8
1.6
1.4
1.2
1.0
I_o / I
0.0
5.0x10^{-6}
1.0x10^{-5}
1.5x10^{-5}
2.0x10^{-5}
2.5x10^{-5}
3.0x10^{-5}
[Zn(OAc)$_2$] (M)

c)

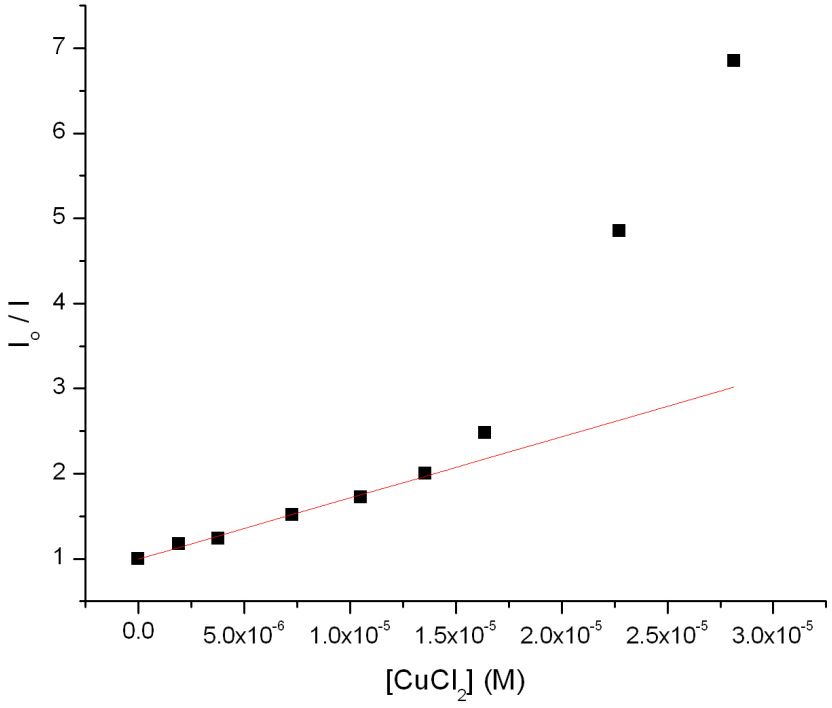
7
6
5
4
3
2
1
I_o / I
0.0
5.0x10^{-6}
1.0x10^{-5}
1.5x10^{-5}
2.0x10^{-5}
2.5x10^{-5}
3.0x10^{-5}
[$CuCl_2$] (M)

d)

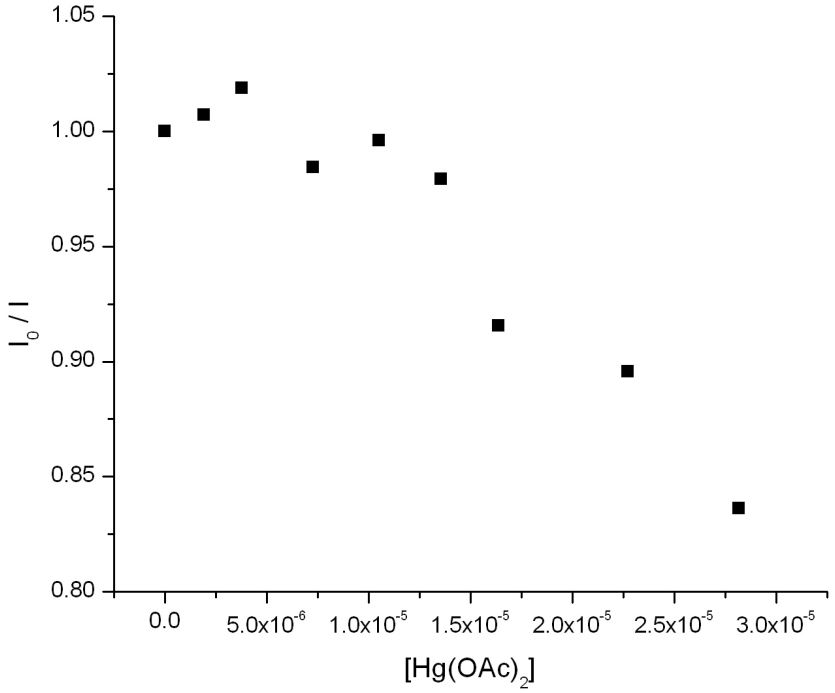
1.05
1.00
0.95
0.90
0.85
0.80
I_0 / I
0.0
5.0x10^{-6}
1.0x10^{-5}
1.5x10^{-5}
2.0x10^{-5}
2.5x10^{-5}
3.0x10^{-5}
[$Hg(OAc)_2$]

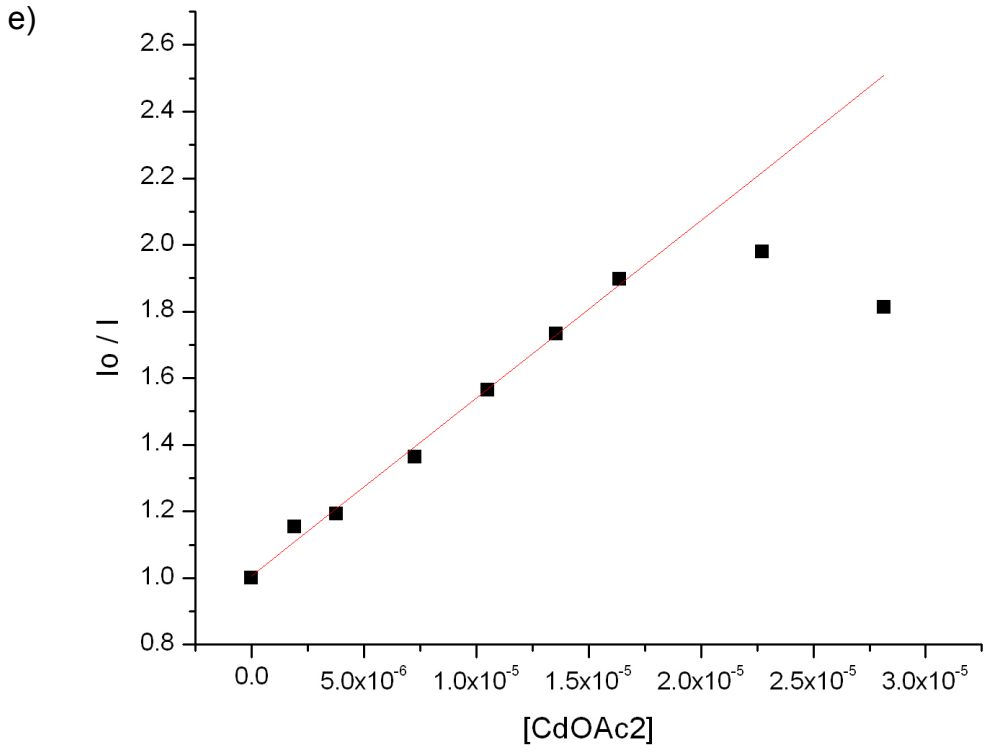

Figure 4.13 Stern-Volmer plots of quenching of ACT-2 fluorescence by a) zinc acetate b) nickel (II) acetate c) copper (II) chloride d) mercury (II) acetate and e) cadmium (II) acetate. Fitting lines for low concentration linear data are shown in red.

4.6 Summary

The 5-acetyl-4*H*-cyclopenta[*c*]thiophene-4,6(5*H*)-dione (ACT) monomer unit was prepared from commercially available thiophene 3,4-dicarboxylic acid in three steps. The yield for the critical step to form the final monomer was moderate at 35%, but the overall yield of ~20% was very high compared to most acceptor units reported in literature due to its short synthetic route.

The monomer exists mainly in one of two enol tautomer forms and not in the nominal 5-acetyl-4,6-cyclopentadione form as evidenced by the asymmetry of the molecule inferred by ^{13}C NMR spectroscopy as well as the stokes shift measurements, which suggest an intramolecular hydrogen bond that facilitates excited-state proton transfer.

The monomer can be successfully polymerized via Stille coupling with bis-triemthylstannylarenes despite the resulting polymers' poor solubility in the Toluene:DMF solvent system. Purification is accomplished by simply precipitating in hexane and washing with toluene.

Polymers based on this novel unit are acidic and are vastly more soluble in organic solvents in their deprotonated forms. This allows them to be dissolved in volatile amine containing solutions coated into films that cannot be washed away with pure organic solvents. This shows great promise for orthogonal solvent processing, and a solar cell based on ACT-1 showed some performance as a proof of concept.

ACT-2 shows some solubility in methanol and DMSO and shows strong photoluminescence in solution that is quenched by a variety of metal ions, with particularly high sensitivity for nickel and copper. The ACT unit could be used as a building block for polymers that are sensitive to these ions by photoluminescence quenching or potentially changes in electrical properties.

4.7 Synthesis Procedures

2,5-dibromo-3,4-thiophenedicarboxylic acid (5): 3,4-thiophenedicarboxylic acid (10 g, 58 mmol) was dissolved in 150 ml of glacial acetic acid in a flask equipped with a reflux condenser and an addition funnel. Liquid bromine (14 ml, 290 mmol) was added dropwise at room temperature over approximately 20 min. The reaction flask was heated to 60 ºC in an oil bath and stirred for 48 h and monitored by thin layer chromatography (TLC) with 10% acetic acid in ethyl acetate as eluent. The reaction mixture was slowly poured into a mixture of ice about 200 g of ice, 200ml of water and 15 g of Na_2SO_3. The liquid was evaporated to dryness leaving a mixture of product and salts. This was washed with about 100 ml of water to remove the salts and leave the majority of the product behind. Boiling water was added to the remaining solid until it was fully dissolved. The solution was then filtered while hot to remove a brown residue and then left to cool forming tan colored needle shaped crystals.

2,5-dibromothiophene-3,4-dicarboxylic anhydride (6): Compound 5 (2 g) was added to 10 ml of acetic anhydride and heated to reflux for 2 hours. The acetic anhydride and acetic acid byproduct were evaporated thoroughly in vacuum. The product was used without further purification.

5-acetyl-1,3-dibromo-6-hydroxy-4H-cyclopenta[c]thiophen-4-one (7): Compound 6 (7.76 g, 24.9 mmol) and 1,1,2,2-tetrachloroethane (25 ml) were put into a flask fitted with a condenser and drying tube. Aluminum chloride (13.45 g, 99.6 mmol) was added in small portions with stirring causing compound 6 to dissolve. Isopropenyl acetate (5.42 ml, 49.8 mmol) was added dropwise and then the temperature was raised to 80 ºC for 3 hours. Then the reaction mixture was cooled to room temperature and

poured into 200 ml of 2 M HCl. The product was then extracted by repeated washings until no product was found in the washings by TLC (6 portions of 100 ml of diethyl ether). The ether solution was dark red. The combined ether washings were then extracted with 6 portions of 100 ml of 1:1 saturated aqueous $NaHCO_3$: DI water. The remaining ether was dark green in color. The aqueous washings were light red at this point. HCl was slowly added to the aqueous solutions until a pH of < 2 was reached. Then the product was extracted with two washings with 100 ml of ether. The ether phase was evaporated and the residue was recrystallized from 100 ml of ethanol. 3.1 g of 7 were collected (35 % yield).

^{1}H NMR (300MHz, CDCl3): δ ppm 2.539 (s)

^{13}C NMR (300MHz, CDCl3): δ ppm 19.71 (s) 111.95 (s) 112.88 (s) 116.23 (s) 140.80 (s) 142.79 (s) 179.42 (s) 187.25 (s) 188.03 (s)

GCMS: m / z = 352

ACT - 1 Polymer: Compound 7 (0.088 g, 0.25 mmol), and (4,8-bis((2-ethylhexyl)oxy)benzo[1,2-b:4,5-b']dithiophene-2,6-diyl)bis(trimethylstannane) were put in a two necked flask fitted with a condenser with a flushing adaptor, a balloon, and a septum. 11.3 ml of toluene and 1.3 ml of DMF was added and ultra high purity argon (obtained from Air Liquide) was bubbled through the mixture for 20 min, before addition of tetrakis-triphenylphosphinepalladium(0) (12.5 mg). The mixture was bubbled with argon five more minutes before the reaction mixture was heated to reflux for 6, 13, or 20 hours. The reaction mix was then poured into 60 ml of hexanes and centrifuged. The supernatant liquid was poured off and replaced with additional hexanes before centrifuging again. This washing procedure was repeated once more with hexanes and

then 3 more times with 12 ml portions of toluene.

ACT - 2 Polymer: Compound 7 (0.088 g, 0.25 mmol), and 2,5-bis-trimethylstannyl thiophene (0.102 g, 0.25 mmol) were put in a two-necked flask fitted with a condenser with flushing adaptor and balloon and a septum. 11.3 ml of toluene and 1.3 ml of DMF was added and ultra high purity argon (obtained from Air Liquide) was bubbled through the mixture for 20 min, before addition of tetrakis-triphenylphosphinepalladium(0) (12.5 mg). The mixture was bubbled with argon five more minutes before the reaction mixture was heated to reflux for 15 hours. The reaction mix was then diluted with 20ml of toluene and centrifuged. The supernatant liquid was poured off and replaced with additional toluene before centrifuging again. This washing procedure was repeated once more with 20 ml portions of toluene.

Chapter 5: Systematic Investigation of Small Molecule Electron Donor Materials With Two Diketopyrrolopyrrole Units

5.1 Introduction

Diketopyrrolopyrrole (DPP) is an electron deficient monomer unit, which has applications in commercially useful fluorescent dye molecules,[86] dye laser media,[87] and sensitizers for dye-sensitized solar cells.[88] The thiophene bearing DPP unit structure is shown in *fig. 5.1*.

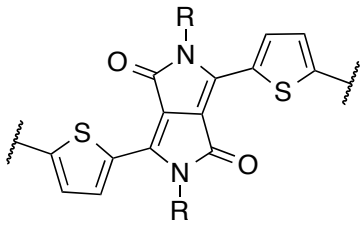

Figure 5.1 3,6-Dithien-2-yl-2,5-dibutylpyrrolo[3,4-c]pyrrole-1,4-dione (DPP) unit

The unit also finds application in polymer[89-91] and small molecule based[72,92-94] OPV devices. Its planar but non-aromatic core gives rise to narrow band gaps in these materials from about 1.5 eV[91] to as low as 1.1 eV[95] for polymers and around 1.7 eV in small molecules with one DPP unit.[72] By incorporating two DPP units in the same molecule, the energy gap can be further reduced to around 1.5 eV[96-98] to take advantage of more of the solar spectrum (see *fig 2.6*). This decrease in band gap, however, leads to a decrease in the open circuit voltage because the HOMO level is increased. The material “DTTDPP” reported in reference 68 uses a dithienothiophene (DTT) unit

between the two DPP units. The strongly electron donating DTT unit would be expected to increase the HOMO level, so in an effort to make materials with a good combination of light absorption and open circuit voltage, a series of small molecules were synthesized with different core units with weaker electron donating and, electron deficient properties.

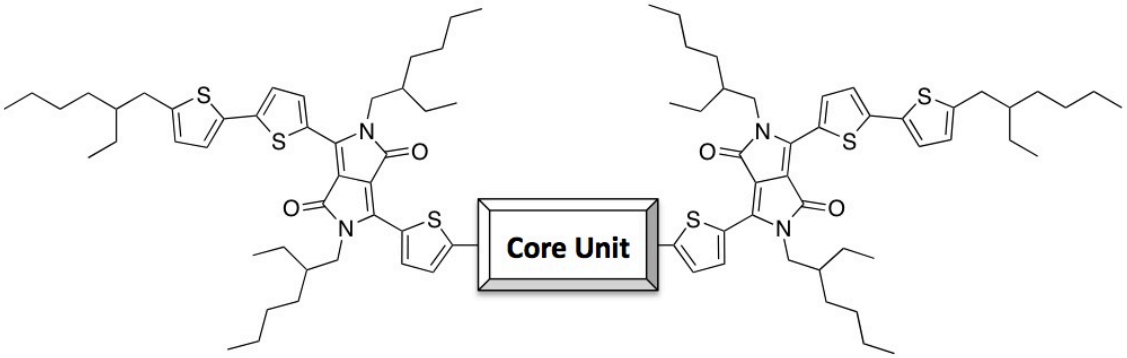

Figure 5.2 General structure of DPP based small molecules investigated

The core units we used were: bis-2-thienyl benzodithiophene (TBDT), di(2-thienyl) benzodithiophene, diphenyl benzodithiophene (PhBDT), nothing (homocoupling), thiophene, 2,2'-bithiophene, and thienopyrrolidione (TPD). All of these units are used as electron-rich donor units in OPV materials with the exception of TPD, which is strongly electron deficient. TPD copolymers, for example, have some of the best open circuit voltages in the literature.[99] The materials were prepared by first making the heterobifunctional DPP unit with one bromine and one 5-alkylthiophene-2-yl group (compound 5-7) as shown in the synthesis section in fig 5.12. With this material in hand, a wide variety of molecules can be prepared by Pd-catalyzed cross coupling reactions. The synthesis of the TPD material was somewhat more difficult since it required converting the bromide of DPP into a pinacolborate ester (compound 5-8) for a Suzuki coupling.

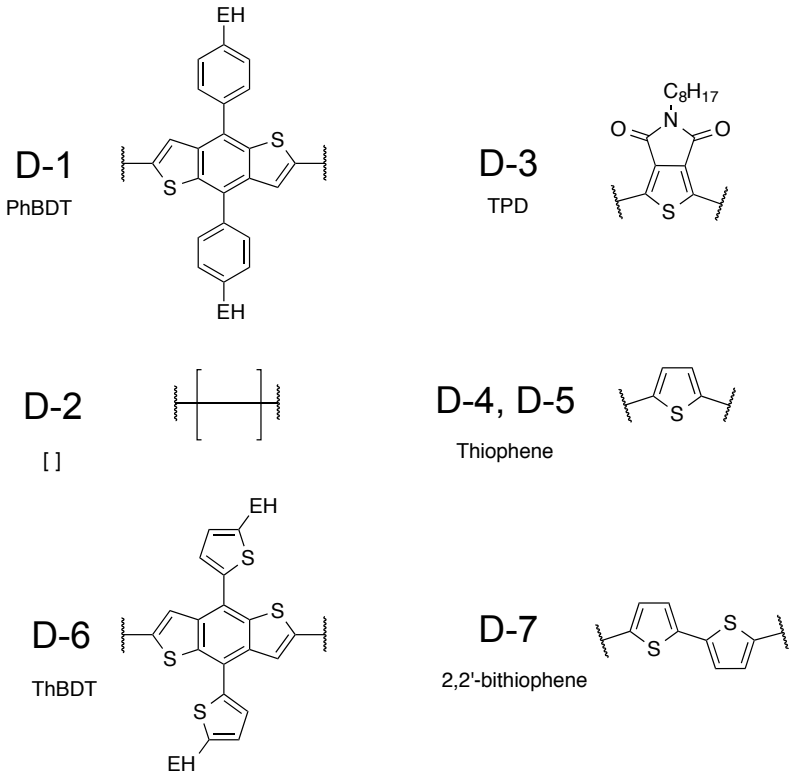

Figure 5.3 structures of core units used in the small molecule series

5.2 Energy Levels

The HOMO levels of all molecules in the series were as expected deeper than DTTDPP from reference 68. They ranged from -5.03 eV for D-7 (2,2'-bithiophene core) to -5.3 eV for D-3 (TPD core). The cyclic voltammetry data for D-1 through D-4 is shown in *figure 5.4*. D-3 was designed to have a lower lying HOMO energy level by switching a donor unit for an acceptor and this lead to devices with the highest open circuit voltage in the series of 0.76 V.

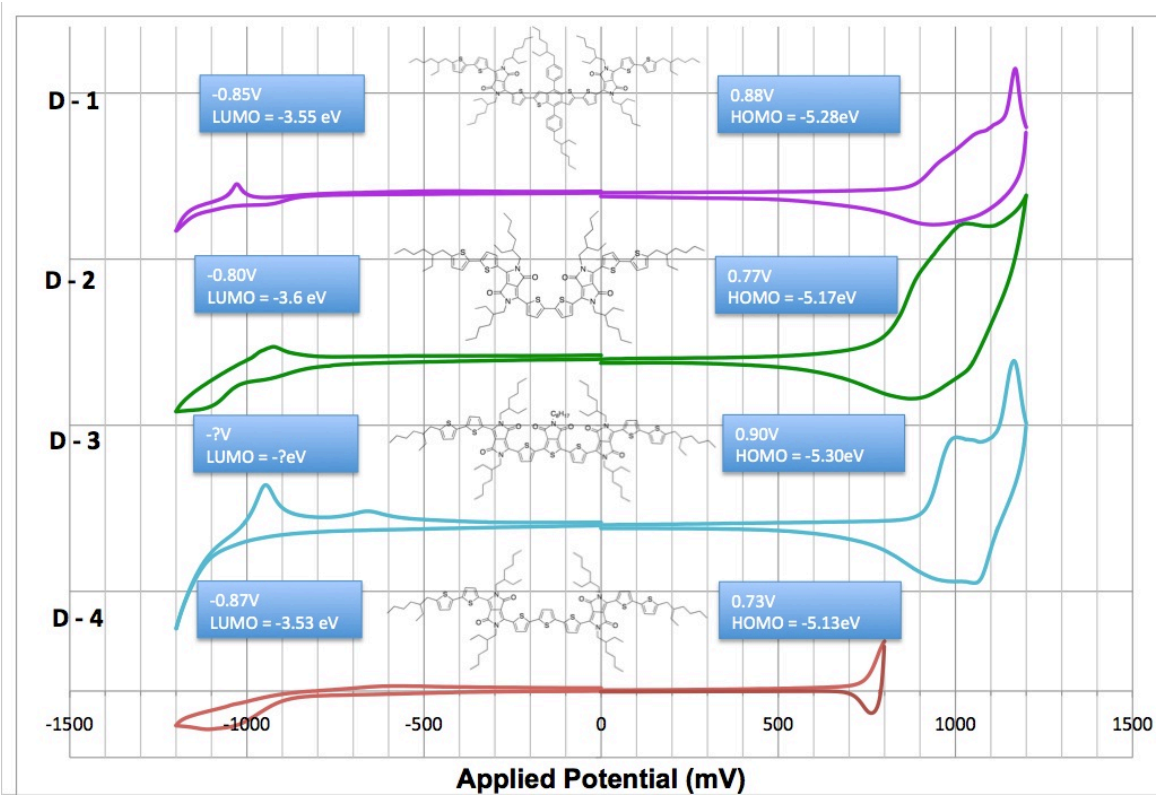

Figure 5.4 Cyclic voltammetry (CV) Curves and energy levels for molecules D-1 through D-4 in acetonitrile / 0.1 M Bu_4NPF_6 at 21 ºC. Pt disk working electrode, silver wire quasi-reference electrode. Ferrocenium / ferrocene couple was used as an external standard for energy level calculations and assumed to lie at - 4.8 eV compared to the vacuum level.

5.3 Device performance and Characterization

OPV Devices were fabricated from the small molecules in the series. C_{60} and C_{70} PCBM were used as acceptor materials; C_{60} for initial tests and C_{70} with the most promising materials. PEDOT on ITO glass was used as the anode and evaporated lithium fluoride / aluminum was used as the cathode. For initial testing to compare the molecules, pure chloroform was used as the solvent and no post treatment was used. Under these conditions, the best performers were D-4 and D-7. D-3 was notable for showing the highest Voc of 0.76 V, but suffered from poor short-circuit current. Fill

factors were generally decent, with 66% being the highest. The currents were quite poor for all materials though, no higher than 3.53 mA/cm^2.

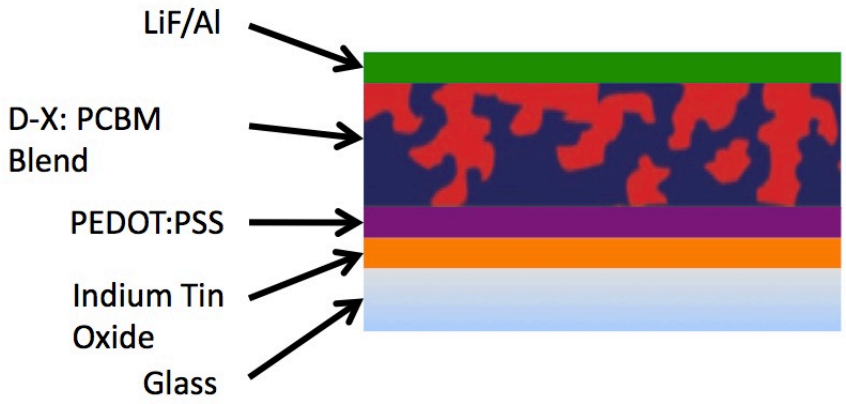

Figure 5.5 General OPV device structure used for materials testing

Table 5.1 Initial testing data for molecules D-1 through D-7. Conditions: D-X:PCBM ratio of 1:0.75, 0.8 wt %, Spin coated films at 2200 rpm from chloroform. No annealing.

Molecule	Core Unit	HOMO (eV)	LUMO (eV)	E_g (eV)	Device V_{OC}	J_{SC} (mA / cm^2)	FF (%)	PCE (%)
D-1	PhBDT	-5.28	-3.55	1.56	0.71	1.06	48.4	0.36
D-2	None	-5.17	-3.60	--	--	--	--	--
D-3	TPD	-5.30	*-3.86	1.44	0.76	1.49	50.4	0.57
D-4	Thiophene	-5.13	-3.53	1.44	0.66	3.20	66.0	1.38
D-5	Thiophene†	--	--	1.38	0.60	1.32	59.1	**0.47
D-6	TBDT	-5.13	-3.50	1.46	0.72	2.67	30.7	0.59
D-7	Bithiophene	-5.03	-3.75	1.43	0.64	3.53	61.9	**1.40

* Calculated from HOMO and E_g **$PC_{71}BM$ used in device test † n-octyl chain on DPP

Since the short circuit current was the parameter most lacking for these initial devices, efforts were made to improve it. Low current can have a variety of causes including incomplete light absorption, parasitic absorbance, geminate recombination (exciton recombination before reaching D-A interface), and non-geminate (free carrier) recombination. Incomplete light absorption was considered, but devices made at lower spin speeds and larger film thickness also showed poor current.

Since small molecules are known to often form oversized domains due to their ease of crystallization,[100] the surface microstructure of the blend films of D-4 was characterized by atomic force microscopy (AFM) and the photoluminescence quenching was measured in the solid state for pure films and D-4:PCBM 1:1 ratio films. The height images from AFM had features approximately 100 nm in size. Phase images measure phase lag between the driving signal and the vibration of the AFM cantilever and give contrast based on mechanical storage and loss moduli.[101] Features in these images usually correspond better to actual D:A domain size.[72] These images showed smaller domain sizes around 50 nm.

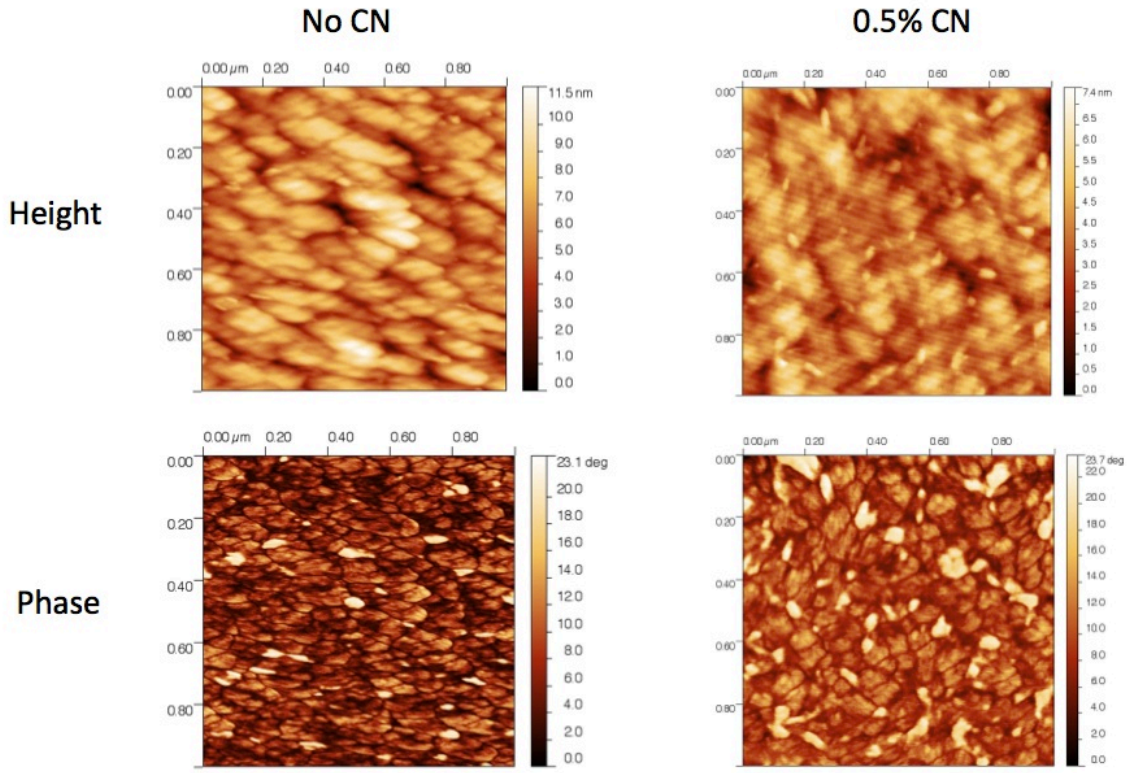

Figure 5.6 AFM images of D-4:$PC_{61}BM$ blend films showing little discernable change in surface morphology as a result of CN solvent additive.

The domain size is larger than the commonly cited 20nm for an ideal bulk heterojunction, so it was suspected that charge separation was incomplete in these

devices. It would account for the low current. Photoluminescence quenching was performed to assess the effectiveness of charge separation in the devices. Photoluminescence in blend films at the same wavelength as the neat polymer can be assumed to result from geminate recombination if separated charge carriers do not emit in that region of the spectrum. Neat films of D-4 and D-4:PCBM were excited at 710 nm and a PL peak around 820 nm was observed. The data is shown in *figure 5.7*. Intensities were normalized using the film absorbance at the excitation wavelength, 710 nm. In the blend films, the PL intensity was reduced to 63 % of the neat film value. This was a strong indication that exciton separation was not occurring effectively.

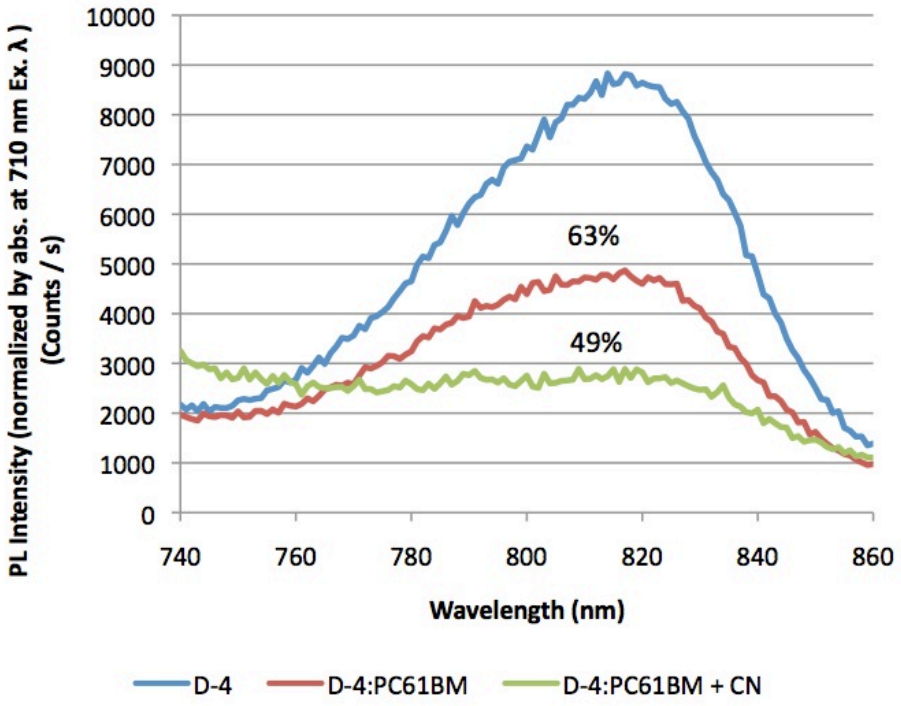

Figure 5.7 Photoluminescence quenching of D-4 by PCBM in thin films. Excited at 710 nm. Intensities were normalized from film absorbance at 710 nm.

With this knowledge, efforts were made to modify the bulk heterojunction morphology in the devices. High boiling-point solvent additives are often used with small

molecules and polymers to change morphology.[2,97,100] Since they are the last solvent to evaporate during the coating process, they can exert a very strong influence on the growth of the donor and acceptor phases. 1,8-diiodooctane (DIO) and 1-chloronapthalene (CN) were employed as solvent additives.

Table 5.2 Effects of solvent additives and annealing on D-4: $PC_{71}BM$ devices

Conditions	Device V_{OC}	J_{SC} (mA / cm^2)	Fill Factor (%)	PCE (%)
No additives	0.66	3.20	66.0	1.38
0.3 % DIO*	0.66	4.21	54.0	1.50
DIO + 95 ºC Anneal*	0.67	3.80	58.6	1.49
0.5 % CN	0.62	5.27	67.7	2.22
1.0 % CN	0.70	1.90	34.6	0.46

*spin speed increased to 2600 rpm to compensate for increased solution viscosity

Adding 0.3% DIO to the processing solvent had a small effect on the device parameters; current was increased, but at the cost of decreased fill factor. The best results were achieved using CN at a concentration of 0.5% by volume. The device performance was increased to 2.22 % PCE as a result of improvements in both current and fill factor.

The effects of CN on device active layer microstructure were studied by AFM, but no noticeable changes in morphology were apparent except for a very slight decrease in surface roughness. As can be seen in figure 5.6, the lateral length scale of the surface features visible in both height and phase images were unchanged.

The PL quenching results tell another story. The PL in films cast from chloroform with 0.5 % v/v CN was clearly more strongly quenched, with the intensity falling to 49% of the value of the neat polymer. Clearly the CN is having an effect based on the device performance and photoluminescence data, but it does not seem from the AFM data that it is related to the domain size. The mechanism for the effect of CN is still unclear. In

future work, TEM images might be able to give a more accurate picture of the subsurface morphology.

Another approach to changing the morphology of the bulk heterojunction is to change the alkyl chains on the donor material. Changing the alkyl chain structure would be expected to effect both the material's tendency to crystallize[102] and its interaction with the acceptor[103]. Molecule D-5 was prepared in order to study the effect of changing the alkyl chain on the DPP unit from a branched 2-ethylhexyl chain to a linear n-octyl chain, thus keeping the number of carbon atoms the same.

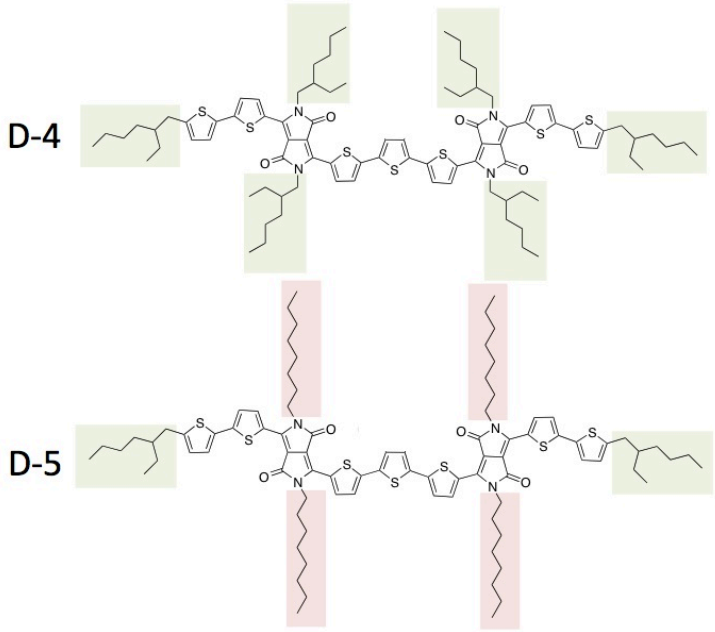

Figure 5.8 Structural modification of D-4 by replacing branched alkyl chains with linear ones

The change was expected to lead to better molecular packing because of the reduced steric hindrance and thus affecting the bulk heterojunction morphology. Blend films were prepared with 1:1 D-5:PCBM ratio with and without added CN. In both cases the feature sizes were in excess of 300 nm, much too large for a good bulk heterojunction. The best results from D-4 and D-5 were obtained with $PC_{71}BM$, and J – V

curves are shown in *figure 5.10.* The device performance of D-5 was worse than D-4 and a maximum efficiency of 0.71 % was obtained when using CN as an additive at 0.3% v/v. The fill factor was somewhat reduced as well. The lower current makes sense in light of the overly large domains observed in the AFM images.

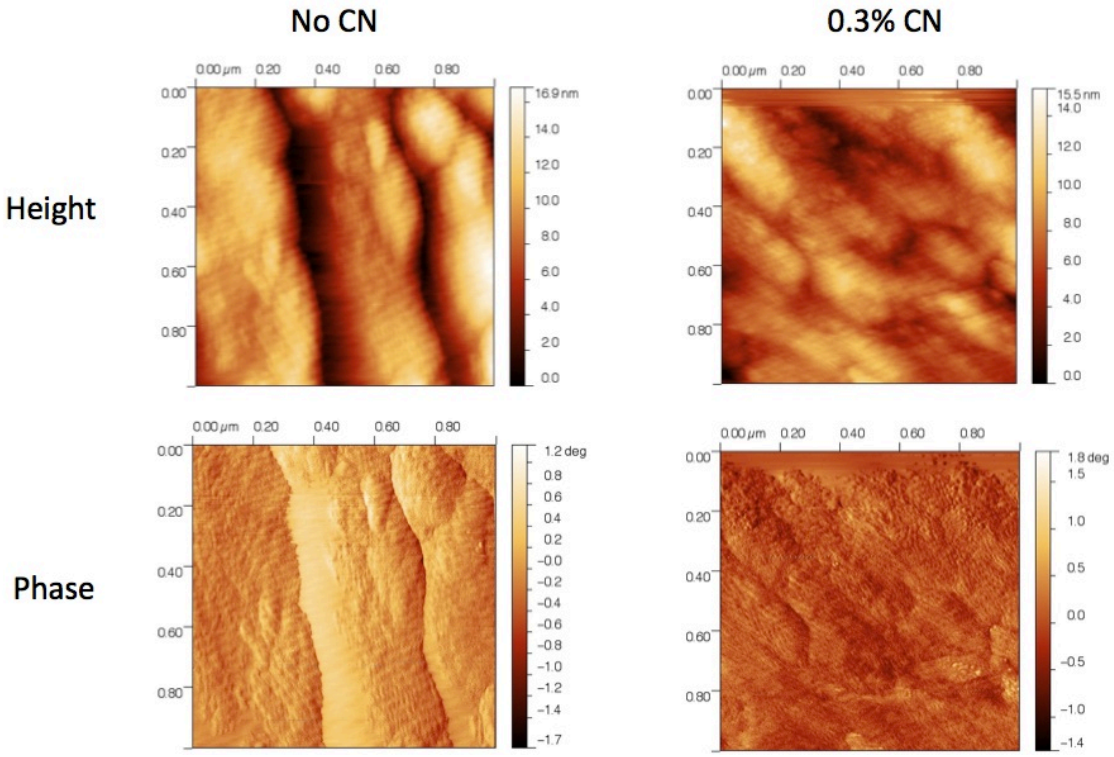

Figure 5.9 AFM images of 1:1 blends of D-5 with $PC_{60}BM$

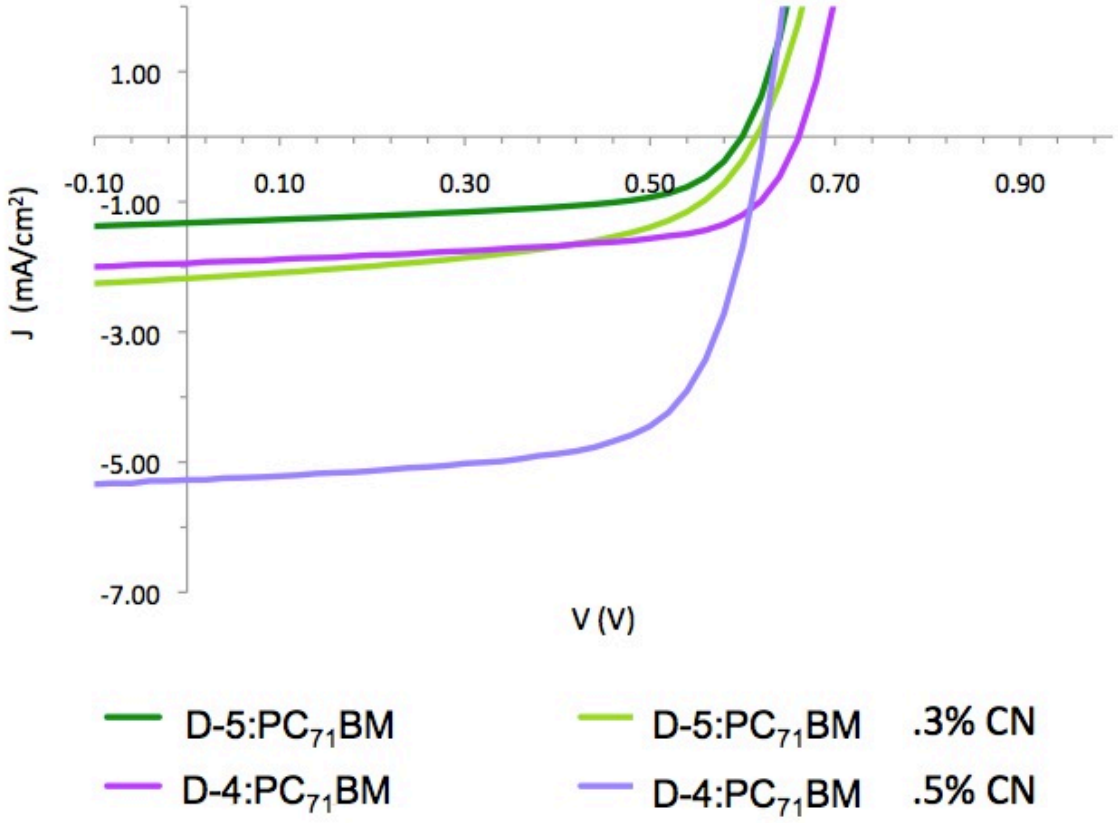

Figure 5.10 J – V curves for D-4 and D-5 in their optimized conditions

Table 5.3 Device data comparison of D-4 and D-5

Materials	Conditions	Voc(V)	Jsc(mA/cm2)	FF(pct)	Eff(pct)
D-4:C70	no CN 2000rpm	0.66	1.95	62.7	0.81
D-5:C70	no CN 2000rpm	0.60	1.32	59.1	0.47
D-4:C70	0.5%CN 2000rpm	0.62	5.27	67.7	2.22
D-5:C70	0.3%CN 2000rpm	0.62	2.18	52.9	0.71

An attempt was made to study the PL quenching behavior of D-4 PCBM films. The weaker PL of D-5 relative to D-4 made accurate determination of the quenching ratio difficult, but a decrease was observed, with a decrease in PL intensity for blends relative to pure D-5, but similar intensity when CN is used as a processing additive. The results can be seen in *figure 5.11*.

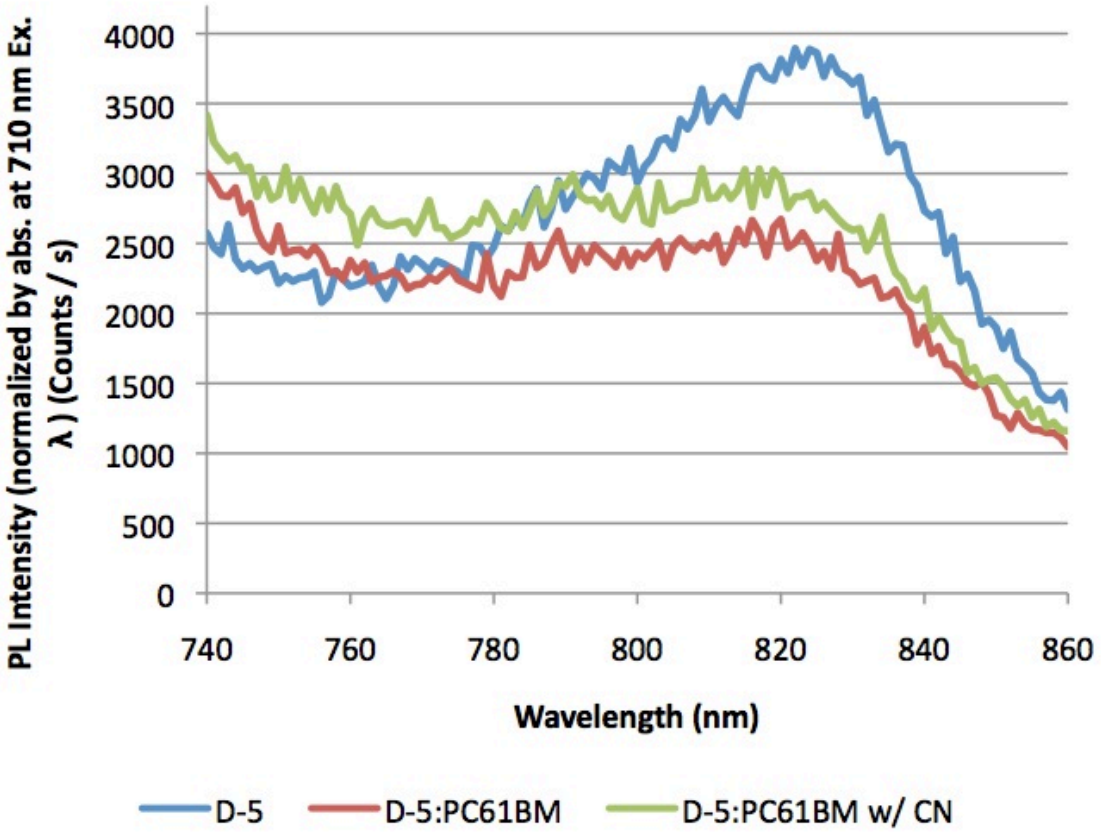

Figure 5.11 Photoluminescence quenching data for D-5 and D-5:PCBM films. Excited at 710 nm. Normalized by film absorption at 710 nm excitation wavelength.

It seems that the exchange of branched alkyl chains for linear ones increased the tendency of the material to crystallize leading to larger domains and decreased, device performance. The photoluminescence intensity was also decreased which makes sense when considering that the steric hindrance is reduced and the molecular packing is expected to be closer. The result is stronger aggregation-induced fluorescence quenching.

5.4 Conclusions

Seven small molecules with two DPP units were designed and synthesized. Changing the core unit between the DPP arms modified frontier orbital energy levels. The highest performing material D-4 had a PCE of 2.2 % after some optimization of processing conditions. The performance of all materials in the series were limited mainly by low short-circuit currents. Open-circuit voltages are improved compared to small molecules with dithienothiophene as the core unit, and molecule D-3 with a thienopyrrolidione core unit showed the highest open circuit voltage of 0.76 V, but its low current lead to low power conversion efficiency. Part of the reason for the low currents appears to be incomplete exciton separation. The significant photoluminescence still present in PCBM blend films of D-4 is evidence for this. 1-chloronapthalene (CN) was effective in increasing the performance of D-4 and D-5 small molecules and reducing, but not eliminating the photoluminescence. The domain sizes in D-4 were found to be larger than ideal at around 50 nm. Changing the alkyl chains on the DPP units from branched to linear made matters worse by increasing the domain sizes further to over 300 nm.

Going forward, in order to improve the performance of materials with this basic structure, something must be done in order to reduce the domain size and or improve exciton diffusion and lifetime. Other processing additives such as 1,8-octanedithiol or N-methylpyrrolidone might be effective in this regard. Another approach would be to increase the size and branching of the alkyl chains in order to reduce the tendency of the materials to crystallize. The energy gaps of these materials are in a good range for use in either single junction or tandem solar cells and the V_{OC} and fill factor are decent for low band gap small molecules. Two DPP unit small molecules would make excellent OPV materials if something can be done about their short circuit current.

5.5 Synthesis Procedures

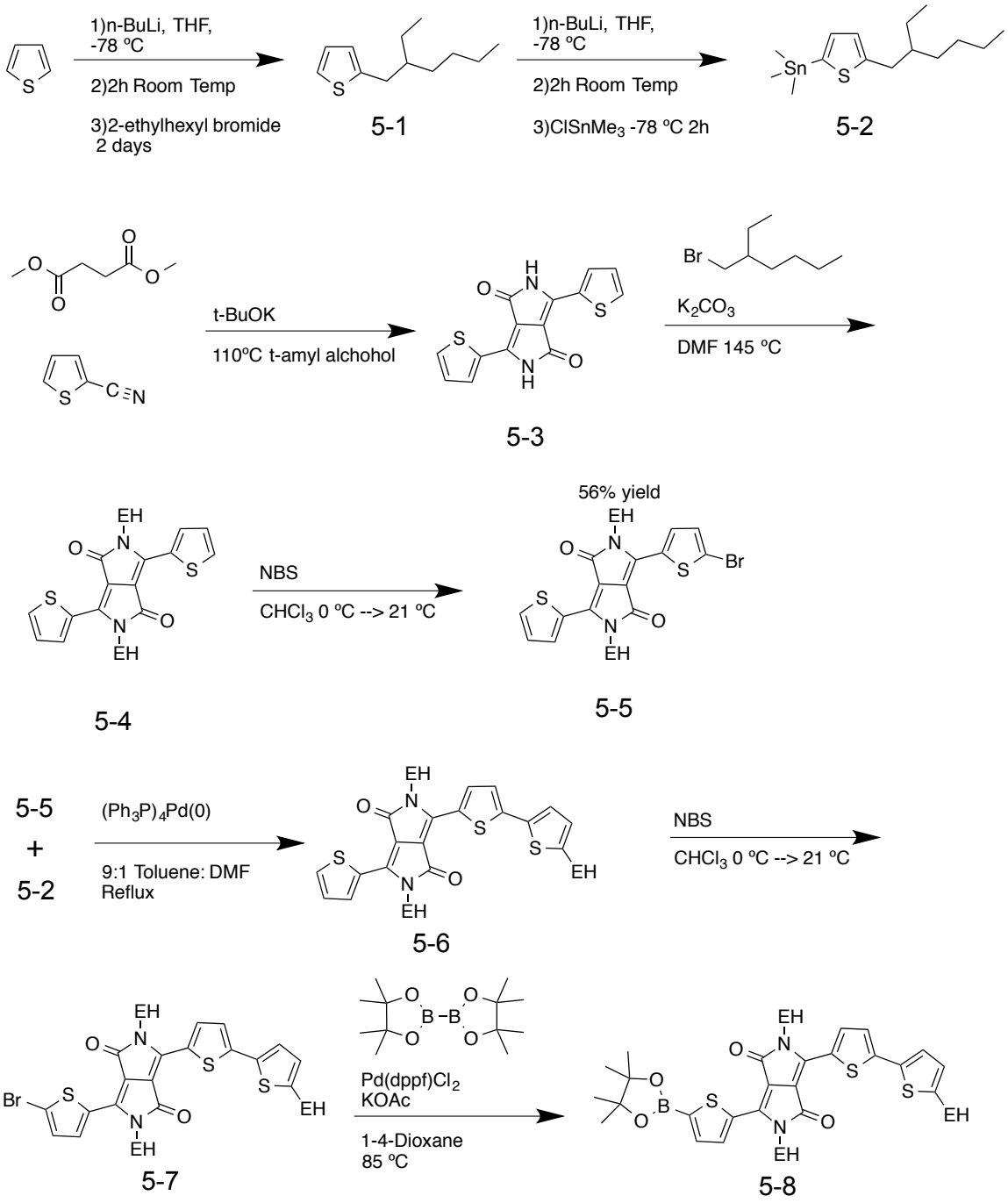

Figure 5.12 Synthetic route to DPP part of small molecule series synthesis

2-(2-Ethylhexyl) thiophene (5-1) Thiophene (15.17 ml, 194 mmol) and THF (300ml) were injected into a flask protected by an argon atmosphere and then were cooled to -78º C. 1.6 M n-butyllithium solution in hexanes (40 ml, 101 mmol) was added dropwise with stirring. The flask was warmed to room temperature and stirred for 2 hours. Then the flask was cooled back to -78º C and 1-bromo-2-ethylhexane (15.4 ml, 86.4 mmol) was added in one portion and the flask was allowed to warm to room temperature naturally and stirred for 48 h. The reaction mixture was then quenched by slow addition of 10 ml of isopropanol and poured into approximately 500 ml of water. The resulting mixture was extracted three times with 50 ml of diethyl ether. The combined ether washings were dried using $MgSO_4$ and filtered before evaporation in vacuum. The resulting oily residue was purified by vacuum distillation with the product fraction boiling at 110 ºC.

GC/MS: M/Z = 196

2-Trimethylstannyl-5-(2-ethylhexyl)thiophene (5-2) 2-(2-Ethylhexyl) thiophene (5-1) (5.0 g, 25.5 mmol) and THF (65 ml) were injected into a flask protected by an argon atmosphere and then were cooled to -78º C. 2.5 M n-butyllithium solution in hexanes (12.2 ml, 30 mmol) was added dropwise with stirring. The flask was warmed to room temperature and stirred for 2 hours. Then the flask was cooled back to -78º C and 1 M trimethyltin chloride in THF (33.2 ml, 33.2 mmol) was added in one portion and the flask was allowed to warm to room temperature naturally and stirred for 12 h. The reaction mixture was poured into approximately 100 ml of water. The resulting mixture was extracted three times with 30 ml of diethyl ether. The combined ether washings were dried using $MgSO_4$ and filtered before evaporation in vacuum. The product was recovered as a light yellow oil.

3,6-Dithien-2-yl-[3,4-c]pyrrole-1,4-dione (5-3) Potassium tert-butoxide (24.4 g, 220 mmol) was added to a flask followed Thiophene-2-carbonitrile (17 ml, 183 mmol) was added followed by tert-amyl alcohol (140 ml). The mixture was heated to 140º C and stirred while dimethyl succinate (7.99 ml, 61 mmol) dissolved in tert-amyl alcohol (50 ml) was added dropwise. The resulting mixture was stirred for 4 hours, then a distillation condenser head was attached to the reaction vessel and the reaction mixture was decreased in volume by ½. The reaction was stirred an additional 4h before cooling to room temperature, dilution with methanol (200 ml) and filtering to collect the solid red product which was washed with methanol and used without further purification.

2,5-bis(2-ethylhexyl)-3,6-di(thiophen-2-yl)-2,5-dihydropyrrolo[3,4-c]pyrrole-1,4-dione (5-4) Compound 5-3 (8 g, 26.6 mmol) was added to DMF (150 ml) and K_2CO_3 (14.72 g, 107 mmol). The mixture was heated to 145 ºC under argon and 1-bromo-2-ethylhexane (21.8 ml, 123 mmol) was added slowly. After 20 h at 145 ºC, the reaction mix was poured into ice water (400 ml). The red solid that precipitated was collected by filtration and washed with water and then methanol. The filtrate was mixed with dichloromethane and washed with brine to remove the water. The material was purified by column chromatography on silica gel with 75% dichloromethane (DCM):hexane as eluent. The title compound was collected as a dark red solid.

3-(5-bromothiophen-2-yl)-2,5-bis(2-ethylhexyl)-6-(thiophen-2-yl)-2,5-dihydropyrrolo[3,4-c]pyrrole-1,4-dione (5-5) Compound 5-4 (2.8 g, 5.34 mmol) was dissolved in chloroform (150 ml), protected from light and cooled to 0 ºC. N-bromosuccinimide (NBS) (0.951 g, 5.34 mmol) solution in 75 ml of chloroform was added in dropwise over 6h with stirring, then stirred at room temperature overnight. The reaction mixture was washed with water and dried over $MgSO_4$ and evaporated. The

residue was purified by column chromatography on silica gel with 60 % DCM : hexanes as eluent. The product was recovered as a reddish solid (1.81 g, 56 % yield)

3-(thiophen-2-yl)-2,5-bis(2-ethylhexyl)-6-(5'-(2-ethylhexyl)-[2,2'-bithiophen]-5-yl)-2,5-dihydropyrrolo[3,4-*c*]pyrrole-1,4-dione (5-6) Compound 5-5 (1.81 g, 3.00 mmol) and compound 5-2 were added to a flask followed by 30 ml of 9:1 v/v Toluene:DMF mixture. The resulting solution was bubbled with argon for 20 min, then the catalyst tetrakis-triphenylphosphinepalladium(0) ($(Ph_3P)_4Pd(0)$) (104 mg, 0.09 mmol) was added. After 5 more minutes of bubbling with argon, the flask was heated to reflux in an oil bath. After 12 h of reaction, the reaction mixture was evaporated in vacuum and the residue purified by column chromatography on silica gel with 60 % DCM : hexanes as eluent. The product was recovered as a dark purple solid in 76% yield.

3-(5-bromothiophen-2-yl)-2,5-bis(2-ethylhexyl)-6-(5'-(2-ethylhexyl)-[2,2'-bithiophen]-5-yl)-2,5-dihydropyrrolo[3,4-*c*]pyrrole-1,4-dione (5-7) Compound 5-6 (1.65 g, 2.29 mmol) was dissolved in chloroform (50ml), protected from light and cooled to 0 ºC. N-bromosuccinimide (NBS) (0.951 g, 5.34 mmol) was added in small portions over 20 min with stirring, then stirred at room temperature overnight. The reaction mixture was washed with 5 % w/v sodium sulfite solution and brine, and then dried over $MgSO_4$ and evaporated. The residue was purified by column chromatography on silica gel with 50 % DCM : hexanes as eluent. The product was recovered as a purple-black solid (1.62 g, 78 % yield).

^{1}H NMR (400 MHz, $CDCl_3$) δ ppm 0.886 – 0.926 (m) 1.27 - 1.63 (m) 1.62 - 1.64 (m, 2H) 1.89 - 1.92 (b, 4H) 2.74-2.76 (d, 2H) 3.91 – 4.03 (b, 4H) 6.71 – 6.72 (d, H) 7.12 – 7.26 (m, 3H) 8.59 – 8.6 (d, H), 8.92 – 8.95 (d, H)

2,5-bis(2-ethylhexyl)-3-(5'-(2-ethylhexyl)-[2,2'-bithiophen]-5-yl)-6-(5-(4,4,5,5-tetramethyl-1,3,2-dioxaborolan-2-yl)thiophen-2-yl)-2,5-dihydropyrrolo[3,4-*c*]pyrrole-1,4-dione (5-8) Compound 5-7 (0.355 g, 0.412 mmol) , bis-pinacolatodiboron (B_2Pin_2) (0.102 g, 0.403 mmol), potassium acetate (0.108 g, 1.10 mmol) and bis-(diphenylphosphino)ferrocene palladium(II) chloride were put in a flask which was then flushed with argon several times. Then argon-degassed 1,4-dioxane (2ml) was injected and the mixture was heated to 85 ºC for 2 hours. A large amount of black precipitate formed. The solids were collected by filtration and washed with hexane. The remaining solid was dissolved in 5 ml of chloroform and dropped into 50 ml of methanol. Water (20 ml) was added to precipitate the desired product while leaving the B_2Pin_2 in solution. Product was collected by filtration and purified by column chromatography on silica gel with 10 % v/v methanol in chloroform as eluent. 0.122 g (35 % yield) of product were recovered as a purple solid.

^{1}H NMR (400 MHz, $CDCl_3$) δ ppm 0.886 – 0.922 (m) 1.25 - 1.37 (m) 1.58 - 1.61 (b, 2H) 1.90 - 1.92 (b, 4H) 2.73-2.75 (d, 2H) 3.96 – 4.15 (b, 4H) 6.70 – 6.71 (d, H) 7.12 – 7.22 (m) 7.96 – 7.97 (d H), 8.92 – 9.00 (m)

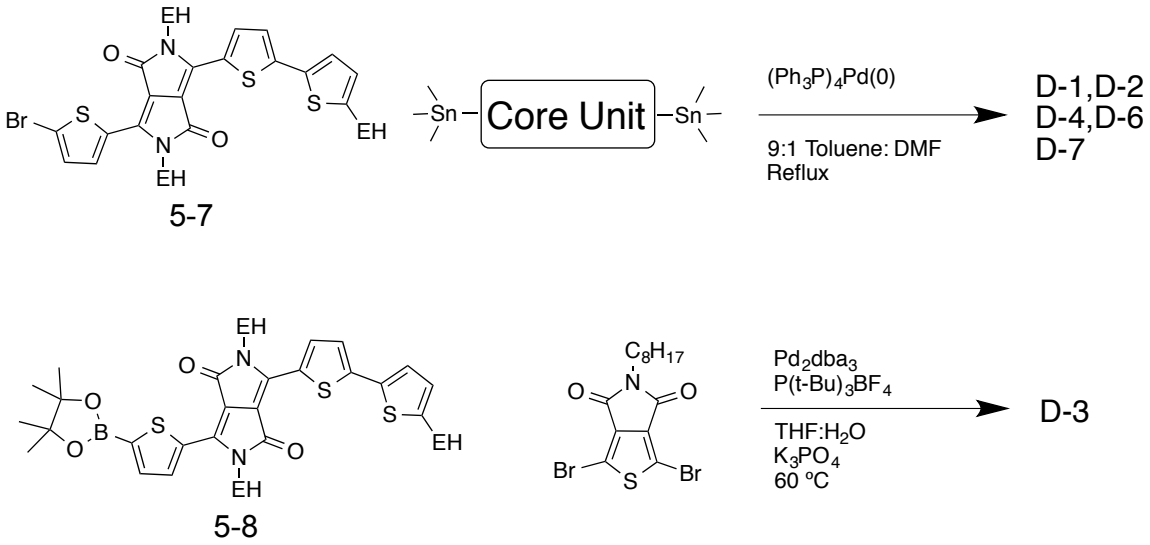

Figure 5.13 Coupling reactions to yield two-DPP unit small molecules.

General coupling reaction to yield compounds D-1, D-, D-4, D-6 and D-7

Compound 3-7 (0.200 g, 0.250 mmol) and the bistrimethylstannyl core unit materials (0.125 mmol) (purchased from Sigma Aldrich and used as received or prepared according to literature[71]) and $(Ph_3P)_4Pd(0)$ (0.05 g) were put in a flask and flushed with argon. 4.5 ml of toluene and 0.5 mol of DMF (degassed with Ar) were injected. The reaction mixtures were then heated to reflux for 3 – 6 h or until the starting material is undetectable by TLC. The reaction mixtures are then washed with water, evaporated in vacuum and purified by column chromatography using slurry-pack dry-load on silica and an 18" tall, 2" wide column. A gradient method was used starting with pure hexane and increasing the DCM concentration until the dark blue-green products move. This procedure is repeated until there are no impurities visible by TLC or NMR.

Chapter 6: Overall Conclusions

A wide variety of novel organic semiconductor materials were described in this thesis. One series of small molecules was based on the recently developed thiophene-substituted isoindigo TII unit, and a strong trend correlating gas-phase ionization energies of the donor units used with the energy levels of the resulting small molecules (and in turn the open circuit voltages of the devices). The power conversion efficiency of 3.75% attained with T-4 represents the highest performance for an OPV material based on the TII structural building block.

An entirely new electron deficient unit was developed for conjugated polymers, and its acidic characteristics lead to interesting properties, including controllable solubility and complexion with metal ions leading to photoluminescence quenching at micromolar concentrations. The synthesis of this material will be reported in a forthcoming paper and it is hoped that additional applications for this unique building block will be discovered in future work.

The work on small molecules with two DPP units lead to materials with performance that is, so far, modest at 2.22 %, but similar materials continue to attract interest in OPV research due in part to their ideal band gaps for tandem solar cell applications. The reason for the low currents obtained in some of these materials appears to be overly large domain size relative to the exciton diffusion length. The incompletely quenched photoluminescence in device films is an indication that some geminate recombination is taking place.

References

(1) Bundgaard, E.; Krebs, F. *Sol. Energ. Mat. Sol. C.* **2007**, *91*, 954.
(2) Sun, Y.; Welch, G. C.; Leong, W. L.; Takacs, C. J.; Bazan, G. C.; Heeger, A. J. *Nat Mater* **2012**, *11*, 44.
(3) Hou, J.; Chen, H.-Y.; Zhang, S.; Li, G.; Yang, Y. *J. Am. Chem. Soc* **2008**, *130*, 16144.
(4) Enchev, V.; Bakalova, S.; Ivanova, G.; Stoyanov, N. *Chem. Phys. Lett.* **1999**, *314*, 234.
(5) Forrest, S. R.; Thompson, M. E. *Chem. Rev.* **2007**, *107*, 923.
(6) Steinberger, S.; Mishra, A.; Reinold, E.; Levichkov, J.; Uhrich, C.; Pfeiffer, M.; Bäuerle, P. *Org. Lett.* **2011**, *47*, 1982.
(7) Cheng, Y.-J.; Yang, S.-H.; Hsu, C.-S. *Chem. Rev.* **2009**, *109*, 5868.
(8) Krebs, F. C.; Fyenbo, J.; Jørgensen, M. *J. Mater. Chem.* **2010**, *20*, 8994.
(9) Spanggaard, H.; Krebs, F. C. *Sol. Energ. Mat. Sol. C.* **2004**.
(10) Pochettino, A. *Sul comportamento foto-elettrico dell'antracene*; Accad. Lincei Rend, 1906; Vol. 15.
(11) Byk, A.; Borck, H. *Ber. deut. physik. ges* **1910**, *8*, 621.
(12) Volmer, M. *Annalen der Physik* **1913**, 775.
(13) Eley, D. D. *Nature* **1948**, *162*, 819.
(14) Wudl, F.; Wobschall, D.; Hufnagel, E. J. *J. Am. Chem. Soc* **1972**, *94*, 670.
(15) Bolto, B. A.; McNeill, R.; Weiss, D. E. *Australian Journal of Chemistry* **1963**.
(16) Shirakawa, H.; Louis, E. J.; MacDiarmid, A. G.; Chiang, C. K.; Heeger, A. J. *J. Chem. Soc., Chem. Commun.* **1977**, 578.
(17) Bernanose, A. *Br. J. Appl. Phys.* **1955**, *6*, S54.
(18) Partridge, R. H. Radiation sources. US 3,995,299 A, November 30, 1976.
(19) Tang, C. W.; VanSlyke, S. A. *Appl. Phys. Lett.* **1987**, *51*, 913.
(20) Kearns, D.; Calvin, M. *Lawrence Berkeley National Laboratory* **1958**.
(21) Tang, C. W. Organic solar cell. US 4,164,431, August 14, 1979.
(22) Tang, C. W. *Appl. Phys. Lett.* **1986**, *48*, 183.
(23) Pakbaz, K.; Heeger, A. J.; Yu, G. *Appl. Phys. Lett.* **1994**, *64*, 3422.
(24) Yu, G.; Gao, J.; Hummelen, J. C.; Wudl, F. *Science-AAAS-Weekly ...* **1995**, *270*, 1789.
(25) Li, G.; Yao, Y.; Yang, H.; Shrotriya, V.; Yang, G.; Yang, Y. **2007**, *17*, 1636.
(26) Heliatek consolidates its technology leadership by establishing a new world record for organic solar technology with a cell efficiency of 12% http://www.heliatek.com/newscenter/latest_news/neuer-weltrekord-fur-organische-solarzellen-heliatek-behauptet-sich-mit-12-zelleffizienz-als-technologiefuhrer/?lang=en (accessed Jun 3, 2014).
(27) You, J.; Dou, L.; Yoshimura, K.; Kato, T.; Ohya, K.; Moriarty, T.; Emery, K.; Chen, C.-C.; Gao, J.; Li, G.; Yang, Y. *Nature Communications* **2013**, *4*, 1446.
(28) Blakemore, J. S. *Solid State Physics*; 2nd ed.; Cambridge University Press: New York.
(29) Miller, R. D.; Michl, J. *Chem. Rev.* **1989**, *89*, 1359.

(30) Podzorov, V.; Menard, E.; Borissov, A.; Kiryukhin, V.; Rogers, J. A.; Gershenson, M. E. *Phys. Rev. Lett.* **2004**, *93*, 086602.
(31) Bredas, J. L.; Street, G. B. *Acc. Chem. Res.* **1985**, *18*, 309.
(32) Knupfer, M. *Appl. Phys. A* **2003**, *77*, 623.
(33) Dimitrov, S. D.; Durrant, J. R. *Chem. Mater.* **2013**.
(34) Chen, K.; Barker, A. J.; Reish, M. E.; Gordon, K. C.; Hodgkiss, J. M. *J. Am. Chem. Soc* **2013**.
(35) Dimitrov, S. D.; Durrant, J. R. *Chem. Mater.* **2014**, *26*, 616.
(36) Chen, K.; Barker, A. J.; Reish, M. E.; Gordon, K. C.; Hodgkiss, J. M. *J. Am. Chem. Soc.* **2013**, *135*, 18502.
(37) Liu, Y.; Zhou, J.; Wan, X.; Chen, Y. *Tetrahedron* **2009**, *65*, 5209.
(38) Liu, Y.; Wan, X.; Wang, F.; Zhou, J.; Long, G.; Tian, J.; You, J.; Yang, Y.; Chen, Y. *Carbon* **2011**, *1*, 771.
(39) Yin, B.; Yang, L.; Liu, Y.; Chen, Y.; Qi, Q.; Zhang, F. *Appl. Phys. Lett.* **2010**, *97*, 023303.
(40) He, Z.; Zhong, C.; Su, S.; Xu, M.; Wu, H.; Cao, Y. *Nature Photon* **2012**, *6*, 591.
(41) Shockley, W.; Queisser, H. J. *J. Appl. Phys.* **1961**, *32*.
(42) Mike, J. F.; Nalwa, K.; Makowski, A. J.; Putnam, D.; Tomlinson, A. L.; Chaudhary, S.; Jeffries-EL, M. *Phys. Chem. Chem. Phys.* **2011**, *13*, 1338.
(43) Patra, A.; Bendikov, M. *J. Mater. Chem.* **2009**, *20*, 422.
(44) Chen, H. Y.; Hou, J.; Zhang, S.; Liang, Y.; Yang, G.; Yang, Y.; Yu, L.; Wu, Y. *Nature Photon.* **2009**, *3*, 649.
(45) Huo, L.; Li, Z.; Guo, X.; Wu, Y.; Zhang, M.; Ye, L.; Zhang, S.; Hou, J. *Polym. Chem.* **2013**, *4*, 3047.
(46) Liang, Y.; Yu, L. *Acc. Chem. Res.* **2010**, *43*, 1227.
(47) Chen, H.-Y.; Hou, J.; Zhang, S.; Liang, Y.; Yang, G.; Yang, Y.; Yu, L.; Wu, Y.; Li, G. *Nature Photon.* **2009**, 1.
(48) Rolczynski, B. S.; Szarko, J. M.; Son, H. J.; Liang, Y.; Yu, L.; Chen, L. X. *J. Am. Chem. Soc.* **2012**, *134*, 4142.
(49) Cao, Y.; Smith, P.; Heeger, A. J. *Synthetic Metals* **1992**, *48*, 91.
(50) Lee, O. P.; Yiu, A. T.; Beaujuge, P. M.; Woo, C. H.; Holcombe, T. W.; Millstone, J. E.; Douglas, J. D.; Chen, M. S.; Fréchet, J. M. J. *Adv. Mater. Weinheim* **2011**, *23*, 5359.
(51) Liu, J.; Zhang, Y.; Phan, H.; Sharenko, A.; Moonsin, P.; Walker, B.; Promarak, V.; Nguyen, T.-Q. *Adv. Mater.* **2013**, *25*, 3645.
(52) Yang, L.; Tumbleston, J. R.; Zhou, H.; Ade, H.; You, W. *Energy Environ. Sci.* **2012**, *6*, 316.
(53) Subramaniyan, S.; Xin, H.; Kim, F. S.; Shoaee, S.; Durrant, J. R.; Jenekhe, S. A. *Macromolecules* **2011**, *1*, 854.
(54) Zhou, H.; Yang, L.; Xiao, S.; Liu, S.; You, W. *Macromolecules* **2010**, *43*, 811.
(55) Biniek, L.; Fall, S.; Chochos, C. L.; Anokhin, D. V.; Ivanov, D. A.; Leclerc, N.; Lévêque, P.; Heiser, T. *Macromolecules* **2010**, *43*, 9779.
(56) Steinberger, S.; Mishra, A.; Reinold, E.; Müller, C. M.; Uhrich, C.; Pfeiffer, M.; Bäuerle, P. *Org. Lett.* **2011**, *13*, 90.
(57) Walker, B.; Tamayo, A. B.; Dang, X.-D.; Zalar, P.; Seo, J. H.; Garcia, A.; Tantiwiwat, M.; Nguyen, T.-Q. *Adv. Funct. Mater.* **2009**, *19*, 3063.

(58) Griffiths, J. *Colour and constitution of organic molecules*; Academic Press: London, 1976.
(59) Lei, T.; Cao, Y.; Fan, Y.; Liu, C.-J.; Yuan, S.-C.; Pei, J. *J. Am. Chem. Soc* **2011**, *133*, 6099.
(60) Lei, T.; Cao, Y.; Zhou, X.; Peng, Y.; Bian, J.; Pei, J. *Chem. Mater.* **2012**, *24*, 1762.
(61) Mei, J.; Kim, D. H.; Ayzner, A. L.; Toney, M. F.; Bao, Z. *J. Am. Chem. Soc* **2011**, *133*, 20130.
(62) Chen, M. S.; Niskala, J. R.; Unruh, D. A.; Chu, C. K.; Lee, O. P.; Fréchet, J. M. J. *Chem. Mater.* **2013**, *25*, 4088.
(63) Ashraf, R. S.; Kronemeijer, A. J.; James, D. I.; Sirringhaus, H.; McCulloch, I. *Chem. Commun.* **2012**, *48*, 3939.
(64) Wang, E.; Ma, Z.; Zhang, Z.; Vandewal, K.; Henriksson, P.; Inganäs, O.; Zhang, F.; Andersson, M. R. *J. Am. Chem. Soc.* **2011**, *133*, 14244.
(65) Wang, E.; Ma, Z.; Zhang, Z.; Henriksson, P.; Inganäs, O.; Zhang, F.; Andersson, M. R. *Chem. Commun.* **2011**, *47*, 4908.
(66) Stalder, R.; Grand, C.; Subbiah, J.; So, F. *Polym. Chem.* **2012**.
(67) Mei, J.; Graham, K. R.; Stalder, R.; Reynolds, J. R. *Org. Lett.* **2010**, *12*, 660.
(68) Ide, M.; Koizumi, Y.; Saeki, A.; Izumiya, Y.; Ohkita, H.; Ito, S.; Seki, S. *J. Phys. Chem. C* **2013**, *117*, 26859.
(69) Koizumi, Y.; Ide, M.; Saeki, A.; Vijayakumar, C.; Balan, B.; Kawamoto, M.; Seki, S. *Polym. Chem.* **2013**, *4*, 484.
(70) Siddiqui, S.; Spano, F. C. *Chem. Phys. Lett.* **1999**, *308*, 99.
(71) Karsten, B. P.; Janssen, R. A. J. *Macromol. Chem. Phys.* **2011**, *212*, 515.
(72) Shin, W.; Yasuda, T.; Watanabe, G.; Yang, Y. S.; Adachi, C. *Chem. Mater.* **2013**, *25*, 2549.
(73) **NIST Chemistry WebBook**
.
(74) Nardes, A. M.; Kemerink, M.; de Kok, M. M.; Vinken, E.; Maturova, K.; Janssen, R. A. J. *Organic Electronics* **2008**, *9*, 727.
(75) Zilberberg, K.; Trost, S.; Schmidt, H.; Riedl, T. *Adv. Energy Mater.* **2011**, *1*, 377.
(76) Wetzelaer, G. A. H.; Kuik, M.; Lenes, M.; Blom, P. W. M. *Appl. Phys. Lett.* **2011**, *99*, 153506.
(77) Thomsen, I.; Clausen, K.; Scheibye, S.; Lawesson, S. O. *Org. Synth.* **1984**, *62*, 158.
(78) Groenendaal, L.; Jonas, F.; Freitag, D.; Pielartzik, H.; Reynolds, J. R. *Adv. Mater.* **2014**, *12*, 481.
(79) Huang, J.; Miller, P. F.; de Mello, J. C.; de Mello, A. J.; Bradley, D. D. C. *Synthetic Metals* **2003**, *139*, 569.
(80) Nguyen, T.-Q.; Martel, R.; Bushey, M.; Avouris, P.; Carlsen, A.; Nuckolls, C.; Brus, L. *Phys. Chem. Chem. Phys.* **2007**, *9*, 1515.
(81) Weedon, A. C.; Morrison, J. S. *Can. J. Chem.* **2008**, *86*, 791.
(82) Merényi, F.; Nilsson, M.; Rodmar, S.; Nihlgård, B.; Nilsson, L. *Acta Chemica Scandinavica* **1964**, *18*, 1368.
(83) Ahmedova, A.; Mantareva, V.; Mitewa, M. *International Journal of Cosmetic*

Science **2002**, 103.
(84) Kumar, A.; Sista, S.; Yang, Y. *J. Appl. Phys.* **2009**, *105*, 094512.
(85) Enchev, V.; Ahmedova, A.; Ivanov, G.; Wawer, I.; Stoyanov, N.; Heiney, P. A.; Mitewa, M. *J. Mol. Struct.* **2001**, *595*, 67.
(86) Grandidier, Y.; Riegler, A.; Ruf, K.; Schlatter, U.; Deno, T. C.I.Pigment Red 254 having improved colouristic properties - European Patent Office - EP 1411092 B1C.I.Pigment Red 254 having improved colouristic properties - European Patent Office - EP 1411092 B1. EP 1 411 092 B1, September 14, 2011.
(87) Mula, S.; Hablot, D.; Jagtap, K. K.; Heyer, E.; Ziessel, R. *New J. Chem.* **2013**, *37*, 303.
(88) Qu, S.; Wu, W.; Hua, J.; Kong, C.; Long, Y.; Tian, H. *J. Phys. Chem. C* **2010**, *114*, 1343.
(89) Li, W.; Roelofs, W. S. C.; Wienk, M. M.; Janssen, R. A. J. *J. Am. Chem. Soc.* **2012**, *134*, 13787.
(90) Qu, S.; Tian, H. *Chem. Commun.* **2012**, *48*, 3039.
(91) Dou, L.; Gao, J.; Richard, E.; You, J.; Chen, C.-C.; Cha, K. C.; He, Y.; Li, G.; Yang, Y. *J. Am. Chem. Soc* **2012**, *134*, 10071.
(92) Walker, B.; Tamayo, A. B.; Dang, X.-D.; Zalar, P.; Seo, J. H.; Garcia, A.; Tantiwiwat, *Adv. Funct. Mat.* M.; Nguyen, T.-Q. **2009**, *19*, 3063.
(93) Ripaud, E.; Demeter, D.; Rousseau, T.; Boucard-Cétol, E.; Allain, M.; Po, R.; Leriche, P.; Roncali, J. *Dyes and Pigments* **2012**, *95*, 126.
(94) Tamayo, A. B.; Dang, X. D.; Walker, B.; Seo, J. *Appl. Phys. Lett.* **2009**, *94*, 103301.
(95) Zhou, E.; Cong, J.; Hashimoto, K.; Tajima, K. *Energy Environ. Sci.* **2012**, *5*, 9756.
(96) Wang, L.; Zhang, X.; Tian, H.; Lu, Y.; Geng, Y.; Wang, F. *Chem. Commun.* **2013**, *49*, 11272.
(97) Park, J. K.; Kim, C.; Walker, B.; Nguyen, T.-Q.; Seo, J. H. **2012**, *2*, 2232.
(98) Loser, S.; Bruns, C. J.; Miyauchi, H.; Ortiz, R. P.; Facchetti, A.; Stupp, S. I.; Marks, T. J. *J. Am. Chem. Soc.* **2011**, *133*, 8142.
(99) Yuan, J.; Zhai, Z.; Dong, H.; Li, J.; Jiang, Z.; Li, Y.; Ma, W. **2012**, *23*, 885.
(100) Love, J. A.; Proctor, C. M.; Liu, J.; Takacs, C. J.; Sharenko, A.; van der Poll, T. S.; Heeger, A. J.; Bazan, G. C.; Nguyen, T.-Q. **2013**, *23*, 5019.
(101) James, P. J.; Antognozzi, M.; Tamayo, J.; McMaster, T. J.; Newton, J. M.; Miles, M. J. *Langmuir* **2001**, *17*, 349.
(102) Lee, O. P.; Yiu, A. T.; Beaujuge, P. M.; Woo, C. H.; Holcombe, T. W.; Millstone, J. E.; Douglas, J. D.; Chen, M. S.; Fréchet, J. M. J. *Adv. Mater.* **2011**, *23*, 5359.
(103) Miller, N. C.; Cho, E.; Gysel, R.; Risko, C. *Adv. Energy Mater.* **2012**, *2*, 1208.